

**STUDIES ON OXIDATIVE PROTEIN FOLDING  
AND THE DEVELOPMENT OF  
GENETICALLY ENCODED PROBES FOR  
ANALYTE SPECIFIC RATIOMETRIC IMAGING**

by

Devin A. Hudson

A dissertation submitted to the Faculty of the University of Delaware in partial fulfillment of the requirements for the degree of Doctor of Philosophy in Chemistry and Biochemistry

Winter 2018

© 2018 Devin A. Hudson  
All Rights Reserved

**STUDIES ON OXIDATIVE PROTEIN FOLDING  
AND THE DEVELOPMENT OF  
GENETICALLY ENCODED PROBES FOR  
ANALYTE SPECIFIC RATIOMETRIC IMAGING**

by

Devin A. Hudson

Approved: \_\_\_\_\_

Brian J. Bahnson, Ph.D.  
Chair of the Department of Chemistry and Biochemistry

Approved: \_\_\_\_\_

George H. Watson, Ph.D.  
Dean of the College of Arts and Sciences

Approved: \_\_\_\_\_

Ann L. Ardis, Ph.D.  
Senior Vice Provost for Graduate and Professional Education

I certify that I have read this dissertation and that in my opinion it meets the academic and professional standard required by the University as a dissertation for the degree of Doctor of Philosophy.

Signed:

---

Colin Thorpe, Ph.D.  
Professor in charge of dissertation

I certify that I have read this dissertation and that in my opinion it meets the academic and professional standard required by the University as a dissertation for the degree of Doctor of Philosophy.

Signed:

---

Brian J. Bahnson, Ph.D.  
Member of dissertation committee

I certify that I have read this dissertation and that in my opinion it meets the academic and professional standard required by the University as a dissertation for the degree of Doctor of Philosophy.

Signed:

---

John T. Koh, Ph.D.  
Member of dissertation committee

I certify that I have read this dissertation and that in my opinion it meets the academic and professional standard required by the University as a dissertation for the degree of Doctor of Philosophy.

Signed:

---

Wilfred Chen, Ph.D.  
Member of dissertation committee

Dedicated to the memory of my father, Michael Hudson.

## ACKNOWLEDGMENTS

I would like to thank my advisor, Dr. Colin Thorpe for his guidance and support during the duration of my graduate work. Dr. Thorpe's input and training has allowed me to grow as a scientist and researcher. I would also like to thank the current and past Thorpe lab members with whom I shared so much of my time here at the University of Delaware. I would like to thank Dr. Benjamin Israel for being my mentor and teaching me biochemistry methodology. The scientific and non-scientific discussions with my lab mates and other students in the Chemistry and Biochemistry department have made these last six years enjoyable. I would also like to thank my thesis committee members for guidance and support.

I would like to acknowledge the Chemistry and Biochemistry department and the Chemistry and Biology Interface program for the opportunities that have been afforded to me. The environment that Chemistry and Biochemistry department has been built with great students, faculty, and equipment have enabled me to develop as a researcher. In addition, the collaborative environment that has fostered productive collaborations between myself and the Joseph Fox laboratory. I would also like to thank the Delaware Biotechnical Institute and Dr. Jeffery Caplan for his assistance, insight, and guidance in confocal microscopy and intercellular imaging.

I would like to thank my friends, and family whom have supported me during the duration of my doctoral work. I would like to acknowledge Dr. Robert Luttrell whose advice and mentorship led me to applying for graduate school. I would especially like thank my wife, Jordan Hudson for her support and unending

encouragement that kept me going, even during some of the hardest and most trying times over the last six years.

## TABLE OF CONTENTS

|  |     |
|--|-----|
| LIST OF TABLES .....   | x   |
| LIST OF FIGURES .....  | xi  |
| ABSTRACT .....   | xiv |
| Chapter  |     |
| 1 OXIDATIVE PROTEIN FOLDING.....   | 1   |
| 1.1 Introduction and Background.....   | 1   |
| 1.1.1 Protein Folding.....   | 1   |
| 1.1.2 Oxidative Protein Folding.....   | 4   |
| 1.1.3 Oxidative folding in Prokaryotes.....  | 4   |
| 1.1.4 Oxidative Folding in Eukaryotes.....   | 8   |
| 1.1.5 Secretory Apparatus .....  | 9   |
| 1.1.6 Mitochondrion.....   | 12  |
| 1.1.7 Chloroplasts.....  | 14  |
| REFERENCES.....  | 18  |
| 2 OXIDATIVE PROTEIN FOLDING: FROM THIOL-DISULFIDE<br>EXCHANGE REACTIONS TO THE REDOX POISE OF THE<br>ENDOPLASMIC RETICULUM ..... | 22  |
| 2.1 Introduction .....   | 22  |
| 2.2 Chemical Aspects of Thiol-Exchange Reactions .....   | 23  |
| 2.2.1 Oxidative Protein Folding --- Enzymes and Oxidants .....   | 26  |
| 2.1 PDI – Second Pathways.....   | 30  |
| 2.2 PDI and Glutathione Interaction Kinetics .....   | 32  |
| 2.3 Preamble to Redox Poise Measurements in the Mammalian ER .....   | 35  |
| 2.4 ER Glutathione Redox Poise.....  | 36  |
| 2.5 Redox State of PDI in the Mammalian ER .....   | 40  |
| 2.6 Chemical Trapping of PDI Redox State.....  | 42  |
| 2.7 The Influence of PDI Redox State on In Vitro Oxidative Protein<br>Folding.....   | 47  |

|                  |  |     |
|------------------|--|-----|
| 2.8              | Future Directions .....  | 52  |
| 2.9              | Envoi.....   | 57  |
| REFERENCES ..... |  | 61  |
| 3                | MIA40 IS A FACILE OXIDANT OF UNFOLDED REDUCED<br>PROTEINS BUT SHOWS MINIMAL ISOMERASE ACTIVITY .....   | 70  |
| 3.1              | Introduction and Background .....  | 70  |
| 3.2              | Experimental Procedures .....  | 73  |
| 3.2.1            | Materials and General Methods.....   | 73  |
| 3.2.2            | Expression and Treatment of Proteins.....  | 73  |
| 3.2.3            | RNase Activity Assay.....  | 74  |
| 3.2.4            | Insulin Reductase Assay .....  | 75  |
| 3.2.5            | Stopped Flow Methods.....  | 75  |
| 3.2.6            | Sequence Analysis.....   | 75  |
| 3.3              | Results and Discussion .....   | 76  |
| 3.3.1            | Mia40/IfALR is a general catalysis of protein oxidation .....  | 76  |
| 3.3.2            | Reduced RNase interacts with oxidized Mia40.....   | 80  |
| 3.3.3            | Does Mia40 show significant protein disulfide isomerase<br>activity? .....                             | 82  |
| 3.4              | Conclusions .....  | 87  |
| REFERENCES ..... |  | 88  |
| 4                | DESIGNING FLAVOPROTEIN-GFP FUSION PROBES FOR<br>ANALYTE-SPECIFIC RATIOMETRIC FLUORESCENCE IMAGING..... | 94  |
| 4.1              | Introduction to Genetically Encode Fluorescent Protein Sensors .....                                   | 94  |
| 4.2              | Genetically Encode Fluorescent Proteins .....  | 95  |
| 4.2.1            | Limitations and Deficits in Our Current Tools to Measure<br>Intracellular Redox Molecule Pools .....   | 96  |
| 4.3              | Materials and Methods .....  | 100 |
| 4.3.1            | Materials.....   | 100 |
| 4.3.2            | General Procedures.....  | 101 |
| 4.3.3            | Protein Expression in <i>E. coli</i> .....   | 101 |
| 4.3.4            | Protein Handling.....  | 102 |

|        |   |     |
|--------|---|-----|
| 4.3.5  | NADPH Reductase Activity of TrxR-mCherry and TrxR <sub>GV</sub> -mCherry.....                     | 103 |
| 4.3.6  | In Vitro TrxR <sub>GV</sub> -mCherry Reduction Assay.....   | 103 |
| 4.3.7  | Thioredoxin Titration of TrxR <sub>GV</sub> -mCherry.....   | 103 |
| 4.3.8  | In Vivo TrxR <sub>GV</sub> -mCherry Reduction Assay.....  | 104 |
| 4.3.9  | Imaging <i>E. coli</i> Cells.....   | 104 |
| 4.3.10 | LipDH-mCherry Reduction and Titration Experiments.....  | 105 |
| 4.3.11 | Mammalian Cell Culture and Imaging.....   | 105 |
| 4.3.12 | Image and Data Processing for Bacterial and Mammalian Sensors.....                                | 106 |
| 4.3.13 | Redox Measurements.....   | 106 |
| 4.4    | Results and Discussion.....   | 107 |
| 4.4.1  | Design of a New Probe for Thioredoxin Proteins.....   | 107 |
| 4.4.2  | Expression and Characterization of Thioredoxin Sensors.....                                       | 109 |
| 4.4.3  | Thioredoxin Sensor Responds to Intracellular Thioredoxin.....                                     | 113 |
| 4.4.4  | TrxR <sub>GV</sub> -mCherry Sensor Imaged in Live <i>E. coli</i> Cells.....                       | 118 |
| 4.5    | Design of a New Probe for NAD <sup>+</sup> /NADH.....   | 120 |
| 4.5.1  | Expression and Characterization of NAD <sup>+</sup> /NADH Sensor.....                             | 122 |
| 4.5.2  | NAD <sup>+</sup> /NADH Sensor Interacts Reversibly with Intracellular NAD <sup>+</sup> /NADH..... | 125 |
| 4.6    | CONCLUSIONS.....  | 128 |
|        | REFERENCES.....   | 131 |
|        | Appendix  |     |
| A      | CHAPTER 4 DNA AND PROTEIN SEQUENCES.....  | 139 |

## LIST OF TABLES

|            |   |    |
|------------|---|----|
| Table 2.1: | Measurement of glutathione redox state in the mammalian ER. ....                          | 39 |
| Table 2.2: | Determination of the redox state of PDIs within the ER.....                               | 42 |
| Table 2.3: | Redox potentials and projected redox state of selected human PDI-<br>family members. .... | 50 |
| Table 2.4: | Tryptic peptides of PDI-family members carrying CxxC redox-active<br>motifs.....          | 59 |

## LIST OF FIGURES

|              |  |    |
|--------------|--|----|
| Figure 1.1:  | Diagram of the multiple pathways of protein folding. ....  | 2  |
| Figure 1.2:  | The conceptual two-step process of oxidative protein folding.....  | 3  |
| Figure 1.3:  | Schematic of gram-negative bacterial periplasmic oxidative folding. ....   | 5  |
| Figure 1.4:  | Selected cellular schematic for known sites of oxidative protein folding in eukaryotic cells. ....                               | 8  |
| Figure 1.5:  | Oxidative protein folding in the endoplasmic reticulum.....  | 9  |
| Figure 1.6   | Oxidative protein folding in the innermembrane space of mitochondria.....  | 12 |
| Figure 1.7   | Oxidative folding in the thylakoid space of chloroplasts.....  | 15 |
| Figure 2.1:  | Mechanistic aspects of thiol-disulfide exchange reactions. ....  | 25 |
| Figure 2.2:  | Structure of human PDI.....  | 28 |
| Figure 2.3:  | An example of a PDI-first pathway in oxidative protein folding.....  | 29 |
| Figure 2.4:  | Some enzymatic and non-enzymatic oxidants for reduced PDI.....   | 30 |
| Figure 2.5:  | PDI-second pathways of oxidative folding. ....   | 32 |
| Figure 2.6:  | Reduction of PDI by GSH.....   | 33 |
| Figure 2.7:  | A potential pathway for redox cycling in the ER.....   | 35 |
| Figure 2.8:  | Electron micrograph of a plasma cell from guinea pig bone marrow showing an extensive reticular network of ER.....               | 44 |
| Figure 2.9:  | The use of NEM to trap intraluminal redox state within the ER.....   | 46 |
| Figure 2.10: | The rate of oxidative refolding of riboflavin binding protein in the presence of PDI redox buffers of defined concentration..... | 49 |

|   |     |
|---|-----|
| Figure 2.11: Schematic diagram of equilibrating and non-equilibrating redox species in the ER. ....   | 54  |
| Figure 2.12: A suggested protocol for a more global analysis of the redox state of thiol-disulfide oxidoreductases within the ER (see the Text). .... | 55  |
| Figure 3.1: The flow of reducing equivalents during the oxidation of a protein dithiol catalyzed by Mia40 and IfALR. ....                             | 71  |
| Figure 3.2: ScanProsite analysis of non-cognate substrates. ....  | 77  |
| Figure 3.3: Oxidative of non-cognate substrates. ....   | 78  |
| Figure 3.4: Reduction of Mia40 by RNase. ....   | 81  |
| Figure 3.5: Isomerization of scrambled RNase. ....  | 83  |
| Figure 3.6: Insulin turbidity assay by Mia40. ....  | 85  |
| Figure 4.1: Three-dimensional structure of green fluorescent protein. ....  | 95  |
| Figure 4.2: Three types of genetically encoded fluorescent protein sensors ....   | 98  |
| Figure 4.3: A new class of genetically encoded probes. ....   | 99  |
| Figure 4.4: <i>E. coli</i> thioredoxin reductase: structure, reactions and probe design. ...  | 109 |
| Figure 4.5: UV-Vis spectrum of thioredoxin reductase-mCherry sensors. ....  | 110 |
| Figure 4.6: Characterization of TrxR <sub>GV</sub> -mCherry. ....   | 111 |
| Figure 4.7: Suppressing NADPH activity in <i>E. coli</i> thioredoxin reductase. ....  | 113 |
| Figure 4.8: Reduction of TrxR <sub>GV</sub> -mCherry in vitro and in <i>E. coli</i> . ....  | 114 |
| Figure 4.9: Reduction of <i>Ec</i> Trx1 followed by tryptophan fluorescence. ....   | 116 |
| Figure 4.10: Interrogating Thioredoxin Redox Poise in Live <i>E. coli</i> cells. ....   | 117 |
| Figure 4.11: Confocal field of view of <i>E. coli</i> cells expressing TrxR <sub>GV</sub> -mCherry sensor. ....                                       | 119 |
| Figure 4.12: Lipoamide Dehydrogenase: structure, reactions and probe design. ....   | 121 |
| Figure 4.13: UV-Vis spectrum of the LipDH-mCherry NAD <sup>+</sup> /NADH sensor. ....   | 123 |

|   |     |
|---|-----|
| Figure 4.14: Characterization of LipDH-mCherry. ....  | 124 |
| Figure 4.15: Interrogating NADH/NAD <sup>+</sup> Redox in Live HEK283T Cells. ....                              | 126 |
| Figure 4.16: Confocal field of view for one of the NAD <sup>+</sup> /NADH sensor flow cell<br>experiments. .... | 127 |
| Figure 4.17: Characterization of the TrxR <sub>GV</sub> -mRuby2 sensor.....                                     | 129 |

## ABSTRACT

Disulfide bond formation *in vivo* is linked to many essential intracellular processes; protein regulation and signaling, chemical transformations, and oxidative protein folding. Oxidative protein folding is an enzyme catalyzed process which is controlled by dedicated protein thiol oxidoreductases. In this work the oxidative protein folding within the mammalian endoplasmic reticulum (ER) is examined from an enzymological perspective. Evidence for the rapid reduction of PDI by reduced glutathione is presented in the context of PDI-first pathways. Next, strategies and challenges for the determination of the concentrations of reduced and oxidized glutathione and of the ratios of PDI<sub>red</sub>:PDI<sub>ox</sub> is discussed. After a discussion of the use of natively encoded fluorescent probes to report the glutathione redox poise of the ER, a complementary strategy to discontinuously survey the redox state of as many redox-active disulfides as can be identified by ratiometric LC-MS-MS methods in order to better understand redox linked species. Next, we investigate the specificity of the human Mia40/IfALR system towards non-cognate unfolded protein substrates to assess whether the efficient introduction of disulfides requires a particular amino acid sequence context or the presence of an IMS targeting signal. Mia40 is found to be effective oxidant of non-cognate substrates, but is an ineffective protein disulfide isomerase when its ability to restore enzymatic activity from scrambled RNase is compared to that of protein disulfide isomerase. Mia40's ability to bind amphipathic peptides tested by the insulin reductase assay. The consequences of these studies, mitochondrial oxidative protein folding, and the transit of polypeptides is discussed.

Finally, the development of disulfide linked genetically encoded fluorescent probes for analyte-specific imaging are demonstrated. Current classes of intracellular probes depend on the selection of binding domains that either undergo conformational changes on analyte binding or can be linked to thiol redox chemistry. Here, novel probes were designed by fusing a flavoenzyme, whose fluorescence is quenched on reduction by the analyte of interest, with a GFP domain to allow for rapid and specific ratiometric sensing. Two flavoproteins, *Escherichia coli* thioredoxin reductase and *Saccharomyces cerevisiae* lipoamide hydrogenase, were successfully developed into thioredoxin and NAD<sup>+</sup>/NADH specific probes respectively and their performance was evaluated *in vitro* and *in vivo*. These genetically encoded fluorescent constructs represent a modular approach to intracellular probe design that should extend the range of metabolites that can be quantitated in living cells.

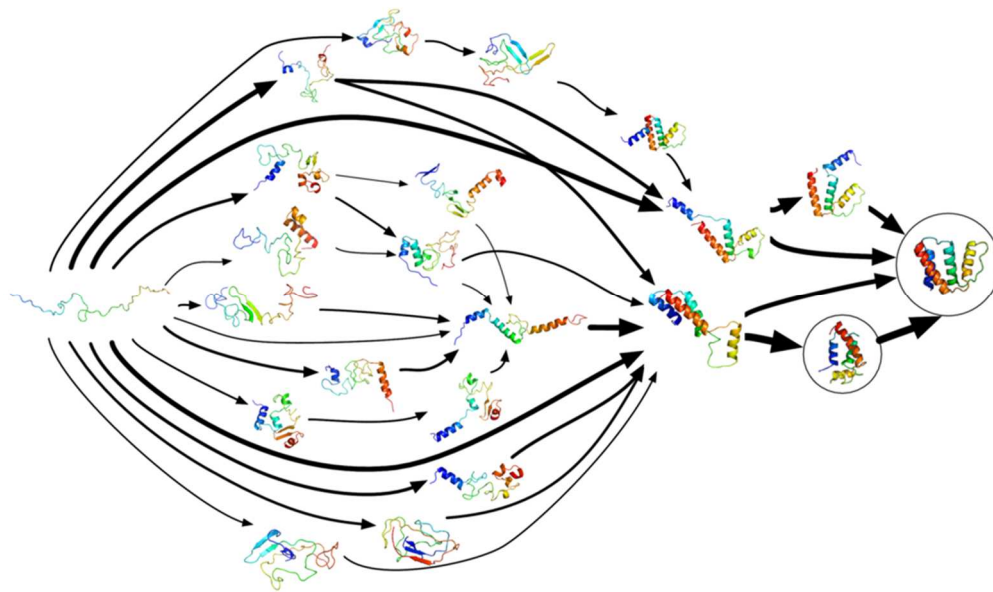
## **Chapter 1**

### **OXIDATIVE PROTEIN FOLDING**

#### **1.1 Introduction and Background**

##### **1.1.1 Protein Folding**

Protein folding begins with a series of transfers that convert information contained within DNA, into proteins. This information transfer is a twostep process; first information in DNA is transcribed into RNA, and secondly translated into a polypeptide. Protein folding is defined as a process by which a polypeptide acquires its three-dimensional structure, or native fold. The native fold is the conformation of a polypeptide that is biologically functional and active [1]. This process is dictated by the primary sequence of the polypeptide (Anfinsen's dogma) and the non-covalent interactions of the polypeptide with its environment [2]. These interactions, primarily due to solvation effects, drive the protein folding via a combination of free energy minimizing steps.

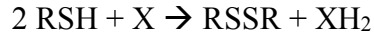


A Markov state model illustrating 15 of the highest-flux folding pathways between the unfolded (left) and native state (right) of ACBP, an 86-residue helix-bundle protein. Line thicknesses are proportional to pathway folding flux. Image by Vincent Voelz, distributed under a CC BY-SA 3.0 license.

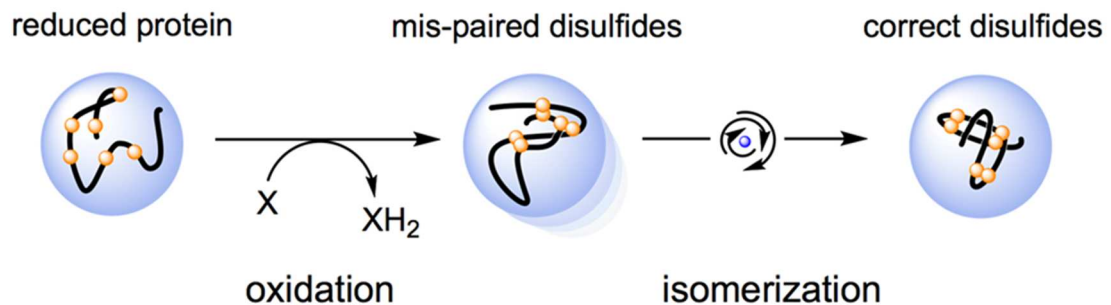
**Figure 1.1: Diagram of the multiple pathways of protein folding.**

Protein folding, as depicted in Figure 1.1, is a complex process that comprises multiple pathways leading to the native fold. Protein folding can further be complicated by the requirement in some proteins for post-translational modifications [3]. One common post-translation modification that impacts protein folding is the oxidation of cysteine residues to form disulfide bonds. Disulfide bonds are often found in secreted and structural proteins where this modification reinforces the protein's native fold structure and enhances stability [4].

The formation of disulfide bonds is an oxidation reaction, where two cysteine thiols are oxidized to form one disulfide bond (reaction equation below).



Historically the oxidation of protein cysteine residues to disulfide bonds in aerobic solutions has been attributed to a spontaneous oxidation by molecular oxygen, but this reaction is formally spin-forbidden as molecular oxygen is a ground-state triplet and thiols are ground-state singlets [5, 6]. This reported spontaneous reactivity between protein thiols and molecular oxygen is commonly catalyzed by trace metal ions, such as copper, which often contaminate labware and commercially-available reagents [7]. In addition to molecular oxygen, a number of other common biologically significant small molecules have been observed to spontaneously oxidize thiols, including hydrogen peroxide and L-dehydroascorbic acid [8]. The chemistry of cysteine oxidation, thiol exchange reactions and the steric requirements of this reaction are described in detail in Chapter 2. When cysteine oxidation chemistry is coupled with protein folding, this process is known as oxidative protein folding.



In the first step, cysteine residue pairs in the polypeptide undergo oxidation yielding disulfide bonds. In the second step, mispaired disulfide bonds undergo isomerization to yield the native protein fold.

**Figure 1.2: The conceptual two-step process of oxidative protein folding.**

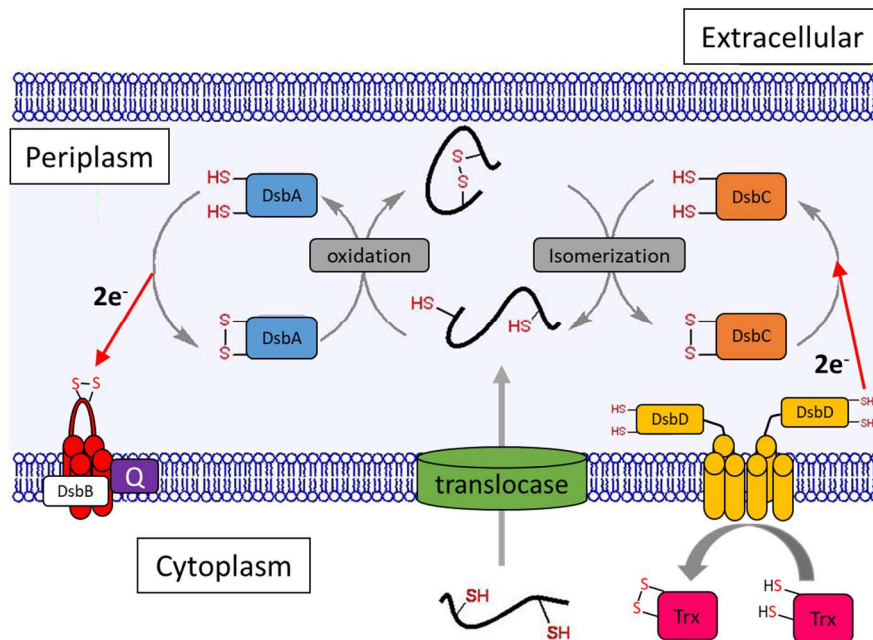
### 1.1.2 Oxidative Protein Folding

Oxidative protein folding is conceptually a two-step process. In the first step, *oxidation* (see Figure 1.2), free thiols on a reduced unfolded protein are net oxidized by the transfer of one or more pairs of electrons to form disulfide bonds. The number of fully oxidized polypeptide isomers generated by the oxidation of cysteine residues is directly related to the number of cysteines in the original peptide. Bovine RNaseA contains 8 cysteines and can be fully oxidized to yield 105 isomers, while hen egg white riboflavin binding protein contains 18 cysteines with 34,459,425 possible oxidized isomers. In the second step, *isomerization* (see Figure 1.2), mispaired disulfide bonds generated during the first step are rearranged by repeated rounds of disulfide exchange to yield the protein's native fold with correct disulfide connectivity. In cells, both steps of oxidative protein folding are catalyzed by a protein thiol oxidoreductase. In disulfide-containing proteins, the oxidation and isomerization of disulfide bonds represents the slow step in oxidative protein folding [8]. In biology, oxidative folding is found in all clades of life including prokaryotes, archaea, and eukaryotes [9]. A common feature in all oxidative folding systems is that this specialized machinery is confined to specific organelles and locations separate from the bulk of the living cell. Following are overview summaries discussing the known oxidative folding strategies and machineries found in both prokaryotes and eukaryotes.

### 1.1.3 Oxidative folding in Prokaryotes

Before the discovery of the first catalyst of oxidative folding in prokaryotes by Bardwell *et al.* in 1991, disulfide bond formation in prokaryotes was widely believed to occur spontaneously [10]. The best studied model prokaryote oxidative protein folding is found in *Escherichia coli* (*E.coli*), where this machinery is isolated to a

gram-negative bacterial compartment known as the periplasm. The periplasm is a membrane-enclosed compartment found between the inner and outer membranes of gram-negative bacteria. A schematic of the gram-negative bacterial oxidative folding system, including participating enzymes and small molecules is depicted in Figure 1.3.



Bacterial oxidative folding is catalyzed within the periplasmic space. DsbA is the dedicated oxidant of cysteine residue, inserting disulfide bonds into imported reduced polypeptides. DsbA is recycled by the membrane anchored DsbB, that in turn, is reoxidized by coenzyme Q. DsbC and its homologs catalyze the isomerization and reduction of mispaired disulfide bonds. DsbC is maintained in its functional reduced state by DsbD and electrons transferred through the membrane from cytosolic thioredoxin.

**Figure 1.3: Schematic of gram-negative bacterial periplasmic oxidative folding.**

In gram-negative bacteria, the oxidation and isomerization of reduced proteins are handled by two separate, but co-localized protein assemblies. The oxidation of

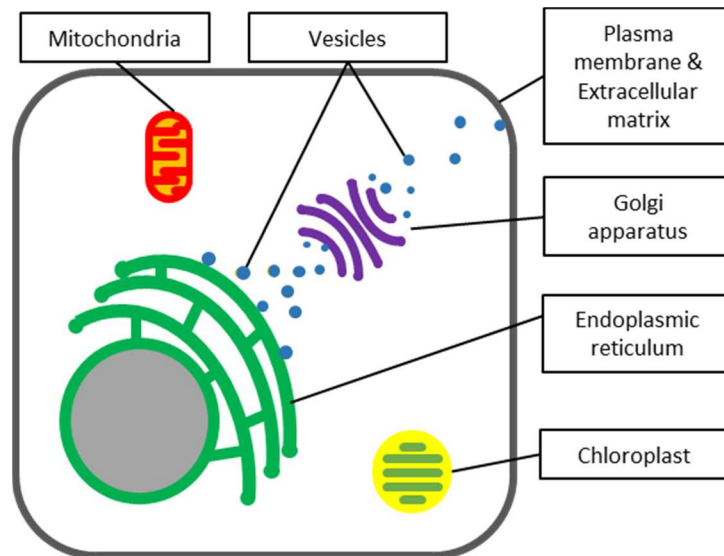
unfolded polypeptides folding is catalyzed by DsbA/DsbB system, while the isomerization and reduction of dispaired disulfides is catalyzed by the DsbC/DsbD system [9, 11]. Cysteine-containing polypeptides that cross the inner membrane via a membrane bound protein translocase (green, Figure 1.3) are potential substrates of this oxidative folding machinery. Reduced polypeptides are oxidized by transferring a pair of electrons onto thioredoxin fold protein DsbA (blue, Figure 1.3). DsbA contains the most highly oxidizing redox active CxxC motif recognized to date at -121 mV, which allows oxidized DsbA to effectively transfer a disulfide to polypeptides [12]. Reduced DsbA is recycled to its oxidized form by transferring the reducing equivalents to a membrane bound partner protein, DsbB (red, Figure 1.3). DsbB is a membrane protein containing two redox active disulfides and a binding pocket for quinone (purple, Figure 1.3). DsbB undergoes a series of internal thiol exchange reactions, transferring the electrons to the terminal small molecule electron acceptor, quinone, completing the catalytic cycle. Isomerization of oxidized polypeptide products produced by the DsbA/DsbB system is catalyzed by the DsbC/DsbD system [9, 11]. DsbD (yellow, Figure 1.3) is an integral membrane protein with redox active disulfides in both the transmembrane domain and a terminal thioredoxin-like domain. Electrons from reduced thioredoxin (pink, Figure 1.3) in the cytoplasm are transferred to DsbD via thiol exchange reactions which connect the reducing potential of the bacterial cytoplasm to the periplasmic space. Reducing equivalents received by DsbD are then passed to the partner protein DsbC (orange, Figure 1.3). DsbC is a disulfide isomerase that contains a dual thioredoxin motif separated by a protein binding domain. DsbC is the active catalyst that corrects the mispaired disulfide polypeptide products of the DsbA/DsbB system. DsbC corrects mispaired polypeptide disulfides via multiple

round of disulfide exchange reactions between unfolded substrate thiols and DsbC. The energetically favorable disulfide arrangement of substrate forms after multiple rounds of DsbC catalyzed isomerization, resulting in the attainment of the native form of the substrate protein [9, 11]. While an examination of Figure 1.3 suggest the potential for a futile cycle in which cytosolic reducing potential could be diverted to coenzyme Q without participating in oxidative protein folding, strict steric clashes between these catalysts results in kinetic isolation between the DsbA/DsbB and DsbC/DsbD systems [4].

While the oxidative folding machinery of *E. coli* may be the best studied gram-negative bacterial system to date, recently increasing diversity among bacterial oxidative folding machineries has been recognized [13]. Genetic analysis has shown that some organisms within the cyanobacteria, actinobacteria, and proteobacteria phylum lack the gene for DsbB, while still retaining oxidative folding capacity. In these organisms, an integral membrane protein named vitamin K epoxide reductase (VKOR) acts as the direct oxidant of DsbA, or can act as a direct oxidant of polypeptides via a C-terminal thioredoxin domain. VKOR, like DsbB, utilizes the terminal electron acceptor quinone. Due to the absence of an outer membrane and accompanied periplasmic compartment, gram-positive bacteria are thought to lack the capacity to catalyze oxidative protein folding. Recently, evidence of oxidative folding in the exoplasm of actinobacteria, a phylum of gram-positive bacteria, has been demonstrated [14]. Additionally, disulfide rich proteins have been found in the cytoplasm of thermophilic archaea, and it has been proposed that oxidative protein folding machinery to catalyze these protein disulfide bonds must exist in this unusual bacterial compartment [15].

### 1.1.4 Oxidative Folding in Eukaryotes

Eukaryotic cells contain several evolutionarily divergent sets of oxidative folding machineries isolated to discrete organelles. [9] Figure 1.4 depicts a schematic of a eukaryotic cell with selected organelles where protein oxidative folding is known to occur. In eukaryotes several unique and separate oxidative protein folding machineries have been identified in the endoplasmic reticulum, Golgi apparatus, plasma membrane, mitochondrion, and chloroplast (See Figure 1.4). Substrates of these oxidative folding machineries are encoded by nuclear genes, and thus must be transported into their final locales by specific signal sequences located in nascent peptides [9, 16, 17].

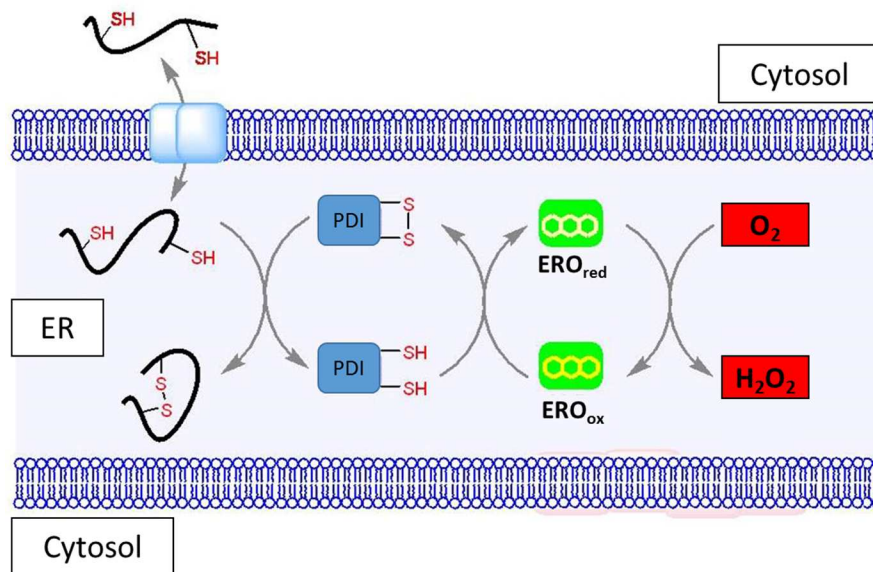


The secretory system, made up of the endoplasmic reticulum (green), Golgi apparatus (purple), and vesicles (blue), is known as the main site for oxidative protein folding and quality control. Other sites of oxidative protein folding include the mitochondria (red), chloroplast (yellow), outward facing plasma membrane and extracellular matrix.

**Figure 1.4: Selected cellular schematic for known sites of oxidative protein folding in eukaryotic cells.**

### 1.1.5 Secretory Apparatus

The secretory system has been long recognized as the main site of protein oxidative folding in the eukaryotic cell and as the processor of secreted and plasma membrane proteins. The typical eukaryotic cell process approximately ~1/3 of their proteome through the secretory network [4, 16]. Secretory network peptides start translation in the cytosol, where an internal ER-targeting signal stalls ribosomal synthesis and targets the nascent peptide to the ER translocation lumen via a peptide transporter channel (light blue) [4, 8]. A schematic for one mode of ER oxidative protein folding can be seen in Figure 1.5.



Cytosolically expressed reduced polypeptides are imported into the ER and are net oxidized by oxidized protein disulfide isomerase (blue). Mismatched disulfides generated by this oxidation are isomerized by reduced protein disulfide isomerase. Net oxidation of PDI is catalyzed by a variety of oxidants including ERO (green). Reduced ERO is reoxidized by transfer of electrons to the final acceptor molecular oxygen (red).

**Figure 1.5: Oxidative protein folding in the endoplasmic reticulum.**

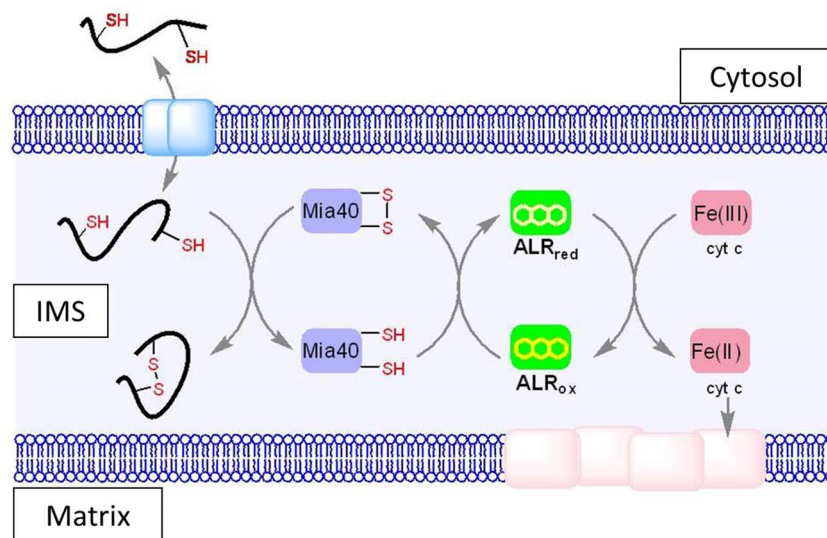
Imported unfolded reduced polypeptides undergo the first step of oxidative folding by transferring reducing equivalents to the oxidized form of the thiol oxidoreductase protein disulfide isomerase (PDI, dark blue, Figure 1.5). PDI is a tetra-thioredoxin domain protein arranged as a “V” that contains two opposed redox active cysteine pairs as well as a hydrophobic protein binding domain which has affinity for partially folded peptides [8]. Figure 1.5 shows that reduced PDI can be recycled by thiol exchange with endoplasmic reticulum oxidoreductin 1 (ERO1, green, Figure 1.5). ERO1 is a thiol oxidoreductase that contains a bound flavin cofactor and a bridged-redox active CxxCxxC motif. Electrons accepted by ERO1 from PDI, are transferred to the terminal acceptor molecular oxygen (red, Figure 1.5) to form hydrogen peroxide. In addition to ERO1, reduced metazoan PDI is recycled by several other oxidants, including enzymes such as peredoxin 4, glutathione peroxidase 7/8, VKOR, and small molecules such as H<sub>2</sub>O<sub>2</sub>, GSSG, and dehydroascorbate [4, 8]. These multiple routes of the reoxidation of PDI are described in detail in Chapter 2.

Unlike prokaryotic oxidative folding, where the oxidation and isomerization catalysts are independent and kinetically isolated systems, both steps are largely catalyzed by PDI. Reduced PDI utilizes the affinity of unfolded polypeptides for its hydrophobic protein binding domain to correct mispaired disulfide bonded peptides via multiple rounds of thiol exchange reactions [4, 18]. Due to the duality of the roles of PDI the redox status of PDI has profound effects on the rate of secretory system oxidative folding. The consequences of PDI redox states on oxidative protein folding is analyzed in detail in Chapter 2.

Proteins that have successfully undergone oxidative protein folding in the endoplasmic reticulum are transported to the Golgi apparatus, where additional post-translational modifications and sorting can occur. Quality control mechanisms in the Golgi apparatus screen out improperly folded proteins and return these products to the ER via retrograde transport. Secreted and plasma membrane proteins that pass this quality control step pass through the Golgi apparatus to be packaged into vesicles targeted for fusion into the plasma membrane (Figure 1.4) [19, 20]. Additional opportunities for oxidative protein folding may occur in the Golgi apparatus and the late-secretory pathways. Localized to the Golgi apparatus, cell surface, and extracellular spaces is a sulfhydryl oxidase known as Quiescin-sulfhydryl oxidase (QSOX) [21-23]. QSOX is a pseudo dimeric enzyme, containing a single flavin cofactor and a thioredoxin-like domain containing a redox-active disulfide which directly accepts electrons from reduced unfolded proteins. Reduced QSOX is reoxidized by electron transfer from the thioredoxin domain to the internal flavin cofactor and finally to molecular oxygen, regenerating the catalyst. QSOX is unique in comparison to other protein thiol oxidoreductases in that it both directly interacts with substrate proteins and is self-recycling without a secondary partner oxidase as seen in other oxidative folding systems [24]. The plasma membrane and extracellular matrix is the final destination of many secretory network proteins (see, Figure 1.4), and is a recently recognized location where protein oxidative folding occurs. [4, 21] This is an interesting and exciting new site of oxidative protein folding where the exact actors and players are still being elucidated [4].

### 1.1.6 Mitochondrion

The mitochondrion is an interesting eukaryotic organelle that is believed to have been derived from an ancient endosymbiosis of an oxygen metabolizing prokaryote with an early eukaryotic cell. Mitochondria, like bacteria, possess a double membrane containing an inner membrane space (IMS) analogous to the prokaryotic periplasmic space complete with oxidative protein folding machinery. While derived from an ancient gram-negative bacterium, surprisingly, the oxidative folding system of the mitochondrion and bacteria is not conserved. A schematic of the human mitochondrial oxidative folding machinery can be seen in Figure 1.6.



Reduced unfolded proteins entering the intermembrane space of mitochondria are net oxidized by oxidized Mia40 (blue). Reduced Mia40 is reoxidized by electron transfer to the flavoenzyme augmenter of live regeneration (ALR, Green). Electrons are then transferred from the flavin cofactor of ALR to molecular oxygen or, preferably, to cytochrome C (red) entering the electron transport system (pink).

**Figure 1.6 Oxidative protein folding in the innermembrane space of mitochondria.**

Peptides synthesized by ribosomes in the cytosol targeted to the inner membrane space of mitochondria must first pass through the mitochondria outer membrane via a membrane bound protein translocase pore (light blue, Figure 1.6). Reduced and unfolded polypeptides that are trafficked to the inner membrane space (IMS) are received and oxidized by the thiol oxidoreductase and import receptor, Mia40 (dark blue). Mia40 is a small helix-coil-helix protein that contains a redox active disulfide on a flexible loop and an extensive hydrophobic binding surface with an affinity for unfolded proteins [25, 26]. Historically, IMS resident proteins were thought to have been targeted and trapped in the IMS by interaction with Mia40 via a combination of primary and secondary structure features in IMS peptides. Features found critical to IMS resident peptides required for interactions with Mia40 were identified to be small size (< 20 KDa), conserved cysteine motifs, internal IMS targeting sequence, and helix-coil-helix secondary structure [27, 28]. Recently, advances in proteomics have allowed for identification of a number of Mia40 substrates that are aberrant to the strict definition of canonical Mia40 substrates previously determined [4, 29]. In Chapter 3, the catalytic promiscuity of Mia40 towards unfolded reduced polypeptides and the consequences of this broad substrate tolerance on mitochondrial protein trafficking is discussed and explored in more detail.

Reduced Mia40, is recycled to its active oxidized form by transfer of reducing equivalents to the flavoenzyme long form augments of liver regeneration (ALR, green, Figure 1.6) via a thiol exchange reaction. ALR and its close homolog in yeast, essential for respiration and viability 1 (ERV1), are homodimeric flavoenzymes containing a flavin cofactor and two redox active disulfides [29, 30]. In metazoans,

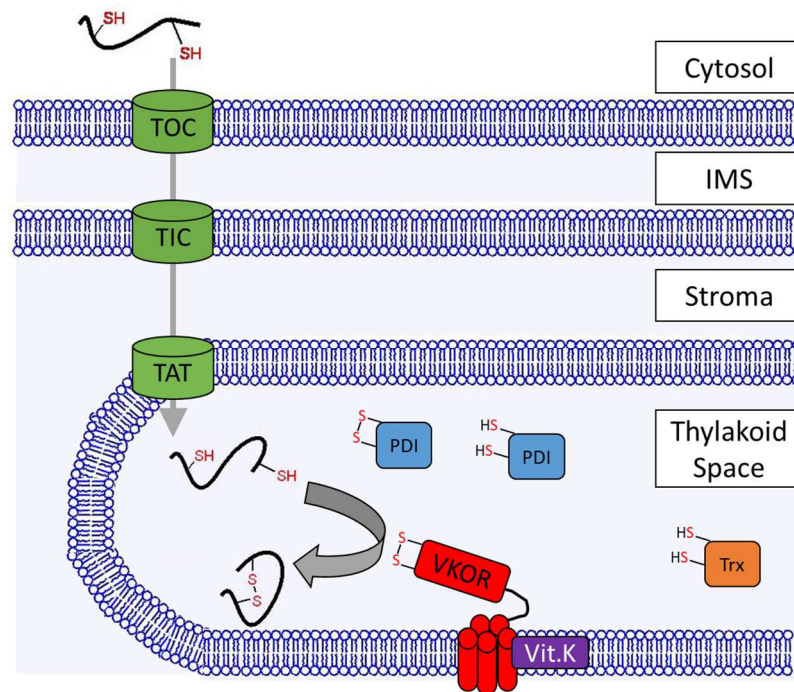
reduced ALR is recycled by transfer of electrons to the terminal electron acceptor cytochrome C (red, Figure 1.6) into the electron transport chain. Under anerobic conditions, yeast recycle reduced ERV1 by transfer of electrons to the fumarate reductase protein (Osm1). In addition, a number of eukaryotes from the kingdom Protista are known to lack a homolog of Mia40. In these protists, a homolog of ALR/ERV1 is capable of directly oxidizing IMS resident proteins without need for the thiol oxidoreductase Mia40 homolog [31, 32].

Unlike the well-established oxidation of IMS resident proteins by Mia40, the identity of a dedicated IMS catalyst of disulfide isomerase has not be elucidated. While many IMS resident proteins tend to be small proteins with simple disulfide connectivities, recent proteomic works has shown a number of IMS residue proteins with much more complicated disulfide connectivities, suggesting the need for a dedicated IMS disulfide isomerase [33, 34]. Mia40 is unlikely to be this isomerase due to its poor isomerase activity towards both native and non-cognate substrate s[29]. Alternately, IMS proteins containing mispaired disulfides may be corrected by IMS-resident reductases[35-37]. Further research on the IMS is needed to fully understand the mechanism of oxidative folding is that critical compartment.

### **1.1.7 Chloroplasts**

The chloroplast is another intriguing eukaryotic organelle that is believed to have been derived from an endosymbiosis between an ancient cyanobacteria with an early eukaryotic cell [38]. Chloroplasts possess a double membrane as well as internal organelles known as thylakoid. Within the thylakoids contain both the photosynthetic and oxidative protein folding machinery [39]. The thylakoid in the chloroplast has only recently been recognized as a site of oxidative folding and as such, this system

and its oxidative folding machinery have been only partially elucidated. The chloroplast and its accompanied oxidative folding machinery is shown in the schematic in Figure 1.7.



Cytosolically-translated reduced polypeptides are imported into the thylakoid space of chloroplasts and are oxidized by the thioredoxin domain of vitamin K epoxide reductase (VKOR). Transfer of reducing equivalents through the membrane-bound VKOR domain to a bound vitamin K cofactor reoxidizes the VKOR thioredoxin domain. Isomerization of mispaired disulfides in proteins may be catalyzed by various thioredoxin and PDI analogs.

**Figure 1.7 Oxidative folding in the thylakoid space of chloroplasts.**

The formation of disulfide bonds in the thylakoid space has a dual function. First, many chloroplast proteins contain disulfides and require oxidative folding for their function. Second, photoreduction of disulfide bonds in Photosystem II (PSII)

proteins under high-light conditions deactivates PSII complexes via disulfide reduction, necessitating disulfide oxidation to restore normal PSII activity [39, 40]. Reduced unfolded peptides targeted to the thylakoid space[16] pass through three protein translocases (TOC, TIC, TAT) and are oxidized by the integral membrane Vitamin K epoxide reductase (VKOR, red, Figure 1.7). Chloroplast VKOR is a dual domain protein containing a transmembrane domain with a vitamin K binding pocket, an internal redox active disulfide and a C-terminal thioredoxin-like domain. VKOR accepts electrons from substrates via the substrate interacting thioredoxin-like domain's surface-exposed redox active disulfide. Transfer of electrons from the thioredoxin domain to the internal disulfide and finally to the final electron acceptor, vitamin K (purple, Figure 1.7), recycles the catalyst. Isomerization in the thylakoid space has been proposed to be carried out by PDI-like thiol isomerases (blue, Figure 1.7) [41]. In higher plants, such as Arabidopsis, gene duplication and diversification of thioredoxin (orange, Figure 1.7) and glutaredoxin domain proteins have resulted in the identification of 10 nuclear genes that encode for five chloroplast resident Trx subtypes. Some of these thylakoid resident chloroplast thioredoxin proteins have been identified to regulate disulfide bonds in thylakoid space, where they participate in both the reduction and isomerization of disulfide bonds[42].

In this Dissertation, the consequences of thiol chemistry and oxidative folding on biology will be explored and detailed in two mammalian systems: the endoplasmic reticulum and the mitochondria. The interplay between the ubiquitous thiol containing cellular glutathione pool and protein disulfide isomerase will be discussed and explored in detail in Chapter 2. The substrate specificity of the thiol oxidoreductase Mia40 is experimentally explored, and consequences on mitochondrial protein

trafficking is discussed in Chapter 3. Finally, in Chapter 4, thiol chemistry is utilized in the design of two novel flavoprotein-GFP fusion probes which represent a new approach to intracellular probe design and allows access to more analytes that are currently measurable.

## REFERENCES

1. Hartl, F.U., A. Bracher, and M. Hayer-Hartl, *Molecular chaperones in protein folding and proteostasis*. Nature, 2011. **475**(7356): p. 324-32.
2. Anfinsen, C.B., *Principles that Govern the Folding of Protein Chains*. Science, 1973. **181**: p. 223-230.
3. Prabakaran, S., et al., *Post-translational modification: nature's escape from genetic imprisonment and the basis for dynamic information encoding*. Wiley Interdiscip Rev Syst Biol Med, 2012. **4**(6): p. 565-83.
4. Fass, D. and C. Thorpe, *Chemistry and Enzymology of Disulfide Cross-Linking in Proteins*. Chem Rev, 2017.
5. Anfinsen, C.B., et al., *The kinetics of formation of native ribonuclease during oxidation of the reduced polypeptide chain*. Proc Natl Acad Sci U S A, 1961. **47**: p. 1309-14.
6. Winterbourn, C.C., *Reconciling the chemistry and biology of reactive oxygen species*. Nat Chem Biol, 2008. **4**(5): p. 278-86.
7. Munday, R., C.M. Munday, and C.C. Winterbourn, *Inhibition of copper-catalyzed cysteine oxidation by nanomolar concentrations of iron salts*. Free Radic Biol Med, 2004. **36**(6): p. 757-64.
8. Hudson, D.A., S.A. Gannon, and C. Thorpe, *Oxidative protein folding: from thiol-disulfide exchange reactions to the redox poise of the endoplasmic reticulum*. Free Radic Biol Med, 2015. **80**: p. 171-82.
9. Herrmann, J.M., F. Kauff, and H.E. Neuhaus, *Thiol oxidation in bacteria, mitochondria and chloroplasts: common principles but three unrelated machineries?* Biochim Biophys Acta, 2009. **1793**(1): p. 71-7.
10. Bardwell, J.C., K. McGovern, and J. Beckwith, *Identification of a protein required for disulfide bond formation in vivo*. Cell, 1991. **67**(3): p. 581-9.
11. Kadokura, H. and J. Beckwith, *Mechanisms of oxidative protein folding in the bacterial cell envelope*. Antioxid Redox Signal, 2010. **13**(8): p. 1231-46.

12. Zapun, A., J.C. Bardwell, and T.E. Creighton, *The reactive and destabilizing disulfide bond of DsbA, a protein required for protein disulfide bond formation in vivo*. *Biochemistry*, 1993. **32**(19): p. 5083-92.
13. Hatahet, F., D. Boyd, and J. Beckwith, *Disulfide bond formation in prokaryotes: history, diversity and design*. *Biochim Biophys Acta*, 2014. **1844**(8): p. 1402-14.
14. Reardon-Robinson, M.E. and H. Ton-That, *Disulfide-Bond-Forming Pathways in Gram-Positive Bacteria*. *J Bacteriol*, 2015. **198**(5): p. 746-54.
15. Mallick, P., et al., *Genomic evidence that the intracellular proteins of archaeal microbes contain disulfide bonds*. *Proc Natl Acad Sci U S A*, 2002. **99**(15): p. 9679-84.
16. Kim, D.H. and I. Hwang, *Direct targeting of proteins from the cytosol to organelles: the ER versus endosymbiotic organelles*. *Traffic*, 2013. **14**(6): p. 613-21.
17. Dudek, J., P. Rehling, and M. van der Laan, *Mitochondrial protein import: common principles and physiological networks*. *Biochimica et biophysica acta*, 2013. **1833**(2): p. 274-85.
18. Wilkinson, B. and H.F. Gilbert, *Protein disulfide isomerase*. *Biochimica Et Biophysica Acta-Proteins and Proteomics*, 2004. **1699**(1-2): p. 35-44.
19. Glick, B.S. and A. Nakano, *Membrane traffic within the Golgi apparatus*. *Annu Rev Cell Dev Biol*, 2009. **25**: p. 113-32.
20. Teasdale, R.D. and M.R. Jackson, *Signal-mediated sorting of membrane proteins between the endoplasmic reticulum and the golgi apparatus*. *Annu Rev Cell Dev Biol*, 1996. **12**: p. 27-54.
21. Ilani, T., et al., *A secreted disulfide catalyst controls extracellular matrix composition and function*. *Science*, 2013. **341**(6141): p. 74-6.
22. Israel, B.A., et al., *Disulfide bond generation in mammalian blood serum: detection and purification of quiescin-sulfhydryl oxidase*. *Free Radic Biol Med*, 2014. **69**: p. 129-35.
23. Thorpe, C., et al., *Sulfhydryl oxidases: emerging catalysts of protein disulfide bond formation in eukaryotes*. *Arch Biochem Biophys*, 2002. **405**(1): p. 1-12.

24. Kodali, V.K. and C. Thorpe, *Quiescin sulfhydryl oxidase from Trypanosoma brucei: catalytic activity and mechanism of a QSOX family member with a single thioredoxin domain*. *Biochemistry*, 2010. **49**(9): p. 2075-85.
25. Banci, L., et al., *MIA40 is an oxidoreductase that catalyzes oxidative protein folding in mitochondria*. *Nat Struct Mol Biol*, 2009. **16**(2): p. 198-206.
26. Sideris, D.P., et al., *A novel intermembrane space-targeting signal docks cysteines onto Mia40 during mitochondrial oxidative folding*. *Journal of Cell Biology*, 2009. **187**(7): p. 1007-1022.
27. Banci, L., et al., *Molecular chaperone function of Mia40 triggers consecutive induced folding steps of the substrate in mitochondrial protein import*. *Proceedings of the National Academy of Sciences of the United States of America*, 2010. **107**(47): p. 20190-5.
28. Milenkovic, D., et al., *Identification of the Signal Directing Tim9 and Tim10 into the Intermembrane Space of Mitochondria*. *Molecular Biology of the Cell*, 2009. **20**(10): p. 2530-2539.
29. Hudson, D.A. and C. Thorpe, *Mia40 is a facile oxidant of unfolded reduced proteins but shows minimal isomerase activity*. *Arch Biochem Biophys*, 2015. **579**: p. 1-7.
30. Lisowsky, T., *Dual function of a new nuclear gene for oxidative phosphorylation and vegetative growth in yeast*. *Mol Gen Genet*, 1992. **232**(1): p. 58-64.
31. Eckers, E., et al., *Divergent molecular evolution of the mitochondrial sulfhydryl:cytochrome C oxidoreductase Erv in opisthokonts and parasitic protists*. *J Biol Chem*, 2013. **288**(4): p. 2676-88.
32. Basu, S., et al., *Divergence of Erv1-associated mitochondrial import and export pathways in trypanosomes and anaerobic protists*. *Eukaryot Cell*, 2013. **12**(2): p. 343-55.
33. Nuebel, E., P. Manganas, and K. Tokatlidis, *Orphan proteins of unknown function in the mitochondrial intermembrane space proteome: New pathways and metabolic cross-talk*. *Biochim Biophys Acta*, 2016. **1863**(11): p. 2613-2623.
34. Hung, V., et al., *Proteomic mapping of the human mitochondrial intermembrane space in live cells via ratiometric APEX tagging*. *Mol Cell*, 2014. **55**(2): p. 332-41.

35. Vogtle, F.N., et al., *Intermembrane space proteome of yeast mitochondria*. Mol Cell Proteomics, 2012. **11**(12): p. 1840-52.
36. Kojer, K., et al., *Kinetic control by limiting glutaredoxin amounts enables thiol oxidation in the reducing mitochondrial intermembrane space*. Molecular Biology of the Cell, 2015. **26**(2): p. 195-204.
37. Cardenas-Rodriguez, M. and K. Tokatlidis, *Cytosolic redox components regulate protein homeostasis via additional localisation in the mitochondrial intermembrane space*. FEBS Lett, 2017. **591**(17): p. 2661-2670.
38. Jensen, P.E. and D. Leister, *Chloroplast evolution, structure and functions*. F1000Prime Rep, 2014. **6**: p. 40.
39. Kieselbach, T., *Oxidative folding in chloroplasts*. Antioxid Redox Signal, 2013. **19**(1): p. 72-82.
40. Jarvi, S., M. Suorsa, and E.M. Aro, *Photosystem II repair in plant chloroplasts--Regulation, assisting proteins and shared components with photosystem II biogenesis*. Biochim Biophys Acta, 2015. **1847**(9): p. 900-9.
41. Onda, Y., *Oxidative protein-folding systems in plant cells*. Int J Cell Biol, 2013. **2013**: p. 585431.
42. Yoshida, K. and T. Hisabori, *Distinct electron transfer from ferredoxin-thioredoxin reductase to multiple thioredoxin isoforms in chloroplasts*. Biochemical Journal, 2017. **474**(8): p. 1347-1360.

## Chapter 2

# OXIDATIVE PROTEIN FOLDING: FROM THIOL-DISULFIDE EXCHANGE REACTIONS TO THE REDOX POISE OF THE ENDOPLASMIC RETICULUM

### 2.1 Introduction

Understanding the mechanisms by which disulfide bonds are both inserted and isomerized during oxidative protein folding remains a significant intellectual challenge some 50 years after the classic studies of Anfinsen and colleagues on the refolding of reduced ribonuclease A (RNase) [1]. Indeed, while the disulfide bond is one of the most recognized forms of post-translational modification, fundamental aspects of oxidative folding remain unclear. For example, why such a proliferation of cellular strategies for the formation of disulfides in higher eukaryotes? How can these various pathways operate with the prevailing concentrations of reduced glutathione (GSH) in mammalian cells, and how can futile cycles between them be avoided? Finally, how is the choreography between folding and disulfide generation managed from one protein to the next?

There have been a number of recent comprehensive reviews dealing with oxidative protein folding in a variety of organisms and cellular locales (e.g. see [2-8]). In this Chapter we principally address disulfide bond generation within the secretory apparatus of animal cells, while acknowledging the major contributions from complementary studies on yeast [9-11]. Rather than presenting a detailed account of the discovery and characteristics of the various catalysts of disulfide bond generation,

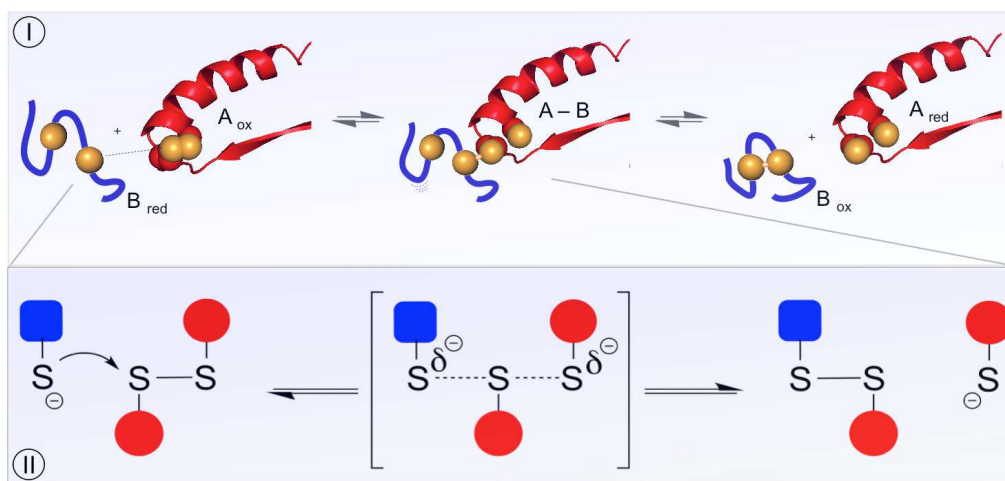
we will focus on conceptual issues and future challenges that seem relevant to a deeper understanding of oxidative protein folding within the mammalian secretory apparatus. We will first briefly address key biochemical aspects of thiol-disulfide exchange reactions. Recognized actors in various oxidative folding pathways in the mammalian endoplasmic reticulum (ER) will then be introduced. We then discuss the role of redox poise in the ER from the perspective of two major participants: the small molecule glutathione, and oxidoreductases of the protein disulfide isomerase (PDI) family. We recount methodological advances in the estimation of glutathione and PDI redox states in the ER and discuss issues with their implementation. The likelihood of redox equilibration between glutathione and PDI-family members will be discussed and whether equilibration could be reconciled with the efficient generation of disulfides in the ER. Finally we propose an expanded toolbox of methods to complement the continuous fluorescent probes that have so transformed the field of redox biology.

## **2.2 Chemical Aspects of Thiol-Exchange Reactions**

Thiol-disulfide exchange reactions are central to oxidative protein folding and key to the mechanism of almost all enzymes that generate and isomerize disulfide bonds [3, 12-14]. During the successful folding of a protein with multiple disulfide bonds an intensive iteration of disulfide exchanges precedes the emergence of the native fold (see later). Thiol-disulfide exchange reactions are initiated by the nucleophilic attack of a thiolate on a disulfide (Figure 2.1, Panel I). The thiolate is some  $10^{10}$  – fold more reactive than its corresponding thiol form [13, 14]. The relationship between thiol pK values and the intrinsic nucleophilicity of their thiolates is described elsewhere [13, 14]. An important and still under-appreciated aspect of

thiol-disulfide reactions is illustrated in Panel II. The attacking thiolate approaches along the disulfide axis and this requirement for colinearity establishes the orientation necessary for interactions between well-structured redox partners [14-18]. Thus disulfide exchange reactions have significant steric requirements that must be accommodated by the enzymes catalyzing oxidative protein folding. Additionally,

these



stringent requirements impact the rates by which disulfides can be reduced and rearranged non-enzymatically.

Panel I illustrates reduction of a CxxC disulfide motif in A<sub>ox</sub> by an unstructured reduced peptide dithiol (B<sub>red</sub>; blue). Generation of the mixed-disulfide intermediate A-B involves an in-line transition state as depicted in the detail shown in Panel II.

**Figure 2.1: Mechanistic aspects of thiol-disulfide exchange reactions.**

A second nucleophilic attack in Figure 2.1, Panel I, discharges the mixed disulfide (providing that the resolving thiolate can approach in line) yielding a net redox reaction whose equilibrium constant is give by:

$$K = \frac{[A_{red}][B_{ox}]}{[A_{ox}][B_{red}]}$$

The magnitude of this equilibrium constant depends on which of the blue or red couples in Panel I is the stronger thermodynamic reductant. Several comprehensive reviews detail the application of the Nernst equation to thiol-disulfide equilibria (e.g. [19, 20]); the redox potential of a couple, E, is related to E<sup>°</sup>, the corresponding value under standard conditions via:

$$E = E^{\circ} - \left( \frac{2.303RT}{nF} \right) \log_{10} \frac{[red]}{[ox]}$$

The collected terms in parenthesis correspond to about a -30 mV change in the redox potential for every 10-fold increase in the ratio of [red]/[ox] for a particular 2-electron redox couple at 25 °C.

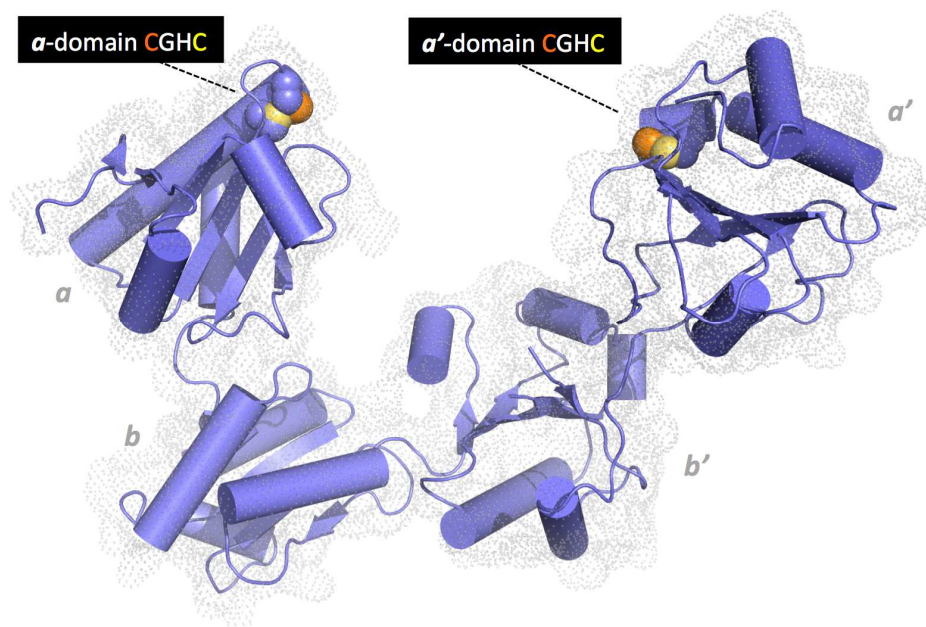
It is important to note that while the difference in standard redox potentials between the couples in Figure 2.1 dictate the overall equilibrium constant between reactants and products, such information provides no guidance concerning the rate of this equilibration; the steric requirements for disulfide-exchange reactions may impose

effective kinetic barriers preventing facile reactions between species that might be expected to react on thermodynamic grounds. Conversely, even if the reaction is thermodynamically far uphill - when products (**A<sub>red</sub>** and **B<sub>ox</sub>**) are strongly disfavored with respect to reactants (**A<sub>ox</sub>** and **B<sub>red</sub>**) the **A-B** mixed-disulfide intermediate that forms between the reactants might be very stable thermodynamically [21]. Obviously, arguments based on thermodynamics and redox potentials need to be applied with an appreciation of their limitations. A significant issue in this Chapter is whether equilibrium conditions prevail between any of the thiol-disulfide couples in the secretory apparatus.

### **2.2.1 Oxidative Protein Folding --- Enzymes and Oxidants**

Oxidative protein folding comprises two conceptually separate stages. The first represents the net generation of disulfide bonds; each disulfide bond generated from a pair of thiols involves the removal of a pair of electrons. Since disulfides are frequently major determinants in the stability of secreted proteins [22] the insertion of disulfides linkages, particularly in early phases of oxidative folding where conformations resembling the native fold are likely to be poorly populated, is generally error-prone. Hence the second aspect of oxidative protein folding is the rearrangement of disulfide bonds via PDI enzymes. A strong case can be made that the isomerization of mispaired disulfide bonds is the linchpin of oxidative folding. In comparison, the net generation of disulfides is chemically much less demanding - from the inorganic oxidants that can be used *in vitro* (e.g. molecular iodine, ferricyanide, tetrathionate and hydrogen peroxide; [23, 24]) to the small molecule and enzymatic oxidants that contribute to disulfide formation *in vivo* (see later). The multiplicity of enzymes with PDI activity in various cell types perhaps speaks to the specialization of

these catalysts for particular client types. There are about 20 proteins in the human PDI-family containing up to 5 thioredoxin domains and from 0-4 redox-active CxxC motifs [3, 25, 26]. A crystal structure of P4HB (hereinafter abbreviated PDI) is shown in Figure 2.2 [27]. PDI comprises 4 thioredoxin domain with the outer *a* and *a'* domains carrying CxxC motifs. The first sulfur of each motif is comparatively solvent-accessible whereas its redox partner is buried behind it towards the core of the domain (Figure 2.2). The redox inactive *b'* domain serves an important role in binding unstructured protein substrates [3, 28].

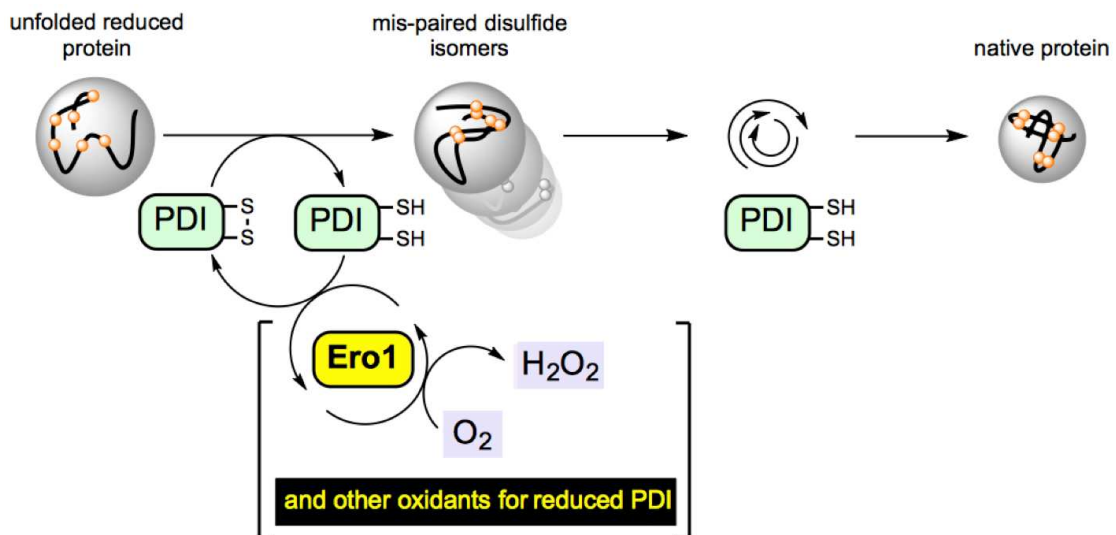


The coordinates for the oxidized protein are from Wang et al. [27]. Redox-active CxxC motifs are found in both *a* and *a'* domains. The N-terminal cysteine sulfur atom of each motif (orange) is solvent accessible and engages in mixed disulfides with redox partners and proteins undergoing disulfide editing. The C-terminal cysteine by contrast is largely buried from solvent (yellow). The *b* and *b'* domains are redox-

inactive. Protein clients of PDI can occupy the central cavity with significant hydrophobic interactions with the b' domain.

**Figure 2.2: Structure of human PDI.**

In many pathways for oxidative folding in the ER PDI is intimately involved in both the initial oxidation of client proteins and in the isomerization steps that are critical to correct mispairings. We will describe these as *PDI-first* pathways to distinguish them from *PDI-second* pathways (in which PDI's role is confined to the isomerization phase of oxidative folding). One PDI-first pathway is depicted in Figure 2.3. It should be noted at the outset that while oxidation and isomerization steps are depicted sequentially, the isomerase activity is likely engaged early in the oxidation phase to avoid the kinetic penalty associated with the accumulation of a concatenation of mispaired disulfides within a client protein.



In the first phase the unfolded reduced protein is oxidized by PDI<sub>ox</sub>. Here, reduced PDI is regenerated by the FAD-linked sulfhydryl oxidase, Ero1, with the formation of

hydrogen peroxide. PDI<sub>red</sub> is then involved in correction of mispaired disulfides prior to the iterative emergence of the native protein fold.

**Figure 2.3: An example of a PDI-first pathway in oxidative protein folding.**

The PDI<sub>red</sub> generated upon oxidation of any given substrate dithiol in Figure 2.3 is recycled by Ero1-family proteins [9, 10, 29-33] with flavin-mediated transfer of a pair of electrons to molecular oxygen to yield hydrogen peroxide [34]. (Note that PDI<sub>red</sub> has negligible direct reactivity towards molecular oxygen and hence should never be described as an “oxidase”, or even a protein with “oxidase activity”. PDI is an oxidoreductase; the term oxidase is reserved for enzymes that oxidize substrates with the direct reduction of dioxygen to hydrogen peroxide [35]). Ero1p was first discovered as an essential protein in yeast [9, 10] and later two mammalian isoforms Ero1 $\alpha$  and Ero1 $\beta$  were uncovered and subjected to detailed cell biological and biochemical scrutiny [29, 31-33, 36]. The general assumption that the mammalian Ero1 oxidases would prove essential in mammals was found to require reexamination as the result of an important study from the Ron laboratory [37]. The mild phenotype associated with the simultaneous ablation of both  $\alpha$ - and  $\beta$ - isoforms [37] invigorated the search for other pathways for disulfide bond generation. Zito et al. [38] and Bulleid and coworkers [39] delineated pathways for the hydrogen peroxide-driven oxidation of PDI<sub>red</sub> catalyzed by peroxiredoxin 4 (PRDX4; Figure 2.4) [7, 8, 40]. Ruddock and colleagues described glutathione peroxidase 7 and 8 (PDI peroxidases) as a further means to the reoxidation of PDI<sub>red</sub> [41]. Rapoport and coworkers showed that vitamin K epoxide reductase provides yet another pathway for oxidative protein folding in the mammalian ER [42]. In addition to these enzymatic routes for the regeneration of PDI<sub>ox</sub>, a number of small molecule oxidants for unfolded reduced

proteins have been described (Figure 2.4). Oxidized glutathione (GSSG) was regarded for decades as an immediate oxidant for protein thiols, including PDI<sub>red</sub>, in the ER (reviewed in [20, 43]). More recently dehydroascorbate [44] and hydrogen peroxide [45] have also been described as candidate oxidants in the ER ([43, 46]).

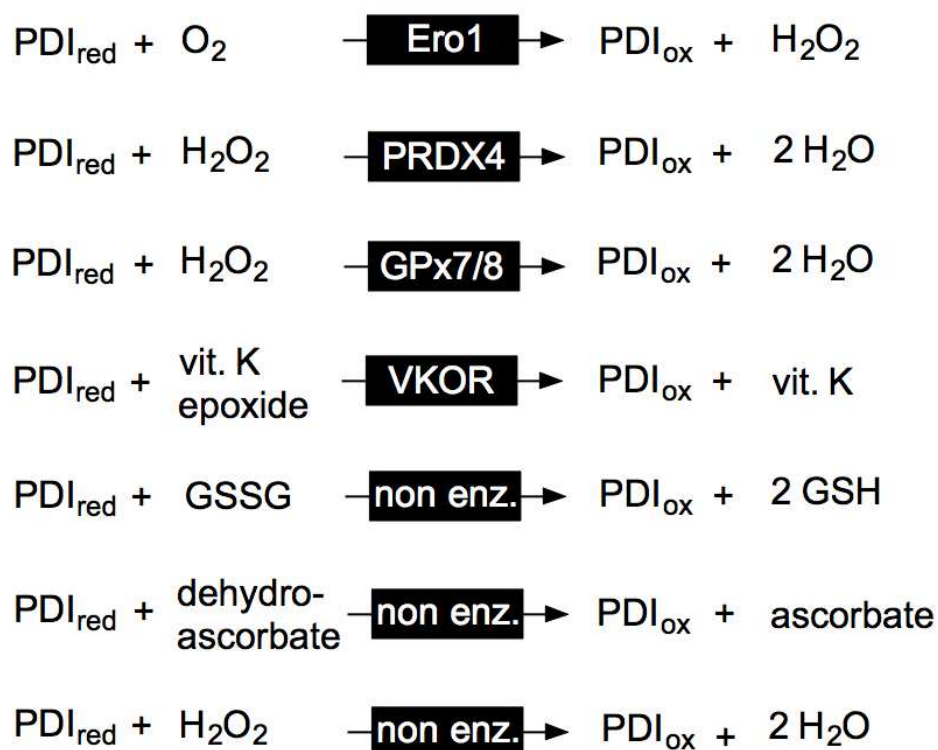
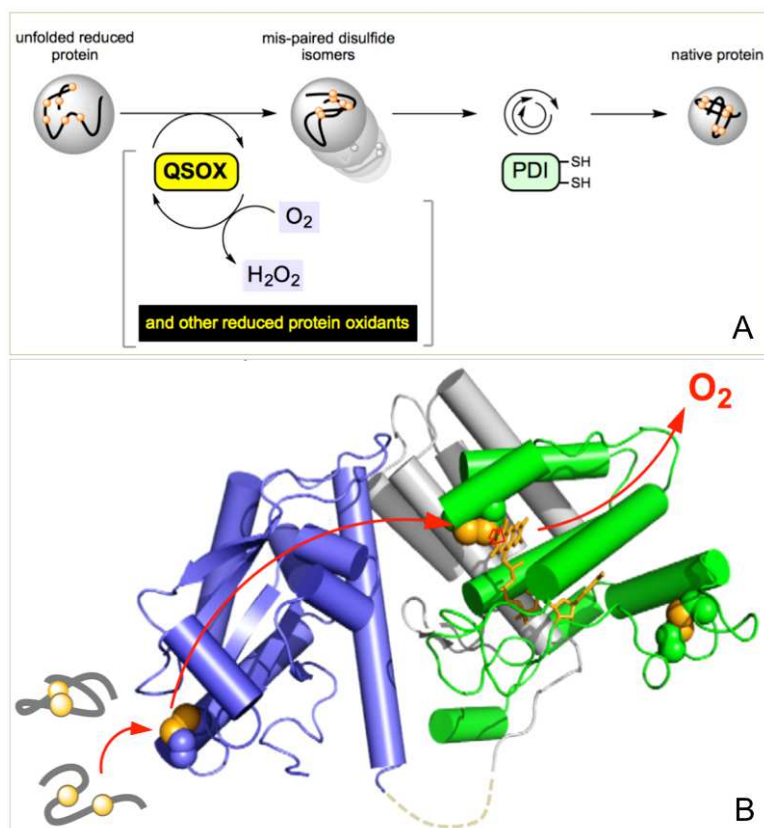


**Figure 2.4: Some enzymatic and non-enzymatic oxidants for reduced PDI.**

## 2.1 PDI – Second Pathways

The small molecules listed in Figure 2.4 represent relatively non-specific oxidants of both protein and non-protein thiols. Hence, to the extent that GSSG, dehydroascorbate and hydrogen peroxide oxidize unfolded proteins directly, they can contribute to PDI-second routes to oxidative folding. However, there is one class of

enzymes that is capable of directly oxidizing unfolded reduced peptides and proteins without significant collateral oxidation of PDI<sub>red</sub> [4, 17, 47-49]. Figure 2.5A shows that members of the Quiescin-sulfhydryl oxidase (QSOX) family of proteins transfer reducing equivalents from client protein dithiols directly to molecular oxygen. QSOX enzymes represent an intriguing amalgamation of PDI-like thioredoxin domains with helix-rich domains of the ERV family (Figure 2.5B) [4, 48, 50-52]. Later we show that efficient oxidative folding can occur when QSOX is the sole oxidant of client proteins and reduced PDI is confined to a role as an isomerization catalyst. These observations provide important perspective regarding the versatility and flexibility of pathways for oxidative folding (see later).

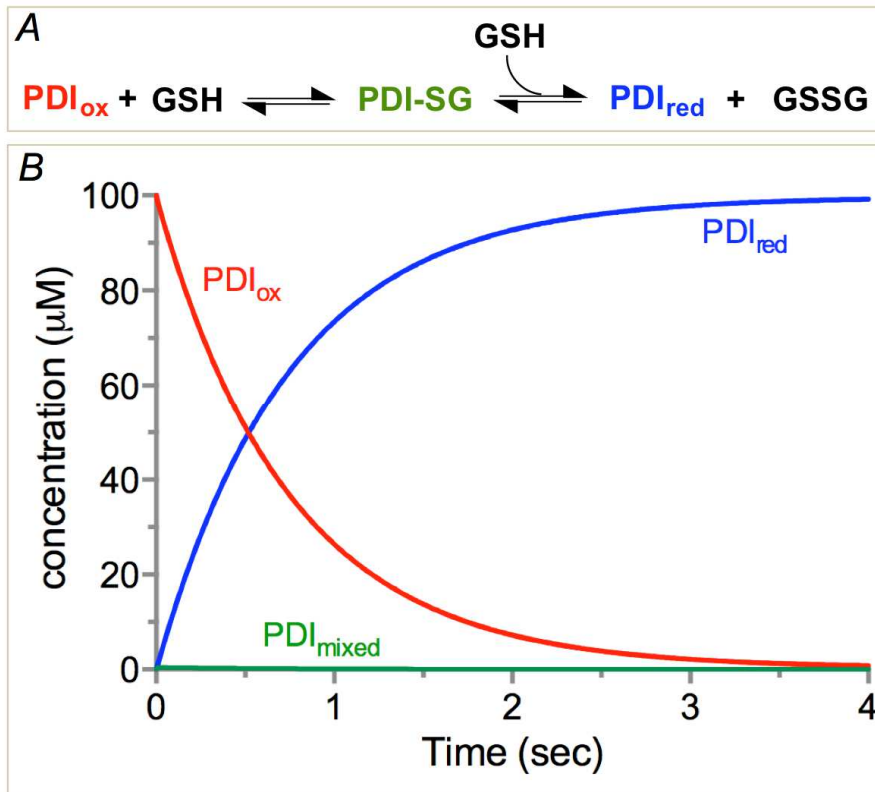


The initial oxidation of reduced proteins is PDI-independent so that PDI is only engaged in the second phase of oxidative protein folding (Panel A). One facile direct oxidant of reduced conformationally-mobile proteins is Quiescin-sulphydryl oxidase. Panel B shows the structure of the open form of QSOX from *Trypanosoma brucei* (3QCP; [52]).

**Figure 2.5: PDI-second pathways of oxidative folding.**

## 2.2 PDI and Glutathione Interaction Kinetics

Three redox systems that likely exert a strong influence on the redox poise within the ER are mentioned here. Glutathione is widely reported to be present at an aggregate concentration (reduced plus oxidized) of  $\sim 10$  mM [53] with even higher concentrations proposed recently [54]. Mammalian PDI is a very abundant largely ER-resident protein with concentrations of perhaps up to 1 mM in certain cell types [3, 55]. The multiplicity of PDI family members will markedly inflate the total concentration of PDI-like thioredoxin domains in the ER. For example, in HEK293T and HeLa cells the concentrations of PDI, ERp57, ERp72, and P5 were approximately comparable [56]. Finally, the ER of professional secretory cells may contain high concentrations of reduced and partially oxidized proteins in transit. While all these species contribute to the overall thiol-disulfide redox poise of the ER, we focus here on the interplay between the glutathione and PDI systems. Thus, how fast does glutathione react with PDI, and do measurements of the concentrations of GSH and GSSG when compared with the ratio of  $\text{PDI}_{\text{red}}:\text{PDI}_{\text{ox}}$  suggest that these couples are in equilibrium in the ER? This discussion is largely focused on PDI since it is the best characterized representative of the mammalian PDI-family from both enzymological and cell biological aspects.



The model and rate constants of Darby and Creighton [57] were used for the *a* domain of human PDI reduced with glutathione (Panel A). Panel B shows the time course for oxidized, reduced and mixed disulfide forms of the single CxxC motif using 100  $\mu\text{M}$  PDI and 5 mM GSH [58]. Under these conditions the half-time for equilibration is 0.52 sec;  $t_{1/2}$  values for 2.5 mM and 10 mM GSH are 1.12 and 0.25 sec respectively.

**Figure 2.6: Reduction of PDI by GSH.**

The classic studies of Darby and Creighton measured the rate constants for the interaction between the isolated *a* and *a'* domains of human PDI in both reductive and oxidative directions using rapid mixing experiments [57]. Their studies suggested that PDI and glutathione could equilibrate with those concentrations of reduced and oxidized glutathione likely to prevail in the ER (see later) with sub-second half-times at pH 7.4 and 25 °C. A reinvestigation and extension of these studies by Lappi et al.

reported comparable rate constants for the reduction of the PDI<sub>ox</sub> *a* domain in the context of a full-length protein whose *a'* domain was disabled by mutations to the CxxC motif [59]. This is to be expected because the *a* and *a'* domains in human PDI seem to have very similar chemical reactivities and redox potentials (see later). To provide a graphic depiction of the reduction of PDI by 5 mM glutathione, the rate constants for the isolated *a* domain [58] were used to simulate the reaction in Figure 2.6A. Reduction shows a half-time of 0.52 sec under these conditions with minimal glutathione mixed disulfide accumulation during this simulation (Figure 2.6B).

This rather rapid equilibration poses interesting issues for PDI-first pathways of oxidative protein folding in the ER. Thus the generally abundant GSH could compete with unfolded reduced proteins for PDI<sub>ox</sub> [35]. To the extent that glutathione prevails, Ero1 would become a *de facto* glutathione oxidase. Possibly this is exactly what the cell intended such that GSH not only drives hydrogen peroxide generation but leverages a second disulfide bond formation via peroxiredoxin 4 and related pathways [7, 8, 38-41]. A series of comprehensive experiments describe the down-regulation of Ero1 activity when a regulatory disulfide is generated by PDI proteins so that overoxidation of the ER is avoided [31, 32, 60, 61]. These studies prompt an interesting question concerning the response to a decreased demand for disulfide-containing secreted proteins. Under this circumstance an increasing proportion of PDI might be reduced by GSH leading to the activation of Ero1 and an elevation of hydrogen peroxide production. The combined action of Ero1 and Prx4/peroxidases would then be expected to lead to a continuous generation of GSSG with the stoichiometry shown in Figure 2.7. The decreased luminal concentration of GSH might then stimulate ingress of cytosolic GSH via the bi-directional transporter [62].

These observations prompt a series of questions: is the ER a constitutive generator of GSSG in the absence of a heavy load of secreted proteins; what role would such a generalized loss of reducing equivalents play in the cellular energy economy; what is the fate of the accumulating impermeant GSSG under these circumstances; and do reservoirs of GSSG exist within the secretory apparatus that fulfill an analogous role to the vacuolar deposits uncovered in yeast by Dick and coworkers [63]?

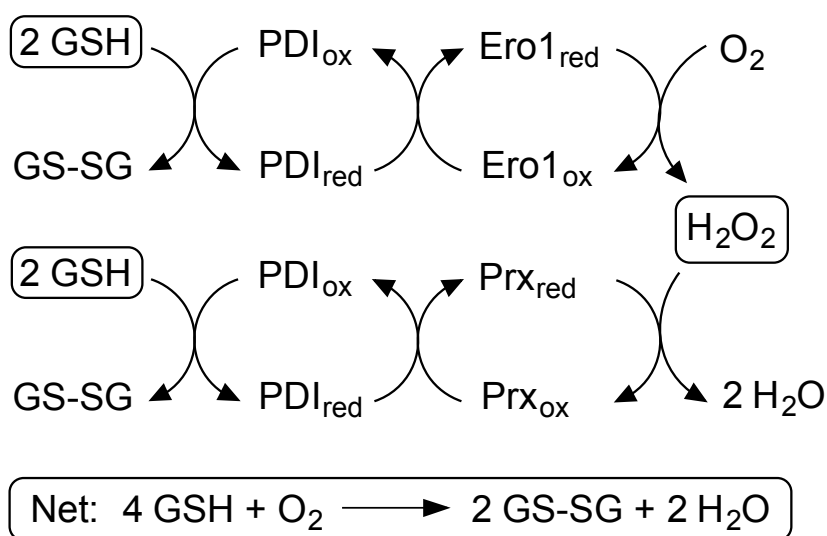


**Figure 2.7: A potential pathway for redox cycling in the ER.**

### 2.3 Preamble to Redox Poise Measurements in the Mammalian ER

As mentioned above, glutathione and PDI can rapidly equilibrate *in vitro* in a reaction that would be mostly complete in 1 sec under the conditions expected to prevail in the mammalian ER. In the following sections, we first review experimental evidence for the concentration and redox poise of intraluminal glutathione. We then describe approaches and challenges to the determination of the redox status of PDI

within the secretory apparatus. Given experimental values for glutathione and PDI, the extent to which these couples approach equilibrium can be assessed. Despite some skepticism concerning the applicability of redox potential measurements for intracellular thiol disulfide reactions involving glutathione [64] we note that the measurement of mass action ratios in cells has proved crucial in identifying the subset of steps in metabolic pathways that are far from equilibrium and thus candidates for control [65]. Hence it seems both relevant and informative to consider whether the PDI/glutathione reactions are close to equilibrium in the ER and if not, why not?

#### **2.4 ER Glutathione Redox Poise**

Hwang et al. in 1992 provided the first quantitative estimation of the redox poise within the ER [66]. Using a membrane-permeant tetrapeptide that was subsequently glycosylated within the ER, they showed that the GSH:GSSG ratio in murine hybridoma cells ranged from 1:1 to 3:1 (Table 2.1). While these studies selected the subset of peptide resident in the ER for their analyses, later work (entries 2 and 3) determined the glutathione status of isolated microsomes by an initial alkylation with monobromobimane [67] or by acid treatment followed by conjugation with dansyl chloride [68]. Isolation of microsomes is associated with two potential complications that might lead to an overestimation of the oxidized status of the ER [54]. The first is the loss of GSH, but not GSSG, from microsomes via a bi-directional transport system [62]; a second is the tendency of the luminal contents to undergo enzyme-mediated oxidation prior to analysis [68]. As detailed earlier [3, 19, 20] the conversion of the ratio of GSH:GSSG deduced from the measurements in entries 1-3 to redox potentials requires knowledge of the net concentration of glutathione within the ER lumen. This is because the monothiol GSH appears as a

squared term ( $[GSH]^2/[GSSG]$ ) in the Nernst equation. Here we have assumed a total luminal glutathione concentration ( $[GSH] + 2[GSSG]$ ) of 10 mM to allow a comparison between the range of entries in Table 2.1. In another approach (entry 4) Montero et al. used a single cysteine glutaredoxin to deduce a GSH:GSSG ratio of <7:1 in HeLa cells [54]. In summary, entries 1-4 predict a redox potential for the ER luminal pool of between about -160 to -200 mV (assuming an aggregate 10 mM glutathione concentration).

The landmark studies of Winther and colleagues introduced a redox-active disulfide bond within a yellow fluorescent variant of GFP (rxYFP) such that the fluorescence was responsive to thiol redox state [69]. Subsequently they fused rxYFP to glutaredoxin to make the probe communicate more specifically and rapidly with glutathione [70]. Remington, Tsien and their coworkers developed a ratiometric GFP probe (roGFP) [71] and variants of this construct have proved useful in interrogating the relatively oxidizing environment of the secretory system. Use of these probes in a range of cultured cell types yield the values shown in entries 5, 7 and 8 (Table 2.1). A value of -231 mV (entry 5) was obtained by Bulleid and colleagues using roGFP1iL expressed in the ER of human fibroblast cells [72]. A similar probe fused to glutaredoxin used by Appenzeller-Herzog, Dick and their colleagues (entry 8) gave a redox potential of -208 mV in the ER of HeLa cells [73]. Ron and colleagues monitored the change in fluorescent lifetime (rather than ratiometric fluorescence intensity) between oxidized and reduced forms of roGFP1iE [74]. They obtained a redox poise for the ER lumen in a pancreatic acinar cell line of -236 mV (Table 2.1, entry 7). While entries 5, 7 and 8 reflect the use of different cell types and methodologies, they yield rather comparable redox potentials averaging – 225 mV. In

contrast, a probe designed by Kolossov and colleagues exploits changes in FRET between enhanced versions of CYP and YFP fused via a cysteine-containing linker region. The construct was records an extremely oxidizing potential of -118 mV in CHO cells (entry 6; [75]). It appears that this probe is responding to redox components within the ER that are not in effective communication with the glutathione redox pool [73] and so we will not consider it further here.

**Table 2.1: Measurement of glutathione redox state in the mammalian ER.**

| Entry | Biological Sample               | Method                      | GSH:GSSG       | Reported redox potential | Adjusted Value  | Year/Reference |
|-------|---------------------------------|-----------------------------|----------------|--------------------------|-----------------|----------------|
| 1     | Murine hybridoma CRL1606 cells  | ER targeted peptide         | 1:1 to 3:1     | -170 to 185 mV (8 mM)    | -164 to -186 mV | 1992/[66]      |
| 2     | Rat liver microsomes            | Microsomal Isolation        | 3:1 to 4:1     | NR                       | -186 to -192 mV | 2004/[67]      |
| 3     | Rat liver microsomes            | Microsomal Isolation        | 4.7:1 to 5.5:1 | NR                       | -194 to -197 mV | 2008/[68]      |
| 4     | HeLa cells                      | sCGrx1pER probe NEM soaking | <7:1           | NR                       | >-201           | 2013/[54]      |
| 5     | Human fibroblast cells (HT1080) | roGFP1iL                    | NR             | -231 mV                  | NA              | 2011/[72]      |
| 6     | CHO cells                       | CY_RL7 fluorescent probe    | NR             | -118 mV                  | NA              | 2012/[75]      |
| 7     | pancreatic acinar cells (AR42j) | roGFP1iE                    | NR             | -236 mV                  | NA              | 2013/[74]      |
| 8     | HeLa cells                      | Grx1_roGFP1iE               | NR             | -208 mV                  | NA              | 2013/[73]      |

Since the redox potential of glutathione buffers depends on the  $[GSH]^2/GSSG$  term, they are dependent on absolute concentration (see the Text). For the purposes of comparison, these values assume a total glutathione concentration (GSH + 2 GSSG) of 10 mM. At a ratio of GSH:GSSG of 3:1 the redox potential would be -186 mV; lower aggregate concentrations of 7.5 and 5 mM glutathione would yield somewhat more positive redox potentials of -182 mV and -177 mV respectively. We have arbitrarily used 10 mM total glutathione to present a comparison with the redox potentials reported for the fluorescent probes entries 5-7.

Assuming that the non-FRET probes are in equilibrium with glutathione pools within the ER, an average potential of -225 mV would predict a GSH:GSSG ratio of 35:1 (using the standard redox potential for glutathione of -240 mV [12], and an aggregate glutathione concentration of 10 mM). In contrast, the experimentally reported values in entries 1-3 in Table 2.1 are considerably more oxidizing (with GSH:GSSG ratios between 1:1 to 5.5:1). In view of the significant experimental difficulties in accurately assessing intraluminal GSH and GSSG concentrations, the fluorescent probes in entries 5, 7 and 8 (Table 2.1) appear to provide the best current measures of redox poise. These probes respond rapidly to glutathione and they report directly from the ER lumen of live cells.

## **2.5 Redox State of PDI in the Mammalian ER**

A redox poise of -225 mV for glutathione in the ER corresponds to a predicted ratio of ~90:1 for PDI<sub>red</sub>:PDI<sub>ox</sub> (see later). Two main methods have been used to measure the redox state of PDI family members within the mammalian ER. The experiments described in entries 1, 2, 4 and 6 (Table 2.2) incubated intact cells with NEM to quench thiols. Subsequent quantitation of oxidized and reduced components employed gel-shift methods detected using Western blots [76]. These studies found various PDI family members to be largely reduced. Studies in HEK-293 cells (entry 4) applied a quantitative analysis procedure that allowed the percentage of each redox state of PDI to be quantified (here 67% of the CxxC motifs are reduced). A recent study (entry 7) by Inaba and colleagues, using HEK293 cells rapidly quenched in TCA showed that PDI was ~80 % reduced [77]. ERp46, ERp57, Erp72 and P5 showed levels of reduction from about 95 – 100% [77]. In contrast a protocol involving microsomal isolation prior to trapping (entry 3) found that both PDI and ERp57 were

predominantly oxidized [78]. As mentioned earlier, this divergent outcome might reflect selective loss of glutathione and/or oxidation of luminal contents of the ER.

**Table 2.2: Determination of the redox state of PDIs within the ER.**

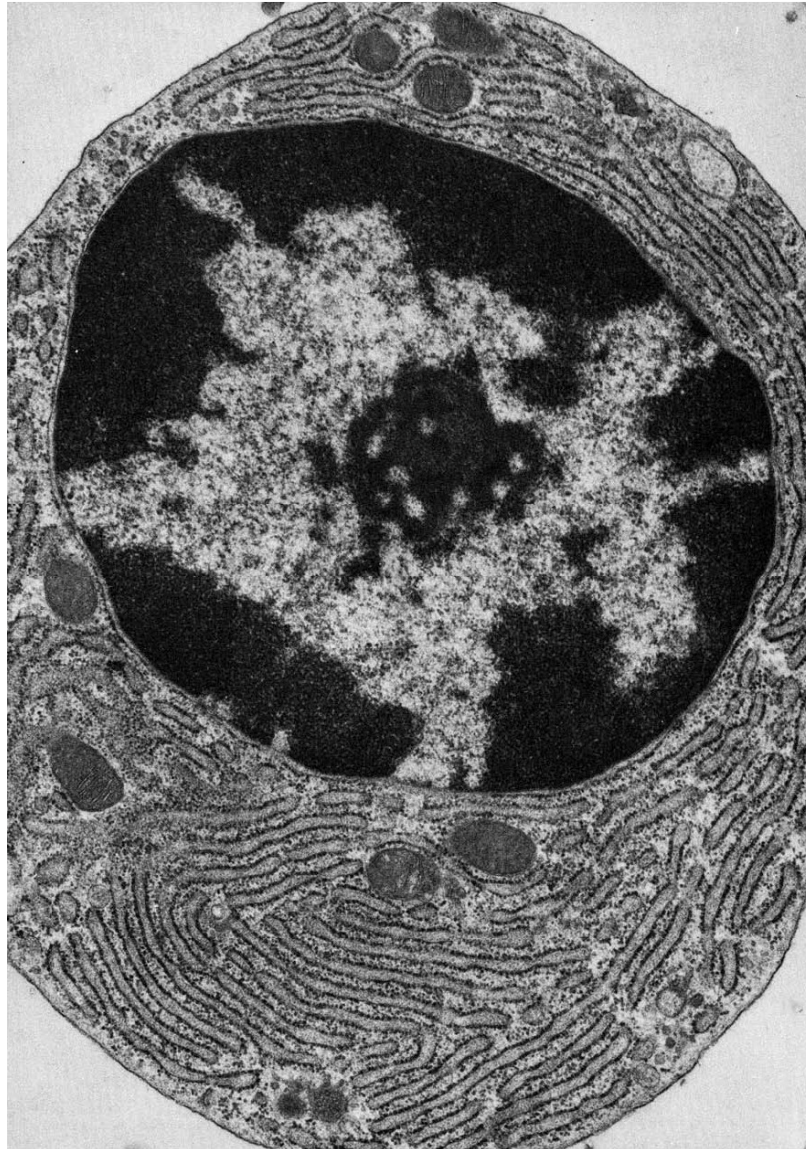
| Entry | Biological Sample     | Method                           | Protein                      | Redox State  | Year/Reference |
|-------|-----------------------|----------------------------------|------------------------------|--|----------------|
| 1     | Hela, COS, U937 cells | TCA/intact cells                 | PDI and ERp57                | Predominantly Reduced  | 2001/[79]      |
| 2     | HT1080 cells          | NEM soaking/intact cells         | PDI, ERp57, ERp72, P5, PDlr  | Predominantly Reduced  | 2004/[53]      |
| 3     | Rat Liver Microsomes  | Microsome Isolation /TCA         | PDI and ERp57                | Predominantly Oxidized   | 2005/[78]      |
| 4     | HEK-293 cells         | NEM soaking/intact cells         | PDI                          | 50% fully reduced, 18% a-oxidized, 15% a'-oxidized, and 16% fully oxidized | 2008/[80]      |
| 5     | Rat Heart Tissue      | Tissue frozen in liquid nitrogen | TMX3<br>PDI                  | Predominantly Reduced  | 2011/[81]      |
| 6     | HeLa cells            | NEM soaking/intact cells         | ERp57                        | Predominantly Reduced  | 2013/[73]      |
| 7     | HEK293                | TCA treatment intact cells       | PDI, ERp46, ERp57, P5, ERp72 | Predominately Reduced<br>0%-20%  | 2013/[77]      |

In a number of references the redox state of PDI family members was not quantified densitometrically. In most cases the overall redox state of PDI family members that carry multiple CxxC motifs is reported in aggregate, without identification of the population of redox isoforms (but see entry 4; here, the percentage of CxxC domains that are reduced totals 67%).

## 2.6 Chemical Trapping of PDI Redox State

Several pioneering early studies of the redox poise of PDI soaked live cells using NEM before application of gel-shift analyses to measure redox state. The use of

NEM was a logical choice because it reacts with thiols some thousand-fold faster than the iodoacetamide [12]. Further NEM is membrane-permeant [3, 53, 82] - although this aspect does not seem to have been quantified. Cells were typically exposed to ice-cold NEM (in a concentration range of 1- 40 mM) prior to a disruption step and the determination of redox status by gel-shift. A relevant question is how fast does trapping have to be? If PDI and glutathione were at equilibrium with a  $t_{1/2}$  of about 500 msec (Figure 2.6), then NEM quenching would need to be completed in 50 – 100 msec to accurately reflect the intraluminal redox state of this oxidoreductase.



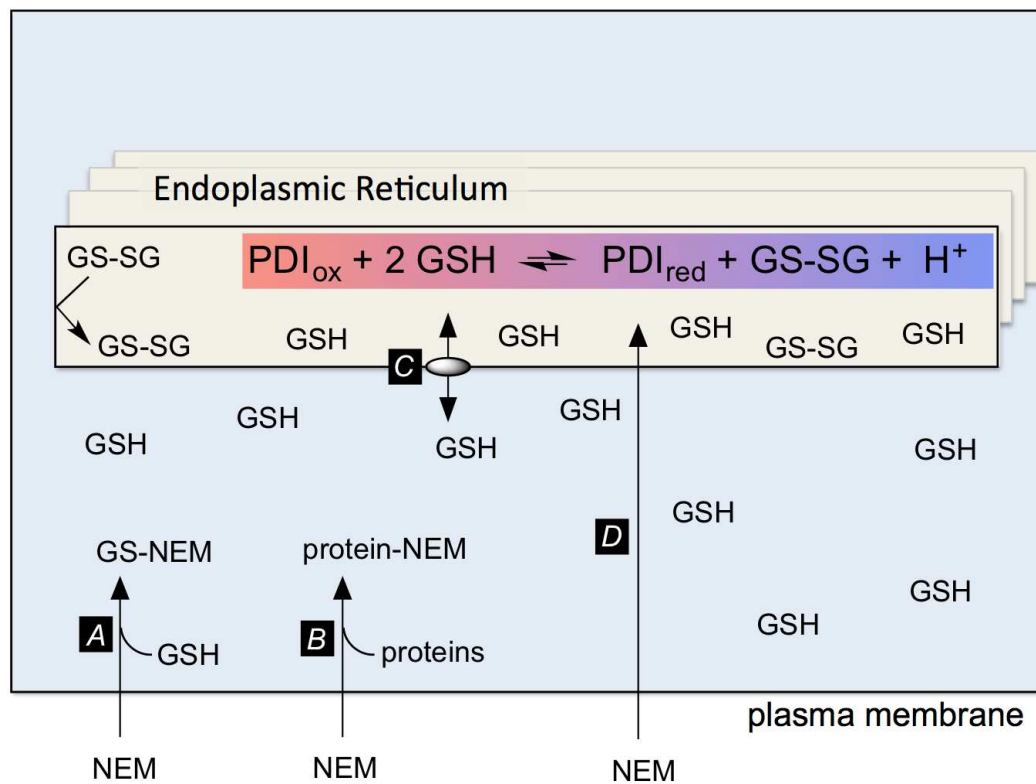
Reproduced from [83].

**Figure 2.8: Electron micrograph of a plasma cell from guinea pig bone marrow showing an extensive reticular network of ER.**

Figure 2.8 shows a micrograph to illustrate some of the cellular features that may delay quenching in an NEM soaking procedure. This professional secretory cell

contains a packed reticular network of rough ER with associated post-ER compartments including the ER-Golgi intermediate complex, cis- and trans-Golgi networks and, finally, the vesicular/granular traffic destined for the plasma membrane. During NEM-soaking protocols the quenching agent must transit not just the plasma membrane but a multiplicity of internal membranes and/or navigate a convoluted path of cytosol separating adjacent luminal sections of ER (Figure 2.8). At the outset NEM diffusing across the plasma membrane will encounter a typical cytosolic GSH concentration of 5-10 mM (Figure 2.9, arrow A) [54, 84, 85]. Since the second-order rate constant for reaction with GSH at neutral pH values is about  $10^4 \text{ M}^{-1}\text{s}^{-1}$  [12] the half-time for NEM capture under these conditions will be of the order of 10 msec. The high protein thiol content within the cytosol [85] will also delay accumulation of unmodified NEM (step B). As the depletion of cytosolic GSH continues release of ER-resident GSH (via step C) could bias the PDI/glutathione equilibrium in favor of  $\text{PDI}_{\text{ox}}$  because GSSG is reported to be impermeant [62]. Finally, as NEM gains entry to the ER by diffusion (step D) it will further deplete the level of thiols in that compartment. Which thiols are preferentially alkylated? If NEM reacts with luminal GSH faster than with  $\text{PDI}_{\text{red}}$ , this would bias the equilibrium in favor of more  $\text{PDI}_{\text{ox}}$ . However, if  $\text{PDI}_{\text{red}}$  is alkylated preferentially, then this will have the opposite effect, leading to an overestimation of  $\text{PDI}_{\text{red}}$ . These issues were recognized as potential artifacts of *in vitro* trapping protocols by Darby and Creighton decades ago [57] In the present case we are unaware of data that allows for a comparison of the bimolecular rate constants for the reaction of NEM with GSH and  $\text{PDI}_{\text{red}}$  at pH 7.4. Finally, while cooling cells on ice is often employed as part of alkylation quenching reactions, it is not immediately apparent that this will help: while a 35 °C drop in

temperature will slow typical enzymatic reactions by a factor of about 5-10, it will also decrease the rate of diffusion of NEM across membranes, and slow the alkylation chemistry itself. These complexities make it uncertain whether the current methodologies used for trapping PDI redox state in live cells using NEM are demonstrably adequate. Trapping could be accomplished more rapidly with isolated microsomes, but the potential for leakage of GSH and for further enzymatic and non-enzymatic oxidation of PDI remain issues of concern (see earlier).



The highlighted equilibrium depicts the reduction of one PDI CxxC motif by GSH. Approximately one proton is released at neutral pH values (see the text).

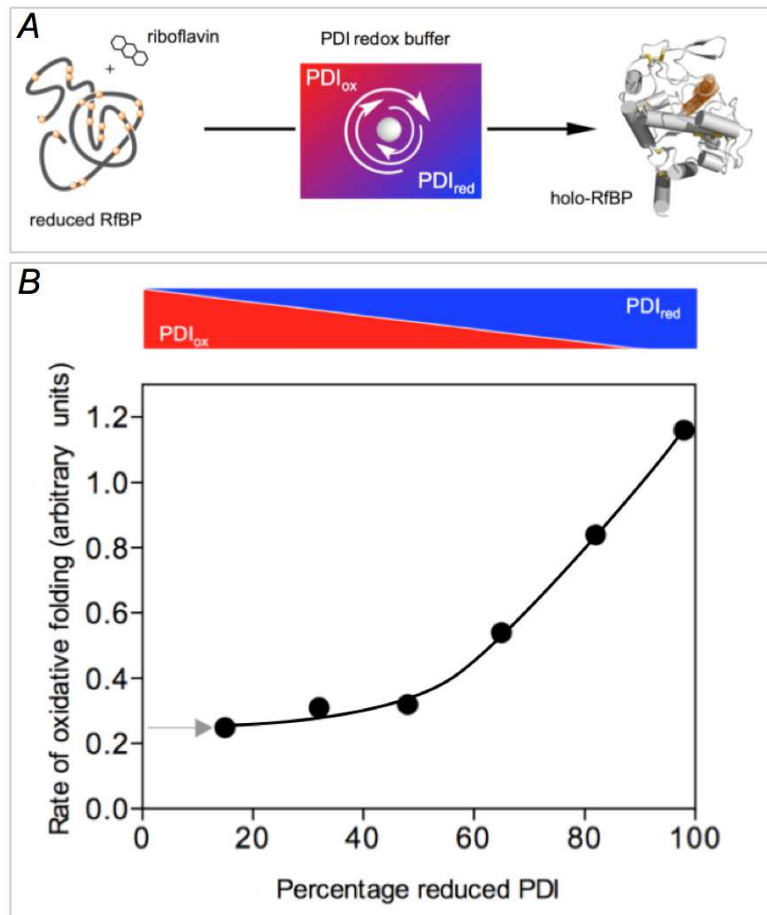
**Figure 2.9: The use of NEM to trap intraluminal redox state within the ER.**

Other trapping methods have been utilized in which pelleted cells, cells in culture, or tissues samples are treated with TCA. These methods are likely to be much more robust providing that denaturing acidification is achieved by rapid mixing methods. An aggressive denaturation is important because some PDIs retain activity at low pH values [3]. In a related issue, it should be noted that the equilibrium between PDI<sub>ox</sub> and GSH is itself pH dependent (Figure 2.9). Since the pK of the GSH thiol group is ~9.7 and that of the surface exposed N-terminal cysteine of reduced CxxC motifs in PDI is 4.4 - 6.7 [3], reduction of each redox-active CxxC disulfide in the isomerase would lead to the release of approximately one proton at pH 7.4. If the pH of the ER is not lowered rapidly enough, acidification will push the equilibrium towards PDI<sub>ox</sub> before the isomerase is inactivated. The time resolution of acid trapping could be further improved by adopting those freeze-quenching procedures already employed for the isolation of enzyme intermediates and for the measurement of metabolite mass action ratios (see later).

## **2.7 The Influence of PDI Redox State on In Vitro Oxidative Protein Folding**

Table 2.3 lists the redox potentials of some other PDI family members and the predicted redox state if they, too, were to equilibrate at a redox poise of -225 mV. Although these predictions initially seem at variance with PDI-first pathways, earlier *in vitro* studies showed that oxidative protein folding occurs efficiently at very low levels of PDI<sub>ox</sub> and that an accumulation of oxidized isomerase actually slowed the emergence of the native fold. The pioneering work of Gilbert and colleagues demonstrated that the oxidative refolding of RNase by PDI is facilitated when the isomerase is largely reduced [86]. RNase has proved a staple of oxidative folding studies and has 4 native disulfide bonds and consequently 105 disulfide isomers for

the fully oxidized enzyme [87]. We wished to explore the influence of the redox state of PDI on the refolding of a protein with a much more complicated disulfide connectivity. Using avian riboflavin binding protein (RfBP; 9 disulfides and >34 million disulfide isomers) enabled Rancy and Thorpe to continuously follow the recovery of riboflavin binding ability by the complete fluorescence quenching that accompanies the association of free riboflavin to apo-RfBP (Figure 2.10A) [49]. Mixtures of PDI<sub>ox</sub> and PDI<sub>red</sub> with an aggregate concentration of 30  $\mu$ M PDI served as redox buffers to drive the oxidative refolding of 1  $\mu$ M reduced RfBP in the complete absence of glutathione [49]. The use of an enzyme in considerable molar excess over its substrate might initially appear unusual, however it is likely to be a frequent occurrence in cellular metabolism [88]. In particular, aggregate PDI concentrations probably approach several mM in the ER (see earlier [56, 89]) and are likely to be comparable to, or higher than, any one particular client protein. Figure 2.10 shows that under the most oxidizing conditions possible (far left; starting with 30  $\mu$ M PDI<sub>ox</sub> and no PDI<sub>red</sub>), the stoichiometric introduction of disulfides into RfBP will generate a redox buffer containing 25.5  $\mu$ M PDI<sub>ox</sub> and 4.5  $\mu$ M PDI<sub>red</sub> (comprising 15% of the total PDI concentration; see arrow at left). Folding under these conditions is relatively slow, but accelerates as the percentage of PDI<sub>red</sub> in the redox buffer increases (rightwards in Figure 2.10). Under the most reducing environment, the redox buffer starts with 85% PDI<sub>red</sub> and 15% PDI<sub>ox</sub> and ends with essentially 100% PDI<sub>red</sub> [49]. Oxidative folding is even faster when fully reduced PDI is used from the outset and disulfides are generated by nanomolar levels of QSOX [49]. Since QSOX cannot oxidize PDI<sub>red</sub> directly [49] the role of the isomerase in this PDI-second model is confined to correcting mispairings introduced by the oxidase.



Refolding was followed continuously by the quenching of riboflavin binding on association with folded oxidized RfBP in the absence of small molecule redox species and without other enzymatic catalysts of disulfide bond generation (panel A). Rates of refolding are plotted as a function of the percentage of  $PDI_{red}$  in the PDI redox buffer (panel B). The concentration of reduced RfBP was  $1 \mu\text{M}$  and the aggregate concentration of reduced and oxidized forms comprising the PDI redox buffer was 30-fold higher (see the Text). Data redrawn from Rancy and Thorpe [49].

**Figure 2.10: The rate of oxidative refolding of riboflavin binding protein in the presence of PDI redox buffers of defined concentration.**

**Table 2.3: Redox potentials and projected redox state of selected human PDI-family members.**

| Protein | Gene Name | Redox Potential (mV)    | Reference | <i>Red:Ox</i> at -225 mV (assuming equilibration) |
|---------|-----------|-------------------------|-----------|---|
| PDI     | P4HB      | -165 (avg) <sup>a</sup> | [90]      | 90:1  |
|         |           | -176 (avg)              | [91]      | 40:1  |
|         |           | -160 (avg)              | [92]      | 130:1   |
|         |           | -162 (avg)              | [56]      | 110:1   |
|         |           | -163 (a)                | [93]      | 100:1   |
|         |           | -169 (a')               | [93]      | 65:1  |
| ERp57   | PDIA3     | -167 (a)                | [94]      | 80:1  |
|         |           | -156 (a')               |           | 175:1   |
|         |           | -155 (avg)              | [56]      | 190:1   |
| ERp72   | PDIA4     | -155 (avg)              | [56]      | 195:1   |
| P5      | PDIA6     | -146 (avg)              | [56]      | 360:1   |
| ERdj5   | DNAJC10   | -190 (avg)              | [95]      | 14:1  |
| ERp18   | TXNDC12   | -165                    | [96]      | 90:1  |
| ERp46   | TXNDC5    | -161 (avg)              | [56]      | 120:1   |
| TMX3    | TMX3      | -157                    | [97]      | 160:1   |

<sup>a</sup>Redox potentials for proteins with multiple CxxC motifs reflect the average redox behavior (denoted by avg) unless explicitly noted. ERp18 and TMX3 contain a single CxxC motif.

These oxidative refolding model studies, using two widely different protein clients, show that efficient oxidative folding can occur under relatively reducing conditions and that increasing levels of PDI<sub>ox</sub> actually slow acquisition of the native disulfide patterns in RfBP [49, 86]. Thus it seems likely that the accumulation of PDI<sub>ox</sub> may be a general impediment to the efficient folding of a range of client proteins within the ER. PDI-first pathways may thus only need to maintain enough PDI<sub>ox</sub> to stoichiometrically oxidize protein clients. In this way PDI-mediated oxidation does not run ahead of the isomerization of mispaired disulfides that is typically rate-limiting in oxidative protein folding [86]. This modest oxidation requirement may partly rationalize the seeming degeneracy of pathways for the oxidation of PDI<sub>red</sub> in mammalian cells; protein folding will only be seriously compromised when the ER can no longer maintain sufficient PDI<sub>ox</sub> to sustain the secretory load. Hence phenotypes associated with enzyme knockouts/knockdowns may emerge more clearly when secretion systems are stretched to capacity.

Table 2.3 contains a prediction of the redox state of PDI-family members if they were in equilibrium with a redox potential of -225 mV (corresponding to a GSH:GSSG ratio of 35:1 at 10 mM total glutathione). This potential is strongly reducing from the perspective of PDI-family members. Even if a potential of -200 mV is used (corresponding to a more oxidizing 5:1 ratio of GSH:GSSG; see earlier) most of the PDIs listed in Table 2.3 would still show reduced:oxidized ratios of >10. The experimental evidence for the redox state of PDI (Tables 2.2 and 2.3) seems generally consistent with both scenarios given the marked difficulties of the measurements.

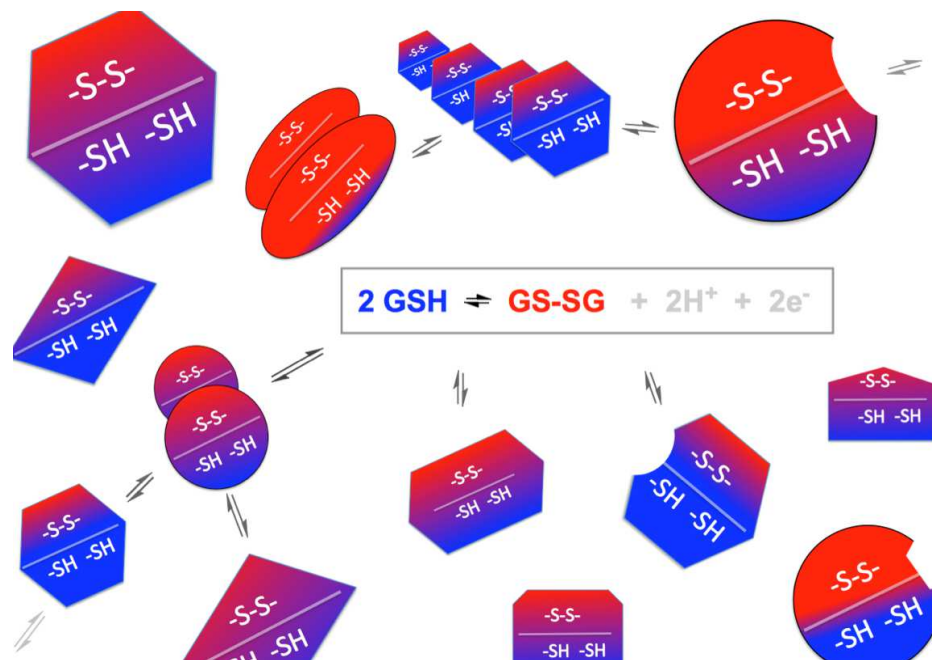
While it appears that the redox potentials of the PDI and glutathione redox pools, when averaged over the ER system, are not widely different, a state of

disequilibrium could be maintained if the oxidation of PDI<sub>red</sub> were to outstrip the rate at which PDI can equilibrate with glutathione. Another possibility is that the secretory system may provide structured microenvironments with clusters of enzymes, or sequestered luminal sections, that protect pools of PDI from equilibration with the bulk glutathione redox pool of the ER. The existence of a multiprotein complex containing molecular chaperones, the isomerases PDI and ERp72, and other component has already been reported in the ER of lymphoma cells [98]. Concentration gradients formed along stretches of the ER lumen might create “hot spots” of oxidation that may not be in equilibrium with the GSH levels that are averaged over the entire contents of the ER.

## 2.8 Future Directions

Current procedures use gel-shift methods [76] combined with Western blots to estimate the redox state of one or other of the PDI family proteins resident in the ER. However what of all the other thiol-disulfide oxidoreductases that are directly or indirectly involved in oxidative folding, or otherwise responsive to changing redox states of the ER? While modern fluorescent probes offer the unparalleled advantage of combining a real-time appraisal of redox poise with the spatial resolution of current fluorescence microscopic methods, they cannot address multiple thiol-disulfide couples simultaneously. In the ER, for example, there are likely to be proteins with CxxC or other redox-active disulfides that are in equilibrium with the glutathione pool, and other protein consortia in redox equilibrium with themselves but not with the glutathione pool (Figure 2.11). There may be other proteins that are far from equilibrium with any of the thiol-disulfide couples that play major roles in modulating redox events within the ER. If measurement of a diverse array of oxidoreductases

with known standard redox potentials (e.g. Table 2.3) predicts a common redox potential, and this consortium of proteins show coordinate redox changes with differing cellular conditions, then these proteins are likely equilibrium partners in a common redox environment [19]. Such equilibration could result from a direct communication between protein networks, as has recently been suggested by Nagata and colleagues [56], or via the intermediacy of a small molecule pool such as that provided by glutathione (Figure 2.11). Such analyses will likely identify components that are far from equilibrium with known redox pools/environments. We suggest that global approaches are likely to provide a useful complement to the real-time fluorescent probes mentioned earlier. All of the logistical steps for the implementation of such method have precedent – from freeze quenching and alkylation procedures, through procedures for the ratiometric mass spectrometric determination of multiple peptides carrying redox active dithiol/disulfide motifs [76, 99]. A flow diagram of this approach is presented in Figure 2.12.



Redox-active proteins are distinguished by their shapes; the state of their redox active disulfides is shown by the blue and red shading. Some species are envisaged as directly in equilibrium with the glutathione redox pool and would have a range of redox states depending on their standard redox potentials. Other proteins are represented as interacting indirectly with the glutathione pool or with consortia of other proteins insulated from small molecular weight redox buffers.

**Figure 2.11: Schematic diagram of equilibrating and non-equilibrating redox species in the ER.**

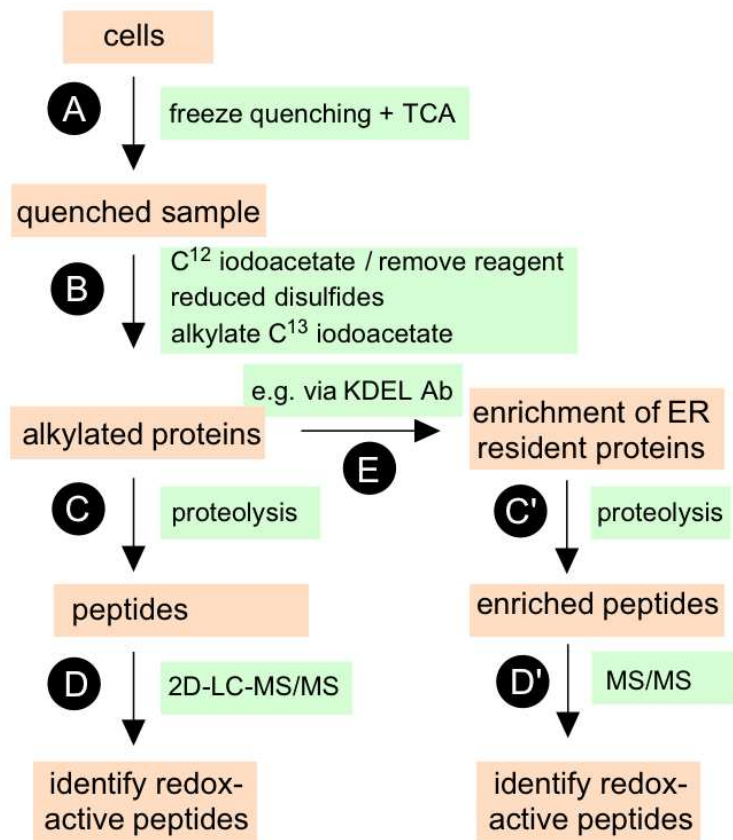


**Figure 2.12: A suggested protocol for a more global analysis of the redox state of thiol-disulfide oxidoreductases within the ER (see the Text).**

Well-established freeze quenching methodologies (step A) provide an alternative to passively soaking cells with NEM. Applied to tissues, they involve very rapid compression of small volumes of material on heavy metal plates cooled in liquid nitrogen [100]. Cell suspensions can be sprayed against rapidly rotating copper wheels that are cooled in liquid nitrogen and the accumulating frozen suspension scraped continuously into liquid nitrogen prior to TCA treatment [101]. Alternatively, a suspension of cells could be sprayed in fine droplets into rapidly stirred acetone at -78 °C followed by acidification with TCA and recovery of the dehydrated acidified

powder by centrifugation at sub-zero temperatures. Cells on surfaces can be rapidly cooled by immersion in a slush of liquid/solid nitrogen (-210 °C) to avoid the generation of an insulating blanket of nitrogen gas [100]. In terms of quenching reagents (step B), while NEM is a facile alkylating agent (see above) it is generally not well suited for general mass spectrometric applications because NEM-adducts are prone to ring opening and are subject to dissociation by reverse Michael reactions [14]. Since the cell samples would be already quenched, a slower and more robust alkylating agent such as iodoacetate is more suitable. Iodoacetate is commercially available in  $^{13}\text{C}$  forms facilitating the application of ratiometric mass spectrometric approaches [76, 99]. In brief, forcing alkylation with normal iodoacetate under denaturing conditions will label all free thiols. Following rigorous removal of alkylating agent, disulfides are reduced with DTT or tris(2-carboxyethyl)phosphine and the liberated thiols labeled with excess  $^{13}\text{C}$  iodoacetate. The ratio of  $^{13}\text{C}/^{12}\text{C}$  labeling peptides then signals their redox status in the original sample. In an important study providing precedent for the method, Bulleid and coworkers used ratiometric mass spectrometry to simultaneously determine the redox potentials of both CxxC motifs of full length PDI using in gel tryptic digestion of carboxymethylated PDI [93] (Table 2.3). The labeled  $^{12}\text{C}$  carboxymethylated CxxC peptides from both **a** and **a'** domains of PDI show distinct masses (of 1944.866 and 1915.814; Table 2.4) and so can be readily distinguished from each other and from their corresponding mass-shifted forms reflecting the proportion of oxidized CxxC motifs in the sample. Importantly, inspection of the sequence databases for human PDI-family members that carry one or more CxxC motifs shows that of the 26 CxxC tryptic peptides from 13 PDIs, only two peptides had identical mass (the **a'** domain of ERp57 and the third

CxxC motif in ERp72; Table 2.4). The remaining peptides have distinguishable masses (from 819.287 to 5102.252 for their  $^{12}\text{C}$  carboxymethylated derivatives) and thus, in principle, can be discerned by mass spectrometry alone. Of course digestion of a whole cell will generate a very large number of peptides and, while a number of mammalian PDI family members are relatively abundant [3, 56, 89], pre-culling of proteins (e.g. by application of KDEL-specific antibodies; step E) may prove advantageous. In summary the scheme outlined in Figure 2.12 will allow searching for alkylated peptides whose mass is already known from the sequences of multiple cellular oxidoreductases both in the ER and beyond. None of the CxxC motifs in human PDI-family members contain inter-cysteine tryptic cleavage sites (Table 2.4). More generally, this method is amenable to any redox-active thiol in the proteome providing that it can be reliably identified mass spectrometrically.

## 2.9 Envoi

Understanding oxidative protein folding in the ER presents formidable challenges for the enzymologist. In a conventional metabolic pathway, individual steps are typically catalyzed by single enzymes that almost always show high specificity for their substrates and exhibit rate enhancements that are typically  $>10^{10}$ -fold greater than the corresponding uncatalyzed reaction [102]. Non-enzymatic transformations very rarely contribute to metabolic flux and the role of an enzyme within a pathway can be identified with confidence. In contrast, many of the catalysts of oxidative folding, particularly PDI-family members, show pedestrian rate enhancements [12, 86, 103]. Further, the rather promiscuous chemical reactivity of thiols leads to the possibility that small molecule oxidants will contribute to the overall flux of disulfide bond generation [43, 44, 46]. Many of the enzymes of oxidative

protein folding have broad and overlapping substrate preferences that compound difficulties in the interpretation of knock-down experiments. As an additional manifestation of the apparent plasticity of oxidative protein folding, the *in vitro* studies described here [49, 86] suggests that oxidative folding *per se* might tolerate all but the most oxidizing conditions within the ER. Nevertheless those model studies show that oxidative folding is more efficient under comparatively reducing conditions and this aligns with most reports of the prevailing averaged redox state for PDI family members within the ER (Table 2.2). It remains to be seen whether the ER shows a heterogeneity of redox environments and whether the redox poise of post ER compartments is significantly different from the bulk ER lumen. We further need to explore the redox protein consortia that are believed to populate the ER and the extent to which network communication is effected directly [56] or via the mediation of glutathione. Finally, we suggest that a discontinuous interrogation of as broad a sampling of redox-active disulfides that can be identified by modern biological mass spectrometry approaches will prove a useful complement to the fluorescent probes that have transformed our understanding of redox homeostasis within cells.

**Table 2.4: Tryptic peptides of PDI-family members carrying CxxC redox-active motifs.**

| Gene Name/accession number | Selected Aliases                                    | CxxC Redox Peptide   | AA Coverage                              | Iodoacetate (C12) Modified                       |
|----------------------------|---|--|--|--|
| DNAJC10/<br>Q8IXB1         | MTHr, ERdj5   | EFDAAVNSGELWVNFYSPGCSHCHDL<br>APTWR<br>NHWVIDFYAPWCGPCQNFAPFELLAR<br>HNEVWMVDFYSPWCHPCQVLMPEWK<br>EPWLVDFFAPWCPPCR | 138-169<br>689-715<br>575-599<br>469-484 | 3771.6267<br>3339.5026<br>3277.4038<br>2078.9138 |
| ERP44/ Q9BS26              | KIAA0573,<br>PDIA10                                 | EITSLDTENIDEILNNADVA<br>LVNFYADWCR   | 30-59                                    | 3514.6318  |
| P4HB/ P07237               | PDI, PROHB,<br>PO4HB,<br>P4Hb                       | YLLVEFYAPWCGHCK<br>NVFVEFYAPWCGHCK   | 43-57<br>387-401                         | 1944.8658<br>1915.8141                           |
| PDIA2/ Q13087              | PDA2, PDIp  | EHPALLVEFYAPWCGHCQALAPEYSK<br>FYAPWCTHCK   | 58-83<br>413-422                         | 3075.4015<br>1371.5496                           |
| PDIA3/ P30101              | P58, ERp61,<br>ERp57,<br>ERp60,                     | ISDTGSAGLMLVEFFAPWCGHCK<br>DVLIEFYAPWCGHCK   | 39-61<br>396-410                         | 2585.1509<br>1896.8295                           |
| PDIA4/ P13667              | ERP70,<br>ERp72                                     | ENFDEVVNDADIILVEFYAP WCGHCK<br>DTVLLLEFYAPWCGHCK<br>DVLIEFYAPWCGHCK  | 185-210<br>80-95<br>545-559              | 3142.3808<br>1997.8771<br>1896.8295              |
| PDIA5/ Q14554              | PDIr,<br>FLJ30401                                   | E EKPLLIMFYAPWCSMCK<br>EHSSVLVMFHAPWCGHCK<br>HTLVMFYAPWCPHCK   | 169-186<br>292-309<br>416-430            | 2305.0411<br>2183.9459<br>1948.8542              |
| PDIA6/ Q15084              | P5, ERp5  | EVIQSDSLWLVEFYAPWCGHCQR<br>NVLDSVDVWVVEFYAPWCGHCK  | 38-60<br>173-194                         | 2882.2912<br>2744.1465                           |
| TMX1/ Q9H3N1               | TMX,<br>PDIA11                                      | ELLEGDWMIIEFYAPWCPACQNLQPEWE<br>SFAEWG-EDLEVNIK  | 41-82                                    | 5102.2520  |
| TMX3/ Q96JJ7               | FLJ20793,<br>PDIA13                                 | NDDIWLVDYAPWCGHCK  | 40-57                                    | 2297.9630  |
| TMX4/Q9H1E5                | DJ971N18.2,<br>PDIA14                               | FYAPWCPCSQQTDSWEAFK  | 59-79                                    | 2610.0587  |
| TXNDC5/<br>Q86UY0          | FLJ90810,<br>EndoPDI,<br>Hcc-2,<br>ERp46,<br>PDIA15 | FYAPWCGHCK<br>FFAPWCGHCK<br>CGHCQR   | 273-282<br>140-149<br>17-22              | 1327.5234<br>1311.5285<br>819.2872               |
| TXNDC12/<br>O95881         | ERp18,<br>ERP19,<br>AGR1,<br>PDIA16                 | SWCGACK  | 64-70                                    | 870.3120   |

Accession numbers correspond to UniprotKB (<http://www.uniprot.org/>) entries. Tryptic peptides were predicted from known UniprotKB sequences using ExPASy PeptideMass ([http://web.expasy.org/peptide\\_mass/](http://web.expasy.org/peptide_mass/)) tool. Out of 25 CxxC containing peptides from 13 PDI-family members, only two peptides exhibit identical masses (underlined).

## REFERENCES

1. Anfinsen, C.B., *Principles that Govern the Folding of Protein Chains*. Science, 1973. **181**: p. 223-230.
2. Riemer, J., N. Bulleid, and J.M. Herrmann, *Disulfide formation in the ER and mitochondria: two solutions to a common process*. Science, 2009. **324**(5932): p. 1284-7.
3. Hatahet, F. and L.W. Ruddock, *Protein Disulfide Isomerase: A Critical Evaluation of Its Function in Disulfide Bond Formation*. Antioxid Redox Signal, 2009. **11**(11): p. 2807-2850.
4. Kodali, V.K. and C. Thorpe, *Oxidative protein folding and the Quiescinsulfhydryl oxidase family of flavoproteins*. Antioxid Redox Signal, 2010. **13**(8): p. 1217-30.
5. Braakman, I. and N.J. Bulleid, *Protein folding and modification in the mammalian endoplasmic reticulum*. Annual review of biochemistry, 2011. **80**: p. 71-99.
6. Sevier, C., *Erv2 and Quiescin Sulfhydryl Oxidases: Erv-Domain Enzymes Associated with the Secretory Pathway*. Antioxidants & Redox Signaling, 2012. **16**: p. 800-808.
7. Oka, O.B. and N.J. Bulleid, *Forming disulfides in the endoplasmic reticulum*. Biochimica et biophysica acta, 2013. **1833**(11): p. 2425-9.
8. Zito, E., *PRDX4, an endoplasmic reticulum-localized peroxiredoxin at the crossroads between enzymatic oxidative protein folding and nonenzymatic protein oxidation*. Antioxidants & Redox Signaling, 2013. **18**(13): p. 1666-74.
9. Frand, A.R. and C.A. Kaiser, *The ERO1 gene of yeast is required for oxidation of protein dithiols in the endoplasmic reticulum*. Mol. Cell, 1998. **1**(2): p. 161-70.
10. Pollard, M.G., K.J. Travers, and J.S. Weissman, *Ero1p: a novel and ubiquitous protein with an essential role in oxidative protein folding in the endoplasmic reticulum*. Mol Cell, 1998. **1**(2): p. 171-82.

11. Sevier, C.S. and C.A. Kaiser, *Ero1 and redox homeostasis in the endoplasmic reticulum*. *Biochim Biophys Acta*, 2008. **1783**(4): p. 549-56.
12. Gilbert, H.F., *Thiol/disulfide exchange equilibria and disulfide bond stability*. *Methods Enzymol.*, 1995. **251**: p. 8-28.
13. Nagy, P., *Kinetics and Mechanisms of Thiol-Disulfide Exchange Covering Direct Substitution and Thiol Oxidation-Mediated Pathways*. *Antioxidants & Redox Signaling*, 2013.
14. Winther, J.R. and C. Thorpe, *Quantification of thiols and disulfides*. *Biochimica et biophysica acta*, 2014. **1840**(2): p. 838-46.
15. Rosenfield, R.E., R. Parthasarathy, and J.D. Dunitz, *Directional Preferences of Nonbonded Atomic Contacts with Divalent Sulfur .1. Electrophiles and Nucleophiles*. *Journal of the American Chemical Society*, 1977. **99**(14): p. 4860-4862.
16. Bach, R.D., O. Dmitrenko, and C. Thorpe, *Mechanism of thiolate-disulfide interchange reactions in biochemistry*. *J Org Chem*, 2008. **73**(1): p. 12-21.
17. Coddling, J.A., B.A. Israel, and C. Thorpe, *Protein Substrate Discrimination in the Quiescin Sulfhydryl Oxidase (QSOX) Family*. *Biochemistry*, 2012. **51**(20): p. 4226-35.
18. Fernandes, P.A. and M.J. Ramos, *Theoretical insights into the mechanism for thiol/disulfide exchange*. *Chemistry*, 2004. **10**(1): p. 257-66.
19. Schafer, F.Q. and G.R. Buettner, *Redox environment of the cell as viewed through the redox state of the glutathione disulfide/glutathione couple*. *Free radical biology & medicine*, 2001. **30**(11): p. 1191-212.
20. Appenzeller-Herzog, C., *Glutathione- and non-glutathione-based oxidant control in the endoplasmic reticulum*. *Journal of cell science*, 2011. **124**(Pt 6): p. 847-55.
21. Israel, B.A., V.K. Kodali, and C. Thorpe, *Going through the Barrier: coupled disulfide exchange reactions promote efficient catalysis in Quiescin sulfhydryl oxidase*. *The Journal of biological chemistry*, 2014. **289**(8): p. 5274-84.
22. Fass, D., *Disulfide Bonding in Protein Biophysics*. *Annu. Rev. Biophys.*, 2012. **41**: p. 43-59.
23. Jocelyn, P.C., *Biochemistry of the SH Group*. 1972, London: Academic Press.

24. Torchinsky, Y.M., *Sulfur in Proteins*. 1981, New York: Pergamon Press. 75-78.
25. Ellgaard, L. and L.W. Ruddock, *The human protein disulphide isomerase family: substrate interactions and functional properties*. EMBO Rep, 2005. **6**(1): p. 28-32.
26. Galligan, J.J. and D.R. Petersen, *The human protein disulfide isomerase gene family*. Human genomics, 2012. **6**(1): p. 6.
27. Wang, C., et al., *Structural insights into the redox-regulated dynamic conformations of human protein disulfide isomerase*. Antioxidants & Redox Signaling, 2013. **19**(1): p. 36-45.
28. Klappa, P., et al., *The b' domain provides the principal peptide-binding site of protein disulfide isomerase but all domains contribute to binding of misfolded proteins*. Embo J, 1998. **17**(4): p. 927-35.
29. Cabibbo, A., et al., *ERO1-L, a human protein that favors disulfide bond formation in the endoplasmic reticulum*. J Biol Chem, 2000. **275**(7): p. 4827-33.
30. Pagani, M., et al., *Endoplasmic reticulum oxidoreductin 1-lbeta (ERO1-Lbeta), a human gene induced in the course of the unfolded protein response*. The Journal of biological chemistry, 2000. **275**(31): p. 23685-92.
31. Tavender, T.J. and N.J. Bulleid, *Molecular mechanisms regulating oxidative activity of the Ero1 family in the endoplasmic reticulum*. Antioxid Redox Signal, 2010. **13**(8): p. 1177-87.
32. Araki, K. and K. Inaba, *Structure, mechanism, and evolution of Ero1 family enzymes*. Antioxidants & Redox Signaling, 2012. **16**(8): p. 790-9.
33. Ramming, T. and C. Appenzeller-Herzog, *The physiological functions of mammalian endoplasmic oxidoreductin 1: on disulfides and more*. Antioxidants & Redox Signaling, 2012. **16**(10): p. 1109-18.
34. Gross, E., et al., *Generating disulfides enzymatically: reaction products and electron acceptors of the endoplasmic reticulum thiol oxidase Ero1p*. Proc Natl Acad Sci U S A, 2006. **103**(2): p. 299-304.
35. Thorpe, C. and D.L. Coppock, *Generating disulfides in multicellular organisms: Emerging roles for a new flavoprotein family*. J Biol Chem, 2007. **282**: p. 13929-13933.

36. Pagani, M., et al., *Endoplasmic reticulum oxidoreductin 1-lbeta (ERO1-Lbeta), a human gene induced in the course of the unfolded protein response*. J Biol Chem, 2000. **275**(31): p. 23685-92.
37. Zito, E., et al., *ERO1-beta, a pancreas-specific disulfide oxidase, promotes insulin biogenesis and glucose homeostasis*. The Journal of cell biology, 2010. **188**(6): p. 821-32.
38. Zito, E., et al., *Oxidative protein folding by an endoplasmic reticulum-localized peroxiredoxin*. Molecular cell, 2010. **40**(5): p. 787-97.
39. Tavender, T.J., J.J. Springate, and N.J. Bulleid, *Recycling of peroxiredoxin IV provides a novel pathway for disulphide formation in the endoplasmic reticulum*. Embo J, 2010. **15**: p. 4185-4197.
40. Kakihana, T., K. Nagata, and R. Sitia, *Peroxides and peroxidases in the endoplasmic reticulum: integrating redox homeostasis and oxidative folding*. Antioxidants & Redox Signaling, 2012. **16**(8): p. 763-71.
41. Nguyen, V.D., et al., *Two endoplasmic reticulum PDI peroxidases increase the efficiency of the use of peroxide during disulfide bond formation*. Journal of molecular biology, 2011. **406**(3): p. 503-15.
42. Schulman, S., et al., *Vitamin K epoxide reductase prefers ER membrane-anchored thioredoxin-like redox partners*. Proc Natl Acad Sci U S A, 2010. **107**(34): p. 15027-32.
43. Ruddock, L.W., *Low molecular weight oxidants involved in disulfide bond formation*. Antioxidants & Redox Signaling, 2011.
44. Banhegyi, G., et al., *Role of ascorbate in oxidative protein folding*. Biofactors, 2003. **17**(1-4): p. 37-46.
45. Karala, A.R., et al., *Efficient Peroxide Mediated Oxidative Refolding of a Protein at Physiological Ph and Implications for Oxidative Folding in the Endoplasmic Reticulum*. Antioxid Redox Signal, 2008. **11**(5): p. 963-970.
46. Margittai, E. and G. Banhegyi, *Oxidative folding in the endoplasmic reticulum: Towards a multiple oxidant hypothesis?* Febs Letters, 2010. **584**(14): p. 2995-2998.
47. Hooper, K.L., et al., *Sulfhydryl oxidase from egg white: a facile catalyst for disulfide bond formation in proteins and peptides*. J. Biol. Chem., 1999. **274**(32): p. 22147-22150.

48. Heckler, E.J., et al., *Generating disulfides with the Quiescin-sulfhydryl oxidases*. *Biochim Biophys Acta*, 2008. **1783**(4): p. 567-77.
49. Rancy, P.C. and C. Thorpe, *Oxidative Protein Folding in vitro: a Study of the Cooperation between Quiescin-sulfhydryl Oxidase and Protein Disulfide Isomerase*. *Biochemistry*, 2008. **47**(46): p. 12047-56.
50. Thorpe, C., et al., *Sulfhydryl oxidases: emerging catalysts of protein disulfide bond formation in eukaryotes*. *Arch Biochem Biophys*, 2002. **405**(1): p. 1-12.
51. Heckler, E.J., et al., *Human quiescin-sulfhydryl oxidase, QSOX1: probing internal redox steps by mutagenesis*. *Biochemistry*, 2008. **47**(17): p. 4955-63.
52. Alon, A., et al., *The dynamic disulphide relay of quiescin sulphhydryl oxidase*. *Nature*, 2012. **488**(7411): p. 414-418.
53. Jessop, C.E. and N.J. Bulleid, *Glutathione directly reduces an oxidoreductase in the endoplasmic reticulum of mammalian cells*. *J Biol Chem*, 2004. **279**(53): p. 55341-7.
54. Montero, D., et al., *Intracellular glutathione pools are heterogeneously concentrated*. *Redox biology*, 2013. **1**(1): p. 508-13.
55. Freedman, R.B., T.R. Hirst, and M.F. Tuite, *Protein disulfide isomerase: building bridges in protein folding*. *Trends Biochem. Sci.*, 1994. **19**: p. 331-336.
56. Araki, K., et al., *Ero1-alpha and PDIs constitute a hierarchical electron transfer network of endoplasmic reticulum oxidoreductases*. *The Journal of cell biology*, 2013. **202**(6): p. 861-74.
57. Darby, N.J. and T.E. Creighton, *Characterization of the active site cysteine residues of the thioredoxin-like domains of protein disulfide isomerase*. *Biochemistry*, 1995. **34**(51): p. 16770-80.
58. Hoops, S., et al., *COPASI--a COmplex PAthway SIMulator*. *Bioinformatics*, 2006. **22**(24): p. 3067-74.
59. Lappi, A.K. and L.W. Ruddock, *Reexamination of the role of interplay between glutathione and protein disulfide isomerase*. *Journal of molecular biology*, 2011. **409**(2): p. 238-49.

60. Appenzeller-Herzog, C., et al., *A novel disulphide switch mechanism in Ero1alpha balances ER oxidation in human cells*. EMBO J, 2008. **27**(22): p. 2977-87.
61. Baker, K.M., et al., *Low reduction potential of Ero1alpha regulatory disulphides ensures tight control of substrate oxidation*. Embo J, 2008. **27**(22): p. 2988-97.
62. Banhegyi, G., et al., *Preferential transport of glutathione versus glutathione disulfide in rat liver microsomal vesicles*. J. Biol. Chem., 1999. **274**: p. 12213-12216.
63. Morgan, B., et al., *Multiple glutathione disulfide removal pathways mediate cytosolic redox homeostasis*. Nature Chemical Biology, 2013. **9**(2): p. 119-125.
64. Flohe, L., *The fairytale of the GSSG/GSH redox potential*. Biochimica Et Biophysica Acta-General Subjects, 2013. **1830**(5): p. 3139-3142.
65. Heinrich, R., S.M. Rapoport, and T.A. Rapoport, *Metabolic regulation and mathematical models*. Progress in biophysics and molecular biology, 1977. **32**(1): p. 1-82.
66. Hwang, C., A.J. Sinskey, and H.F. Lodish, *Oxidized redox state of glutathione in the endoplasmic reticulum*. Science, 1992. **257**(5076): p. 1496-502.
67. Bass, R., et al., *A Major Fraction of Endoplasmic Reticulum-located Glutathione Is Present as Mixed Disulfides with Protein*. J Biol Chem, 2004. **279**(7): p. 5257-62.
68. Dixon, B.M., et al., *Assessment of Endoplasmic Reticulum Glutathione Redox Status Is Confounded by Extensive Ex Vivo Oxidation*. Antioxid Redox Signal, 2008. **10**(5): p. 963-972.
69. Ostergaard, H., et al., *Shedding light on disulfide bond formation: engineering a redox switch in green fluorescent protein*. Embo J, 2001. **20**(21): p. 5853-62.
70. Bjornberg, O., H. Ostergaard, and J.R. Winther, *Mechanistic insight provided by glutaredoxin within a fusion to redox-sensitive yellow fluorescent protein*. Biochemistry, 2006. **45**(7): p. 2362-71.
71. Hanson, G.T., et al., *Investigating mitochondrial redox potential with redox-sensitive green fluorescent protein indicators*. J Biol Chem, 2004. **279**(13): p. 13044-53.

72. van Lith, M., et al., *Real-time monitoring of redox changes in the mammalian endoplasmic reticulum*. Journal of cell science, 2011.
73. Birk, J., et al., *Endoplasmic reticulum: reduced and oxidized glutathione revisited*. Journal of cell science, 2013. **126**(Pt 7): p. 1604-17.
74. Avezov, E., et al., *Lifetime imaging of a fluorescent protein sensor reveals surprising stability of ER thiol redox*. The Journal of cell biology, 2013. **201**(2): p. 337-49.
75. Kolossov, V.L., et al., *Forster resonance energy transfer-based sensor targeting endoplasmic reticulum reveals highly oxidative environment*. Experimental biology and medicine, 2012. **237**(6): p. 652-662.
76. Eaton, P., *Protein thiol oxidation in health and disease: techniques for measuring disulfides and related modifications in complex protein mixtures*. Free radical biology & medicine, 2006. **40**(11): p. 1889-99.
77. Sato, Y., et al., *Synergistic cooperation of PDI family members in peroxiredoxin 4-driven oxidative protein folding*. Scientific reports, 2013. **3**: p. 2456.
78. Nardai, G., et al., *Diabetic changes in the redox status of the microsomal protein folding machinery*. Biochemical and Biophysical Research Communications, 2005. **334**(3): p. 787-95.
79. Mezghrani, A., et al., *Manipulation of oxidative protein folding and PDI redox state in mammalian cells*. Embo J, 2001. **20**(22): p. 6288-6296.
80. Appenzeller-Herzog, C. and L. Ellgaard, *In vivo reduction-oxidation state of protein disulfide isomerase: the two active sites independently occur in the reduced and oxidized forms*. Antioxid Redox Signal, 2008. **10**(1): p. 55-64.
81. Toldo, S., et al., *Altered oxido-reductive state in the diabetic heart: loss of cardioprotection due to protein disulfide isomerase*. Molecular medicine, 2011. **17**(9-10): p. 1012-21.
82. Hansen, R.E. and J.R. Winther, *An introduction to methods for analyzing thiols and disulfides: Reactions, reagents, and practical considerations*. Anal Biochem, 2009. **394**(2): p. 147-58.
83. Brandner, D. and G. Withers, *Image of Plasma Cell from Guinea Pig Bone Marrow CIL:10733*, in *The Cell: An Image Library*. www.cellimagelibrary.org. 2010.

84. Chakravarthi, S., C.E. Jessop, and N.J. Bulleid, *The role of glutathione in disulphide bond formation and endoplasmic-reticulum-generated oxidative stress*. EMBO Rep, 2006. **7**(3): p. 271-5.
85. Hansen, R.E., D. Roth, and J.R. Winther, *Quantifying the global cellular thiol-disulfide status*. Proc Natl Acad Sci U S A, 2009. **106**(2): p. 422-7.
86. Lyles, M.M. and H.F. Gilbert, *Catalysis of the oxidative folding of ribonuclease A by protein disulfide isomerase: dependence of the rate on the composition of the redox buffer*. Biochemistry, 1991. **30**(3): p. 613-9.
87. Narayan, M., et al., *Oxidative folding of proteins*. Acc Chem Res, 2000. **33**(11): p. 805-12.
88. Albe, K.R., M.H. Butler, and B.E. Wright, *Cellular concentrations of enzymes and their substrates*. Journal of theoretical biology, 1990. **143**(2): p. 163-95.
89. Hillson, D.A., N. Lambert, and R.B. Freedman, *Formation and isomerization of disulfide bonds in proteins: protein disulfide-isomerase*. Methods Enzymol, 1984. **107**: p. 281-94.
90. Lundstrom, J. and A. Holmgren, *Determination of the reduction-oxidation potential of the thioredoxin-like domains of protein disulfide-isomerase from the equilibrium with glutathione and thioredoxin*. Biochemistry, 1993. **32**(26): p. 6649-55.
91. Schwaller, M., B. Wilkinson, and H.F. Gilbert, *Reduction-reoxidation cycles contribute to catalysis of disulfide isomerization by protein-disulfide isomerase*. The Journal of biological chemistry, 2003. **278**(9): p. 7154-9.
92. Raturi, A. and B. Mutus, *Characterization of redox state and reductase activity of protein disulfide isomerase under different redox environments using a sensitive fluorescent assay*. Free radical biology & medicine, 2007. **43**(1): p. 62-70.
93. Chambers, J.E., et al., *The reduction potential of the active site disulfides of human protein disulfide isomerase limits oxidation of the enzyme by Ero1alpha*. The Journal of biological chemistry, 2010. **285**(38): p. 29200-7.
94. Frickel, E.M., et al., *ERp57 is a multifunctional thiol-disulfide oxidoreductase*. The Journal of biological chemistry, 2004. **279**(18): p. 18277-87.
95. Ushioda, R., et al., *ERdj5 is required as a disulfide reductase for degradation of misfolded proteins in the ER*. Science, 2008. **321**(5888): p. 569-72.

96. Jeong, W., et al., *ERp16, an endoplasmic reticulum-resident thiol-disulfide oxidoreductase: biochemical properties and role in apoptosis induced by endoplasmic reticulum stress*. The Journal of biological chemistry, 2008. **283**(37): p. 25557-66.
97. Haugstetter, J., T. Blicher, and L. Ellgaard, *Identification and characterization of a novel thioredoxin-related transmembrane protein of the endoplasmic reticulum*. J Biol Chem, 2005. **280**(9): p. 8371-80.
98. Meunier, L., et al., *A subset of chaperones and folding enzymes form multiprotein complexes in endoplasmic reticulum to bind nascent proteins*. Mol Biol Cell, 2002. **13**(12): p. 4456-69.
99. Chouchani, E.T., et al., *Proteomic approaches to the characterization of protein thiol modification*. Current opinion in chemical biology, 2011. **15**(1): p. 120-8.
100. Severs, N. and D. Shotton, *Rapid Freezing of Biological Specimens for Freeze Fracture and Deep Etching*, in *Cell Biology*, J. Celis, Editor. 2006, Elsevier. p. 249-255.
101. Tanaka, M., et al., *Activation of hydrogen peroxide in horseradish peroxidase occurs within approximately 200 microseconds observed by a new freeze-quench device*. Biophysical journal, 2003. **84**(3): p. 1998-2004.
102. Wolfenden, R., *Benchmark reaction rates, the stability of biological molecules in water, and the evolution of catalytic power in enzymes*. Annual review of biochemistry, 2011. **80**: p. 645-67.
103. Wilkinson, B. and H.F. Gilbert, *Protein disulfide isomerase*. Biochimica Et Biophysica Acta-Proteins and Proteomics, 2004. **1699**(1-2): p. 35-44.

## Chapter 3

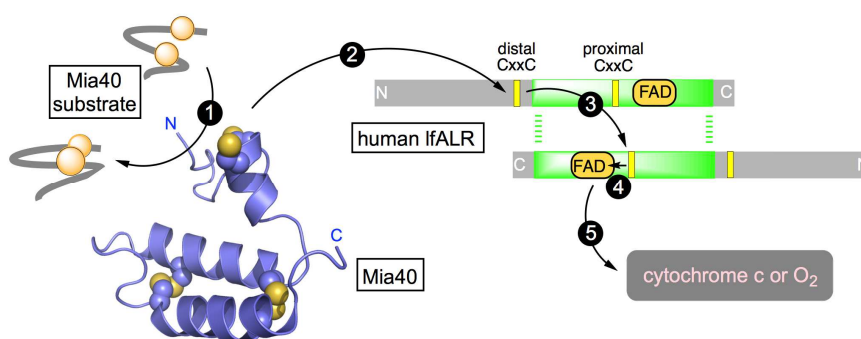
### MIA40 IS A FACILE OXIDANT OF UNFOLDED REDUCED PROTEINS BUT SHOWS MINIMAL ISOMERASE ACTIVITY

#### 3.1 Introduction and Background

The finding that human Quiescin Q6 [1] was a multidomain FAD-dependent sulfhydryl oxidase [2-4] led to the discovery that the yeast growth factor Erv1p (essential for respiration and viability) was also a disulfide-generating enzyme [5]. Both families of flavin-dependent sulfhydryl oxidases share fundamental commonalities in catalytic mechanism: a redox-active disulfide is positioned proximal to a FAD cofactor allowing the oxidation of remote thiol groups to be coupled to the reduction of molecular oxygen or alternate electron acceptors [4, 6-9]. Erv1p functions during oxidative folding in the yeast mitochondrial intermembrane space (IMS; Chapter 1). Here, nascent cytosolic polypeptide chains, carrying a range of targeting sequence motifs, enter the mitochondrial IMS via the outer membrane translocase complex to be subsequently trapped via disulfide bond formation [10-16]. Each disulfide generated releases a pair of reducing equivalents which are passed to the oxidoreductases Mia40 and then to flavoprotein Erv1p [16-18].

Our studies on the human counterpart of Erv1p (augmenter of liver regeneration, ALR; also abbreviated GFER, Growth Factor ERV-like) suggested that cytochrome c was an alternate physiological oxidant of the enzyme [19]. We further demonstrated that human Mia40 was obligatorily oxidized by the distal disulfide of IfALR with the flow of reducing equivalents depicted by arrows 2-5 in the schematic

representation shown in Figure 3.1 [20]. These findings were corroborated with the yeast Erv1p/Mia40 system with the additional insight that redox equilibration between distal and proximal redox centers occurs across the dimer interface (Figure 3.1, step 3) [21-23]. Such inter-subunit redox communication was also proposed for IfALR [24]. The structural aspects of the communication between Mia40 and Erv1p or ALR have received considerable attention [22, 24-26].



Mia40 (PDB 2K3J) is reduced by a reduced substrate (step 1) and then communicates with the distal CxxC disulfide in one subunit of homodimeric IfALR (step 2). Step 3 depicts intersubunit thiol-disulfide exchange, generating the reduced proximal disulfide, followed by transfer of reducing equivalents to the FAD prosthetic group (step 4). Oxidation is completed by reduction of cytochrome c or molecular oxygen (step 5).

**Figure 3.1: The flow of reducing equivalents during the oxidation of a protein dithiol catalyzed by Mia40 and IfALR.**

Three-dimensional structures of both the yeast and mammalian Mia40 proteins [26-28] confirm the presence of a helix-turn-helix motif secured by 2 inter-strand disulfide bonds (Figure 3.1). Substrates bind orthogonally to the helical strands in a shallow hydrophobic depression that contributes to the recognition and retention of substrates, and to their subsequent efficient oxidation by the adjacent CPC redox motif

of Mia40 (shown above the two main helices in Figure 3.1) [26-28]. Analyses of the amino acid sequences of IMS substrates of Mia40 have identified a cysteine-containing sequence (the mitochondrial IMS-targeting signal, MISS; or the IMS-targeting signal, ITS) that was believed to be necessary and sufficient for IMS targeting [11, 29, 30]. Tokatlidis and colleagues have suggested that a 9-residue amphipathic helix contained in client protein substrates within the CX9C and CX3C families forms a mixed disulfide with Mia40 facilitating the emergence of the native fold via a mechanism involving docking and sliding [11, 30]. However, a number of IMS proteins e.g. DRE2, ATP23, Erv1/IfALR, Ccs1, SOD1, and anamorsin contain neither the classical cysteine motifs nor ITS import sequences, although they have been shown to be Mia40 clients in vivo and/or in vitro [15, 31-34]. Schmid and coworkers further probed the substrate specificity of Mia40 by using cysteine mutants of IMS proteins [35, 36]. They demonstrated that rather than a precisely defined sequence, regions of hydrophobicity adjacent to cysteine residues are sufficient for binding and covalent capture by Mia40 [36]. In addition, Herrmann and Reimer and their colleagues have shown that Mia40 can bind a variety of non-cysteine-containing peptides and has chaperone-like activity towards unfolded proteins [31].

These interesting studies leave uncertain the range of protein sequences that comprise substrates of the Mia40/IfALR disulfide generating system. Instead of bona-fide substrates of the IMS, with their generally conserved cysteine motifs and ITS sequences, we wanted to challenge the redox behavior of Mia40/IfALR with potential substrates lacking all of these features. For this work we chose three diverse proteins of the vertebrate secretory apparatus (ribonuclease A, egg white lysozyme, and riboflavin binding protein; RNase, lysozyme and RfBP respectively). We show that

these reduced proteins are competent substrates of the Mia40/IfALR pathway reinforcing the idea that Mia40 dependent oxidative pathways have a broader oxidative scope than originally envisaged. To further investigate the catalytic potential of Mia40 to service structural disulfide bonds, we have benchmarked the suggested isomerase activity of Mia40 against the mammalian protein disulfide isomerase. In addition to providing new insights into Mia40 catalysis, our work identifies potential complications in the interpretation of the insulin reductase assays widely employed to explore the catalytic activities of disulfide oxidoreductases.

## **3.2 Experimental Procedures**

### **3.2.1 Materials and General Methods**

Commercial reagents were obtained as described previously [37-39]. Unless otherwise stated, 50 mM potassium phosphate buffer, pH 7.5, containing 1 mM EDTA was used throughout. Absorbance and fluorescence experiments were performed on HP8453 diode-array spectrophotometers and an SLM-Aminco Bowman 2 luminescence spectrometer respectively. Thiols were routinely quantitated by diluting samples into 180  $\mu$ L of 0.2 mM DTNB in self-masking microcells and recording the increase in absorbance at 412 nm over a corresponding blank using a molar extinction coefficient for the 5-thio-2-nitobenzoate dianion of 14150 M<sup>-1</sup> cm<sup>-1</sup> at 412 nm [40]. Data were visualized using GraphPad Prism software.

### **3.2.2 Expression and Treatment of Proteins**

IfALR was purified as described previously [20]. Wild type Mia40 and Mia40<sub>APA</sub> were prepared in their short linker form as before [20] and quantitated using a molar extinction coefficient of 13.3 mM<sup>-1</sup> cm<sup>-1</sup> at 280 nm (calculated using

ProtParam [41]). Human PDI was purified and quantitated as described previously [42]. Bovine pancreatic RNase A (Sigma), hen egg white lysozyme (Sigma), and hen egg white riboflavin binding protein (prepared as in [43]) were reduced with a 20-fold molar excess of DTT per protein thiol for 1 h at 50 °C in 50 mM phosphate buffer, pH 8.0, containing 1 mM EDTA, 6 M guanidine hydrochloride and 100 mM NaCl. Excess reductant was subsequently removed by gel-filtration of 0.7 mL unfolded reduced protein on PD-10 gel filtration columns (GE Healthcare). Complete separation of reduced protein from excess reductant was verified by sampling small volumes of eluent using DTNB. Reduced RNase (rRNase) was eluted in 2 mM acetate buffer, pH 4.0, containing 1 mM EDTA. Reduced lysozyme and reduced RfBP were eluted in the same buffer supplemented with 3 M urea or 3 M guanidine HCl respectively. Reduced RNase, lysozyme and RfBP were quantitated using molar extinction coefficients of 9800 M<sup>-1</sup> cm<sup>-1</sup> at 278 nm; 34000 M<sup>-1</sup> cm<sup>-1</sup> at 280 nm; and 49000 M<sup>-1</sup> cm<sup>-1</sup> at 280 nm respectively. Scrambled RNase (sRNase) was prepared essentially as described previously [42] except that the oxidized protein in 6 M guanidine HCl was gel filtered using a PD10 column equilibrated with 3.5 mM potassium acetate buffer, pH 4, and stored before use at – 80 °C. The preparation used in this work exhibited 1.3 ± 0.7% activity (a value consistent with the random reformation of 4 disulfide bonds [44]).

### 3.2.3 RNase Activity Assay

Aliquots (20 µL) were withdrawn from incubation mixtures and immediately mixed with 180 µL of 100 mM Tris-HCl buffer, pH 7.0, 25 °C, containing 1.11 mM cCMP and 1 mM EDTA. The increase in absorbance A<sub>296</sub> - A<sub>310</sub> reflects the hydrolysis of cCMP. Subtraction of the absorbance at 310 nm improved the signal to

noise ratio as described previously [35]. Relative activities of the aliquots were determined by comparing the slope of the initial rates with those of an equivalent concentration of native RNase.

### **3.2.4 Insulin Reductase Assay**

Stock solutions of bovine insulin were prepared in water by bringing a suspension of the solid to a pH of 3 with HCl and then returning the clear solution to a pH of 6 with KOH. Reaction mixtures contained 50  $\mu$ M insulin in 50 mM phosphate buffer, pH 7.5, 25 °C, containing 1 mM EDTA in the presence or absence of wild-type Mia40 or the Mia40<sub>APA</sub> double mutant. Reactions were started by the addition of 5 mM DTT and the subsequent increase in light scattering monitored at 600 nm.

### **3.2.5 Stopped Flow Methods**

An SF-61 DX2 stopped-flow spectrometer (Hi-Tech Scientific) was used for rapid mixing kinetics experiments in fluorescence mode exciting at 290 nm with a 300 nm cutoff filter in the emission beam. Oxidized Mia40 was mixed at 25 °C with rRNase to give final concentrations of 0.5  $\mu$ M and 10-50  $\mu$ M respectively in 50 mM phosphate buffer, pH 7.5. Fluorescence traces were visualized and analyzed using the instrument software, KinetAsyst 3, and with KinTek Explorer [45]. The apparent rate constants from biphasic fits to the first 5 s of fluorescence increase were plotted as a function of rRNase concentration. The fast phase was fit to saturation kinetics using GraphPad Prism.

### **3.2.6 Sequence Analysis**

The primary amino acid sequences of RNase, chicken lysozyme and RfBP were analyzed using the ScanProsite tool (<http://prosite.expasy.org/scanprosite/>) for

potential ITS motifs using: [YWF]-x(2)-[AILVIFYWGMP]-[AILVIFYWGMP]-x(2)-C, C-x(2)-[AILVIFYWGMP]-[AILVIFYWGMP]-x(2)-[YWF]. ScanProsite analysis identified no ITS motifs using these sequences. ScanProsite, in conjunction with PDB structures visualized with PyMol (Schrödinger, LLC), showed that neither paired CX<sub>3</sub>C nor CX<sub>9</sub>C motifs are found in the context of helix-coil-helix domains in RNase, lysozyme or RfBP.

### **3.3 Results and Discussion**

#### **3.3.1 Mia40/lfALR is a general catalysis of protein oxidation**

Three diverse disulfide-containing products of the vertebrate secretory apparatus were chosen for this study exploring the ability of Mia40/lfALR to oxidize non-cognate substrates using oxygen as the terminal electron acceptor (Figure 3.1). The proteins show a range of secondary structures, disulfide connectivities, and pI values (RNase, 9.6; lysozyme, 11.35; RfBP, ~ 4.0). ITS sequences are absent in all three proteins (Figure 3.2; see Methods; [29, 30]), as are paired CX<sub>3</sub>C or CX<sub>9</sub>C motifs frequently encountered in the context of helix-coil-helix super secondary structures in IMS-resident proteins (see Methods). RNase, lysozyme and RfBP were reduced under denaturing conditions and freed from excess reductant by size-exclusion chromatography (see Methods). In all three cases efficient oxidation of these proteins requires the presence of both Mia40 and lfALR (Figure 3.3). Panel A shows the disappearance of rRNase thiols mediated by the Mia40/lfALR system. The conditions chosen (500 μM RNase thiols, 20 μM oxidized Mia40 and 1 μM lfALR) require 250 turnovers of lfALR to completely oxidize substrate thiols to disulfides. Under these

conditions the initial rate corresponds to an apparent turnover of  $8.9 \pm 0.1$  RNase disulfide bonds generated/min per lfALR active site.

### RNase

KETAAAKFER QHMDSSTSAA SSSNYC<sup>■</sup>NQMM KSRNLTKDR<sup>■</sup>  
 KPVNTFVHES LADVQAV<sup>■</sup>CSQ KNVA<sup>■</sup>CKNGQT NC<sup>■</sup>YQNSYSTEM  
 SITD<sup>■</sup>RETGS SKYPN<sup>■</sup>CAYKT TQANKHIIVA <sup>■</sup>CEGNPYVPVH  
 FDASV

### Lysozyme

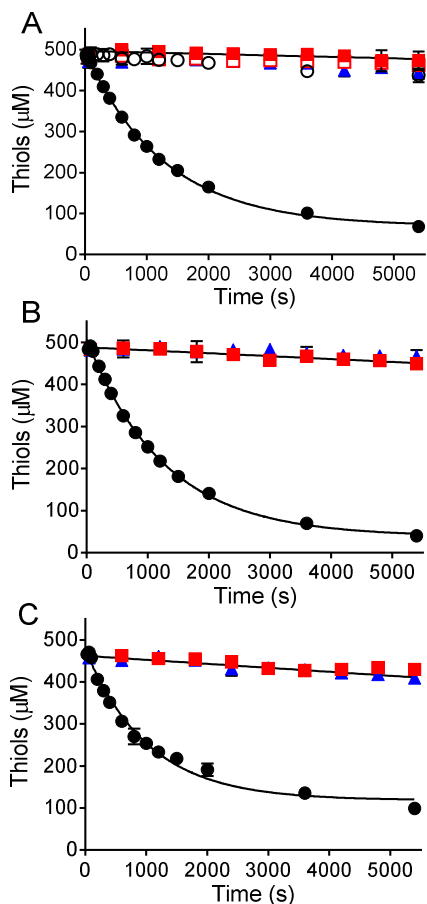
KVFGRC<sup>■</sup>ELAA AMKRHGLDNY RGYSLGNWV<sup>■</sup>C AAKFESNFNT  
 QATNRNTDGS TDYGILQINS RWW<sup>■</sup>CNDGRTP GSRNL<sup>■</sup>CNIPC<sup>■</sup>  
 SALLSSDITA SVN<sup>■</sup>CAKKIVS DNGMNAWVA WRNR<sup>■</sup>CKGTDV  
 QAWIRG<sup>■</sup>CRL

### Riboflavin Binding Protein

QQYG<sup>■</sup>LEGDT HKANPSPEPN MHECTLYSES SCCYANFTEQ  
 LAHSPIIKVS NSYWNRC<sup>■</sup>GQL SKSCEDFTTK IECFYRC<sup>■</sup>SPH  
 AARWIDPRYT AAIQSVPL<sup>■</sup>CQ SFC<sup>■</sup>DDWYEAC<sup>■</sup> KDDSI<sup>■</sup>CAHNW  
 LTDWERDESG ENH<sup>■</sup>CKSK<sup>■</sup>VP YSEMYANGTD MC<sup>■</sup>QSMWGESF  
 KVSESS<sup>■</sup>CL<sup>■</sup>CL QMNKKDMVAI KHLLESSEEE SSSMSSEEH  
 AC<sup>■</sup>QKLLKFE ALQQEEGEER R

RNase, lysozyme and riboflavin binding protein, following their signal sequences, show neither ITS sequences nor paired CX<sub>3</sub>C or CX<sub>9</sub>C motifs (see the Text). Cysteine residues are shown in inverse font. RNase, lysozyme and RfBP contain 4, 4 and 9 disulfides respectively.

**Figure 3.2: ScanProsite analysis of non-cognate substrates.**



Reactions were started by the addition of the enzymes indicated below and aliquots were withdrawn at the indicated times for measurement of thiol titer using DTNB. Panel A represents 62.5  $\mu\text{M}$  of rRNase (8 cysteines; 500  $\mu\text{M}$  thiols) in the additional presence of 1  $\mu\text{M}$  IfALR and 20  $\mu\text{M}$  Mia40 (filled black circles), 1  $\mu\text{M}$  IfALR and 20  $\mu\text{M}$  Mia40<sub>APA</sub> (open black circles), 20  $\mu\text{M}$  Mia40 (red filled squares), 20  $\mu\text{M}$  Mia40<sub>APA</sub> (red open squares), or 1  $\mu\text{M}$  IfALR (blue filled triangles). Panel B shows the incubation of 62.5  $\mu\text{M}$  of reduced lysozyme (8 cysteines) in the presence of 3 M urea to maintain solubility with 1  $\mu\text{M}$  IfALR and 20  $\mu\text{M}$  Mia40 (filled black circles), 20  $\mu\text{M}$  Mia40 (filled red squares), or 1  $\mu\text{M}$  IfALR (filled blue triangles). Panel C shows the comparable treatment of 27.8  $\mu\text{M}$  reduced RfBP (18 cysteines; 500  $\mu\text{M}$  thiols) using 1  $\mu\text{M}$  IfALR and 20  $\mu\text{M}$  Mia40 (filled black circles), 20  $\mu\text{M}$  Mia40 (filled red squares), or 1  $\mu\text{M}$  IfALR (filled blue triangles). All experiments were performed in triplicate at 25 °C in 50 mM phosphate buffer, pH 7.5, containing 1mM EDTA.

**Figure 3.3: Oxidative of non-cognate substrates.**

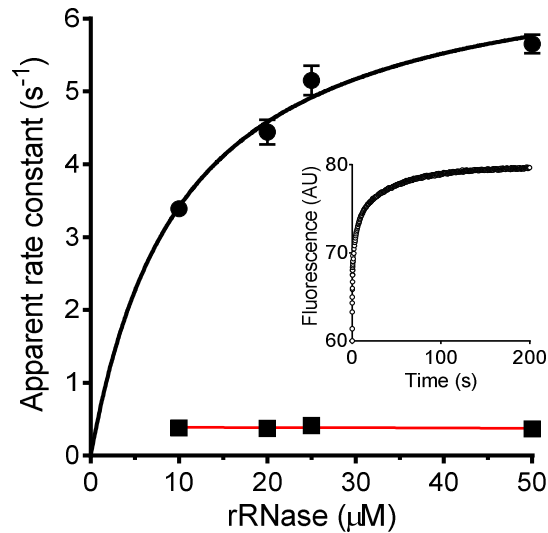
In a previous study, Daithankar et al. examined the concentration dependence for the turnover number of reduced Mia40 by IfALR; at 20  $\mu$ M Mia40 a value of 7/min was found under otherwise identical conditions to those in Figure 3.3 [20]. The similarity between these two turnover numbers for IfALR (encompassing steps 1-5 or 2-5 in Figure 3.1) suggests that the reduction of Mia40 by rRNase thiols (step 1) is not rate-limiting in these experiments. Figure 3.3A also shows that Mia40 is an essential mediator between rRNase and IfALR; reaction mixtures lacking either enzyme give background levels of rRNase autoxidation. Further, when the redox-active CPC motif of Mia40 is replaced with an APA sequence (Mia40<sub>APA</sub>) the oxidation of rRNase is again ablated (Figure 3.3A). The time-dependent slowing of the rate of oxidation observed in Figure 3.3A likely reflects the decreasing access to substrate thiols as the number of disulfides accumulates, as is observed with the oxidation of rRNase catalyzed by QSOX [46-48].

Figure 3.3B shows comparable experiments performed with reduced lysozyme. As observed previously the inclusion of 3 M urea was necessary to avoid precipitation of the unfolded reduced protein. Clearly, the presence of both Mia40 and IfALR were required for significant thiol oxidation in aerobic solution. The turnover number calculated from the initial rate of disulfide bond generation was  $10 \pm 0.4$  /min/per IfALR active site comparable to that obtained for rRNase. Finally, RfBP is a secreted protein with a much more complicated disulfide connectivity than that of RNase or lysozyme. However, upon reduction of this 9-disulfide protein it also becomes a competent substrate in the Mia40/IfALR system with a turnover number of  $11.4 \pm 1.1$  disulfides/min/IfALR active site (Figure 3.3C). In summary, Figure 3.3 shows that

Mia40 can efficiently mediate the transfer of reducing equivalents from diverse non-cognate substrates directly to lfALR.

### **3.3.2 Reduced RNase interacts with oxidized Mia40**

Schmidt and coworkers have used rapid reaction approaches to study the interaction between Mia40 and wild-type and mutant forms of its cognate partner reduced COX17. Utilizing single cysteine mutants of Cox17 they reported apparent rate constants for formation of a mixed disulfide with Mia40 of between 0.12 and 55/s following a rapid pre-equilibrium binding step (with  $K_d$  values from  $\sim 1$  to  $\sim 50 \mu\text{M}$ ; [36]). It was not the purpose of this work to conduct a detailed characterization of the interaction between a reduced unfolded non-cognate substrate and Mia40. Here we are only interested in evaluating whether the interaction between Mia40 and reduced substrate is sufficiently rapid to support the turnover numbers obtained for the experiments in Figure 3.3. We chose rRNase because it does not contain tryptophan residues thus allowing the reaction to be followed more readily. In addition to mixed disulfide bond formation the release of free reduced Mia40 would result in a further increase in the fluorescence of the TRP residue adjacent to the CPC redox active motif [27, 36]. Under pseudo first-order conditions the reaction between  $0.5 \mu\text{M}$  oxidized Mia40 and a 50-fold molar excess of rRNase can be fit to 3 exponentials (inset). The slowest phase (0.02/s) is too slow to be catalytically significant and was not considered further. The concentration dependence of the first and second phases are shown in the main panel of Figure 3.4. The rate constants for the fastest phase can be fit to a  $K_d$  of  $10.4 \pm 0.2 \mu\text{M}$  rRNase with a limiting constant of  $7.0 \pm 0.4/\text{s}$ . In contrast the second phase appears concentration independent over this range ( $\sim 0.36/\text{s}$ ) consistent with resolution of a mixed disulfide between Mia40 and rRNase.



Oxidized Mia40 was mixed with rRNase at 25 °C in a stopped flow spectrofluorimeter to give final concentrations of 0.25  $\mu\text{M}$  Mia40 and 10, 20, 25 and 50  $\mu\text{M}$  rRNase (see Methods). The main panel shows apparent first-order rate constants for first and second phases of a reaction time course that can be fit using 3 exponentials as shown in the inset for 25  $\mu\text{M}$  rRNase. The rate constant for the fast phase saturates at  $7.0 \pm 0.4/\text{s}$  with an apparent  $K_d$  of  $10.4 \pm 0.2 \mu\text{M}$ . The rate constant for the second phase shows insignificant concentration dependence in panel A (averaging  $\sim 0.36/\text{s}$ ). The third phase of  $\sim 0.02/\text{s}$  is significantly slower than the overall turnover number for RNase oxidation ( $\sim 0.15/\text{s}$ ) and was not considered further here.

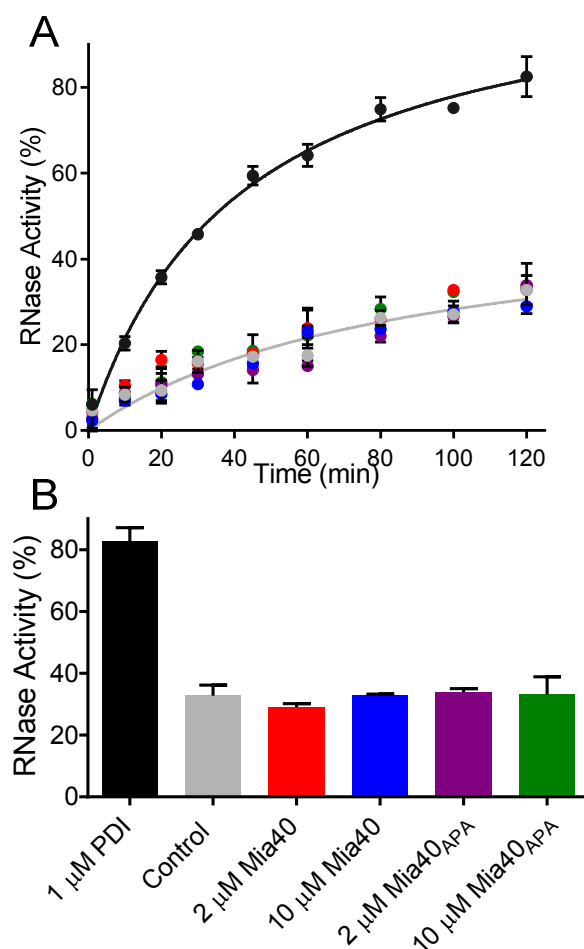
**Figure 3.4: Reduction of Mia40 by RNase.**

Importantly, both processes are fast enough to ensure that the reduction of Mia40 by rRNase is not a serious limitation to the overall oxidation depicted in Figure 3.1 (the overall turnover in Figure 3.3A corresponds to 0.15/s). In sum Mia40 is effectively reduced by a reduced protein lacking ITS sequences [29, 30] at a rate that can support the oxidase activity of IfALR. Further, the  $K_d$  values and rate of disulfide exchange reactions for the non-cognate substrate, rRNase, are comparable to those reported previously for the interaction between reduced Cox17 and Mia40 [36].

### 3.3.3 Does Mia40 show significant protein disulfide isomerase activity?

There has been considerable discussion regarding the need for a protein disulfide isomerase activity in the context of oxidative protein folding within the IMS [16, 31, 32, 35]. While a number of IMS client proteins have simple patterns of disulfide connectivity, and might therefore not require a dedicated isomerase, others proteins show more complicated folds and contain multiple disulfide bonds. In an interesting prior study, Koch and Schmid followed the oxidative refolding of 5  $\mu\text{M}$  rRNase in the presence of 2  $\mu\text{M}$  Mia40 and a glutathione redox buffer (3 mM GSH/0.3 mM GSSG). The regain of enzymatic activity observed over corresponding controls (amounting to  $\sim 25\%$  over 5 h) was very modest considering that the substrate RNase was only present at a 2.5-fold higher concentration over Mia40.

A more stringent assessment of isomerase activity of thiol/disulfide oxidoreductases follows their ability to correct disulfide pairings starting with a fully oxidized RNase populated by random pairings. Scrambled RNase (sRNase; see Methods) shows  $\sim 1\%$  residual activity, as would be expected for a protein containing 4 disulfide bonds. Figure 3.5 uses sRNase in the presence of a GSH/GSSG redox buffer to compare the isomerase activity of protein disulfide isomerase (PDI) to that of Mia40. Using 1  $\mu\text{M}$  PDI, half-maximal RNase activity was recovered in  $\sim 35$  min (Figure 3.5A) with  $83 \pm 5\%$  activity regained in 2h (Figure 3.5B). These activities need to be compared to controls without PDI because the GSH/GSSG redox buffer can directly stimulate non-enzymatic disulfide exchange reactions [49]; in Figure 3.5B, this non-enzymatic component amounts to  $33 \pm 3\%$  activity over 2 h. Importantly, Mia40 proved a negligible isomerase towards sRNase at both 2 and 10  $\mu\text{M}$  (Figure 3.5A and B). Figure 3.5 also shows, as expected, that the redox-inactive Mia40<sub>APA</sub> construct was similarly ineffective at promoting disulfide exchange.

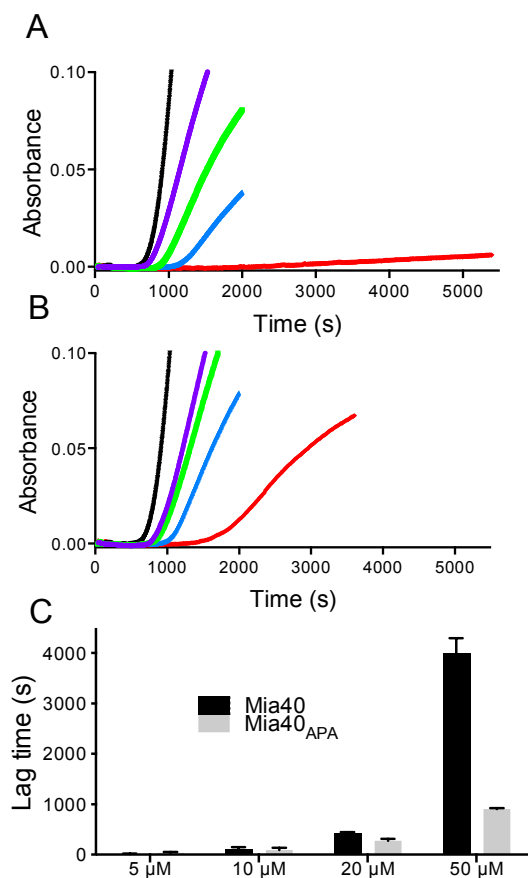


Panel A: mixtures containing 50  $\mu$ M scrambled RNase in 50 mM phosphate buffer, pH 7.5 containing 3 mM GSH and 0.3 mM GSSG, were incubated at 25  $^{\circ}$ C with 1  $\mu$ M PDI (black circles), without (grey), with 2  $\mu$ M Mia40 (red), 10  $\mu$ M Mia40 (blue), 2  $\mu$ M Mia40<sub>APA</sub>(purple) or 10  $\mu$ M Mia40<sub>APA</sub> (green circles). Aliquots were withdrawn and measured for RNase activity (see Methods). The average activity of 3 independent reactions is plotted in Panel A and the values recorded after 2 h are summarized in Panel B.

**Figure 3.5: Isomerization of scrambled RNase.**

It could be argued that Mia40 would be a better catalyst for the isomerization of bona-fide IMS substrates. However Mia40 has been shown to be a poor isomerase

towards scrambled Cox17 in the presence of the same redox buffer used in Figure 3.5 [35]. The Cox17 construct employed for those experiments contained two structural disulfides and no free cysteine residues. Given the permissive conditions used for that experiment (10  $\mu$ M Mia40, 30  $\mu$ M scrambled Cox17 in the presence of 3 mM GSH and 0.3 mM GSSG over 6 h), and the fact that there are only 3 ways to pair 4 cysteine residues, the comparative ineffectiveness of Mia40 in correcting scrambled Cox17 is striking. In summary, Mia40 is ineffective as an isomerase under these conditions towards either cognate proteins with simple disulfide patterns or against non-cognate proteins with more complicated disulfide connectivities.



A solution of 50 μM insulin in 50 mM phosphate buffer, pH 7.5, containing 1 mM EDTA was incubated at 25 °C with 5 mM DTT. Reduction of the two interchain disulfide bonds in insulin leads to the development of turbidity (followed at 600 nm) following a lag phase of ~ 600 s under these conditions (Figure 3.6A). Increasing concentrations of Mia40 (5- 50 μM ) markedly lengthen the lag phase as shown in panel A. Panel B shows the corresponding behavior of the redox-inactive Mia40<sub>APA</sub> construct. Reactions including 0, 5, 10, 20, and 50 μM Mia40, or Mia40<sub>APA</sub>, are shown as black, purple, green, blue, and red traces respectively in panels A and B. In both panels the traces represent the average between two consecutive runs. Panel C: For each indicated Mia40 or Mia40<sub>APA</sub> concentration, the bars reflect the additional lag time required for incubations to reach an absorbance of 0.05 at 600 nm over the corresponding control (black lines panel A and B).

**Figure 3.6: Insulin turbidity assay by Mia40.**

Finally, a range of thiol/disulfide oxidoreductases, including PDI itself, have been characterized by their ability to catalyze the reduction of insulin driven by low concentrations of glutathione, DTT or other disulfide reductants [50-52]. Reduction of the two interchain disulfide bonds between A and B chains of insulin leads to aggregation of the poorly-soluble B chain [53]. The time required for the onset of turbidity has been widely used for assays of PDI activity [39, 54-58]. However, implementation of the insulin reductase assay with Mia40 provided a strikingly different behavior from that found with PDI. Rather than accelerate the onset of turbidity, Figure 3.6A shows that increasing concentrations of Mia40 impede insulin B-chain aggregation; when Mia40 and insulin are equimolar the reaction becomes very slow. The redox-inactive Mia40<sub>APA</sub> form has a less pronounced effect (Panel B) but still significantly retards the onset of turbidity in a concentration-dependent way (Panel C). These data strongly suggest that the isolated reduced insulin B chain can be sequestered by binding to the hydrophobic cleft on Mia40 even in the absence of mixed-disulfide bond formation. It is notable that a previous study identified the ability of Mia40 to bind non-cysteine containing peptides in a form of Atp23 [31]. Further Mia40 has been recognized for its holdase /chaperone activities [27, 31, 32]. On a more practical level, our data shows that the widely-used insulin reductase activity can be undermined by sequestration of B-chains via a combination of hydrophobic binding and covalent mixed disulfide bond formation. Hence the ability of an oxidoreductase to accelerate the reduction of insulin disulfides assessed by this standard turbidometric method might be masked by the tendency of the hydrophobic B-chain to bind to the enzyme under examination.

### 3.4 Conclusions

While the ITS plays an important role in the import of a range of proteins destined for the IMS, our studies reinforce earlier suggestions that it is not an obligatory requirement for oxidative folding at that locale. We report turnover numbers for the insertion of disulfides into non-cognate substrates by the Mia40/IfALR system, and show that overall oxidation is not limited by the transfer of reducing equivalents from unfolded substrates to Mia40. In view of the general lack of substrate specificity observed in this work, all proteins transiting the IMS en route to their final location are potential substrates of the Mia40/IfALR system. However oxidation might be prevented by efficient sequestration during interactions with translocases [12, 13, 59] or chaperones [59, 60], or might be reversed via IMS-resident reductase systems [23, 61-63]. In terms of an expanding role for the Mia40/IfALR system, it is interesting to note that a mitochondrial matrix protein Mrp10 contains two disulfide bonds that are inserted during transit through the IMS [34].

Finally, the minimal isomerase activity observed for a simple potential substrate, scrambled Cox17, and the more challenging example studied here, sRNase, shows that IMS proteins with complex disulfide connectivities would likely need a more proficient isomerase activity to fold correctly. An interesting question for future investigation is the molecular basis for the essential inactivity of Mia40 as an isomerase when benchmarked against PDI itself. Both proteins have redox active disulfide motifs that are solvent accessible; both provide areas of hydrophobic surface for substrate binding, both can be readily reduced by unfolded reduced proteins and both form mixed disulfides with their redox clients. Exploring this question should lead to a more nuanced understanding of both these thiol/disulfide oxidoreductases catalysts of oxidative protein folding.

## REFERENCES

1. Coppock, D.L., D. Cina-Poppe, and S. Gilleran, The Quiescin Q6 gene (QSCN6) is a fusion of two ancient gene families: thioredoxin and ERV1. *Genomics*, 1998. **54**(3): p. 460-468.
2. Hooper, K.L., et al., Homology between egg white sulfhydryl oxidase and quiescin Q6 defines a new class of flavin-linked sulfhydryl oxidases. *J. Biol. Chem.*, 1999. **274**(45): p. 31759-62.
3. Thorpe, C., et al., Sulfhydryl oxidases: emerging catalysts of protein disulfide bond formation in eukaryotes. *Arch Biochem Biophys*, 2002. **405**(1): p. 1-12.
4. Kodali, V.K. and C. Thorpe, Oxidative protein folding and the Quiescin-sulfhydryl oxidase family of flavoproteins. *Antioxid Redox Signal*, 2010. **13**(8): p. 1217-30.
5. Lee, J., G. Hofhaus, and T. Lisowsky, *Erv1p from Saccharomyces cerevisiae is a FAD-linked sulfhydryl oxidase*. *FEBS Letters*, 2000. **477** (1-2): p. 62-66.
6. Thorpe, C. and D.L. Coppock, Generating disulfides in multicellular organisms: Emerging roles for a new flavoprotein family. *J Biol Chem*, 2007. **282**: p. 13929-13933.
7. Heckler, E.J., et al., Human quiescin-sulfhydryl oxidase, QSOX1: probing internal redox steps by mutagenesis. *Biochemistry*, 2008. **47**(17): p. 4955-63.
8. Fass, D., *The Erv family of sulfhydryl oxidases*. *Biochim Biophys Acta*, 2008. **1783**(4): p. 557-66.
9. Heckler, E.J., et al., *Generating disulfides with the Quiescin-sulfhydryl oxidases*. *Biochim Biophys Acta*, 2008. **1783**(4): p. 567-77.
10. Chacinska, A., et al., Importing mitochondrial proteins: machineries and mechanisms. *Cell*, 2009. **138**(4): p. 628-44.
11. Sideris, D.P. and K. Tokatlidis, *Oxidative protein folding in the mitochondrial intermembrane space*. *Antioxidants & Redox Signaling*, 2010. **13**(8): p. 1189-204.

12. Fischer, M. and J. Riemer, *The mitochondrial disulfide relay system: roles in oxidative protein folding and beyond*. International journal of cell biology, 2013. **2013**: p. 742923.
13. Wenz, L.S., et al., *Cooperation of protein machineries in mitochondrial protein sorting*. Biochimica et biophysica acta, 2015. **1853**(5): p. 1119-1129.
14. Riemer, J., N. Bulleid, and J.M. Herrmann, *Disulfide formation in the ER and mitochondria: two solutions to a common process*. Science, 2009. **324**(5932): p. 1284-7.
15. Herrmann, J.M. and R. Kohl, Catch me if you can! Oxidative protein trapping in the intermembrane space of mitochondria. J Cell Biol, 2007. **176**(5): p. 559-63.
16. Deponte, M. and K. Hell, Disulfide bond formation in the intermembrane space of mitochondria. J Biochem, 2009. **146**(5): p. 599-608.
17. Chacinska, A., et al., Essential role of Mia40 in import and assembly of mitochondrial intermembrane space proteins. Embo J, 2004. **23**(19): p. 3735-46.
18. Mesecke, N., et al., A disulfide relay system in the intermembrane space of mitochondria that mediates protein import. Cell, 2005. **121**(7): p. 1059-69.
19. Farrell, S.R., and Thorpe, C., Augmenter of liver regeneration: a flavin dependent sulfhydryl oxidase with cytochrome C reductase activity. Biochemistry, 2005. **44**(5): p. 1532-1541.
20. Daithankar, V.N., S.R. Farrell, and C. Thorpe, Augmenter of liver regeneration: substrate specificity of a flavin-dependent oxidoreductase from the mitochondrial intermembrane space. Biochemistry, 2009. **48**(22): p. 4828-37.
21. Ang, S.K. and H. Lu, Deciphering structural and functional roles of individual disulfide bonds of the mitochondrial sulfhydryl oxidase Erv1p. J Biol Chem, 2009. **284**(42): p. 28754-61.
22. Guo, P.C., et al., Structure of yeast sulfhydryl oxidase Erv1 reveals electron transfer of the disulfide relay system in the mitochondrial intermembrane space. The Journal of biological chemistry, 2012.

23. Bien, M., et al., Mitochondrial disulfide bond formation is driven by intersubunit electron transfer in Erv1 and proofread by glutathione. *Molecular cell*, 2010. **37**(4): p. 516-28.
24. Banci, L., et al., An Electron-Transfer Path through an Extended Disulfide Relay System: The Case of the Redox Protein ALR. *Journal of the American Chemical Society*, 2012.
25. Banci, L., et al., *Molecular recognition and substrate mimicry drive the electron-transfer process between MIA40 and ALR*. *Proceedings of the National Academy of Sciences of the United States of America*, 2011. **108**(12): p. 4811-6.
26. Banci, L., et al., Molecular chaperone function of Mia40 triggers consecutive induced folding steps of the substrate in mitochondrial protein import. *Proceedings of the National Academy of Sciences of the United States of America*, 2010. **107**(47): p. 20190-5.
27. Banci, L., et al., MIA40 is an oxidoreductase that catalyzes oxidative protein folding in mitochondria. *Nat Struct Mol Biol*, 2009. **16**(2): p. 198-206.
28. Endo, T., K. Yamano, and S. Kawano, *Structural basis for the disulfide relay system in the mitochondrial intermembrane space*. *Antioxidants & Redox Signaling*, 2010. **13**(9): p. 1359-73.
29. Milenkovic, D., et al., Identification of the Signal Directing Tim9 and Tim10 into the Intermembrane Space of Mitochondria. *Molecular Biology of the Cell*, 2009. **20**(10): p. 2530-2539.
30. Sideris, D.P., et al., A novel intermembrane space-targeting signal docks cysteines onto Mia40 during mitochondrial oxidative folding. *Journal of Cell Biology*, 2009. **187**(7): p. 1007-1022.
31. Weckbecker, D., et al., Atp23 biogenesis reveals a chaperone-like folding activity of Mia40 in the IMS of mitochondria. *Embo Journal*, 2012. **31**(22): p. 4348-4358.
32. Chatzi, A. and K. Tokatlidis, The mitochondrial intermembrane space: a hub for oxidative folding linked to protein biogenesis. *Antioxidants & Redox Signaling*, 2013. **19**(1): p. 54-62.
33. Banci, L., et al., Anamorsin is a [2Fe-2S] cluster-containing substrate of the Mia40-dependent mitochondrial protein trapping machinery. *Chemistry & biology*, 2011. **18**(6): p. 794-804.

34. Longen, S., et al., The disulfide relay of the intermembrane space oxidizes the ribosomal subunit mrp10 on its transit into the mitochondrial matrix. *Developmental cell*, 2014. **28**(1): p. 30-42.
35. Koch, J.R. and F.X. Schmid, Mia40 combines thiol oxidase and disulfide isomerase activity to efficiently catalyze oxidative folding in mitochondria. *Journal of molecular biology*, 2014. **426**(24): p. 4087-98.
36. Koch, J.R. and F.X. Schmid, Mia40 targets cysteines in a hydrophobic environment to direct oxidative protein folding in the mitochondria. *Nature communications*, 2014. **5**: p. 3041.
37. Schaefer-Ramadan, S.A., S.A. Gannon, and C. Thorpe, Human Augmenter of Liver Regeneration; probing the catalytic mechanism of a flavin-dependent sulfhydryl oxidase. *Biochemistry*, 2013: p. in press.
38. Israel, B.A., V.K. Kodali, and C. Thorpe, Going through the Barrier: coupled disulfide exchange reactions promote efficient catalysis in Quiescin sulfhydryl oxidase. *The Journal of biological chemistry*, 2014. **289**(8): p. 5274-84.
39. Sapra, A., D. Ramadan, and C. Thorpe, Multivalency in the inhibition of oxidative protein folding by arsenic(III) species. *Biochemistry*, 2015. **54**(2): p. 612-21.
40. Eyer, P., et al., Molar absorption coefficients for the reduced Ellman reagent: reassessment. *Anal. Biochem.*, 2003. **312**(2): p. 224-227.
41. Gasteiger, E., et al., *ExpASY: the proteomics server for in-depth protein knowledge and analysis*. *Nucleic Acids Research*, 2003. **31**(13): p. 3784-3788.
42. Rancy, P.C. and C. Thorpe, Oxidative Protein Folding in vitro: a Study of the Cooperation between Quiescin-sulfhydryl Oxidase and Protein Disulfide Isomerase. *Biochemistry*, 2008. **47**(46): p. 12047-56.
43. Miller, M.S. and H.B. White, 3rd, *Isolation of avian riboflavin-binding protein*. *Methods Enzymol*, 1986. **122**: p. 227-34.
44. Haber, E. and C.B. Anfinsen, Side-chain interactions governing the pairing of half-cystine residues in ribonuclease. *J Biol Chem*, 1962. **237**: p. 1839-44.
45. Johnson, K.A., Z.B. Simpson, and T. Blom, Global kinetic explorer: a new computer program for dynamic simulation and fitting of kinetic data. *Analytical biochemistry*, 2009. **387**(1): p. 20-9.

46. Hooper, K.L., et al., *A Sulfhydryl Oxidase from Chicken Egg White*. J. Biol. Chem., 1996. **271**: p. 30510-30516.
47. Hooper, K.L., et al., Sulfhydryl oxidase from egg white: a facile catalyst for disulfide bond formation in proteins and peptides. J. Biol. Chem., 1999. **274**(32): p. 22147-22150.
48. Hooper, K.L. and C. Thorpe, Egg white sulfhydryl oxidase: Kinetic mechanism of the catalysis of disulfide bond formation. Biochemistry, 1999. **38**: p. 3211-3217.
49. Lyles, M.M. and H.F. Gilbert, Catalysis of the oxidative folding of ribonuclease A by protein disulfide isomerase: dependence of the rate on the composition of the redox buffer. Biochemistry, 1991. **30**(3): p. 613-9.
50. Holmgren, A., Thioredoxin catalyzes the reduction of insulin disulfides by dithiothreitol and dihydrolipoamide. J. Biol. Chem., 1979. **254**(19): p. 9627-32.
51. Luthman, M. and A. Holmgren, *Glutaredoxin from calf thymus. Purification to homogeneity*. The Journal of biological chemistry, 1982. **257**(12): p. 6686-90.
52. Lundstrom, J. and A. Holmgren, Protein disulfide-isomerase is a substrate for thioredoxin reductase and has thioredoxin-like activity. J Biol Chem, 1990. **265**(16): p. 9114-20.
53. Sanger, F., *Fractionation of oxidized insulin*. The Biochemical journal, 1949. **44**(1): p. 126-8.
54. Smith, A.M., et al., A high-throughput turbidometric assay for screening inhibitors of protein disulfide isomerase activity. J Biomol Screen, 2004. **9**(7): p. 614-20.
55. Jasuja, R., et al., *Protein disulfide isomerase inhibitors constitute a new class of antithrombotic agents*. The Journal of clinical investigation, 2012. **122**(6): p. 2104-13.
56. Ge, J., et al., Small molecule probe suitable for in situ profiling and inhibition of protein disulfide isomerase. ACS chemical biology, 2013. **8**(11): p. 2577-85.
57. Horibe, T., et al., Discovery of protein disulfide isomerase P5 inhibitors that reduce the secretion of MICA from cancer cells. Chembiochem : a European journal of chemical biology, 2014. **15**(11): p. 1599-606.

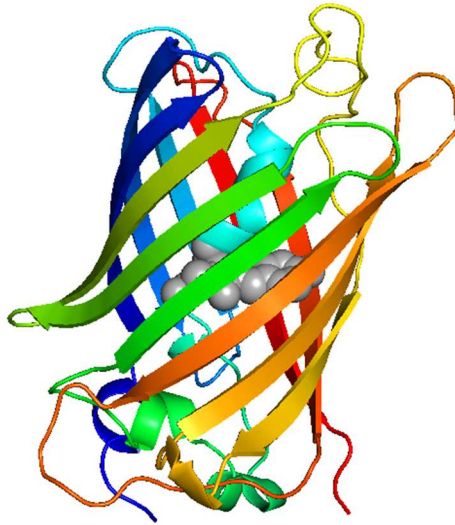
58. Xu, S., et al., Discovery of an orally active small-molecule irreversible inhibitor of protein disulfide isomerase for ovarian cancer treatment. *Proceedings of the National Academy of Sciences of the United States of America*, 2012. **109**(40): p. 16348-53.
59. Dudek, J., P. Rehling, and M. van der Laan, *Mitochondrial protein import: common principles and physiological networks*. *Biochimica et biophysica acta*, 2013. **1833**(2): p. 274-85.
60. Stojanovski, D., et al., *Mechanisms of protein sorting in mitochondria*. *Cold Spring Harbor perspectives in biology*, 2012. **4**(10).
61. Kojer, K., et al., Kinetic control by limiting glutaredoxin amounts enables thiol oxidation in the reducing mitochondrial intermembrane space. *Molecular biology of the cell*, 2015. **26**(2): p. 195-204.
62. Kojer, K. and J. Riemer, Balancing oxidative protein folding: The influences of reducing pathways on disulfide bond formation. *Biochimica et biophysica acta*, 2014.
63. Vogtle, F.N., et al., *Intermembrane space proteome of yeast mitochondria*. *Molecular & cellular proteomics : MCP*, 2012. **11**(12): p. 1840-52.

## Chapter 4

### DESIGNING FLAVOPROTEIN-GFP FUSION PROBES FOR ANALYTE-SPECIFIC RATIOMETRIC FLUORESCENCE IMAGING

#### 4.1 Introduction to Genetically Encode Fluorescent Protein Sensors

The identification of green fluorescent protein (gfp), first isolated from the light-emitting organ of the jellyfish *Aequorea Victoria*, represents a watershed moment for the study of living cells and systems [1]. The subsequent functional and structural characterization of recombinant GFP, has allowed for the development of numerous tools and probes that have revolutionized molecular biology and biochemistry [2-5]. To-date fluorescent proteins (FPs), which in a recent Pubmed (<https://www.ncbi.nlm.nih.gov/pubmed>) search have been mentioned greater than 220,000 times, have demonstrated their value in stunning variety of studies. A three-dimensional representation of a typical GFP, with its characteristic beta-barrel and core chromophore, can be seen in Figure 4.1.



The beta-barrel of green fluorescent protein is shown in rainbow. The developed chromophore is shown as grey spheres in the core of the protein. Image produced in PyMOL is based on PDB accession number, 1GFL.

**Figure 4.1: Three-dimensional structure of green fluorescent protein.**

## 4.2 Genetically Encode Fluorescent Proteins

In living systems, fluorescent proteins have been critical to understanding organization, and function of the cells; uses ranges from being used to labels cells, organelles, proteins, and nucleic acids, to demonstrating protein-protein interactions, promoter activity, enzyme activity, and changes in cellular chemical environment [6]. Genetically encoded fluorescent protein based sensors (GEFPS), based on fluorescent proteins, have been developed to allow the measurement of chemical changes in living cells. The first example of genetically encoded fluorescent protein sensor were the chimeric fusion proteins the yellow cameleons, a fusion between CFP, calmodulin, myosin light chain and YFP [7]. Since this early example of a genetically encoded

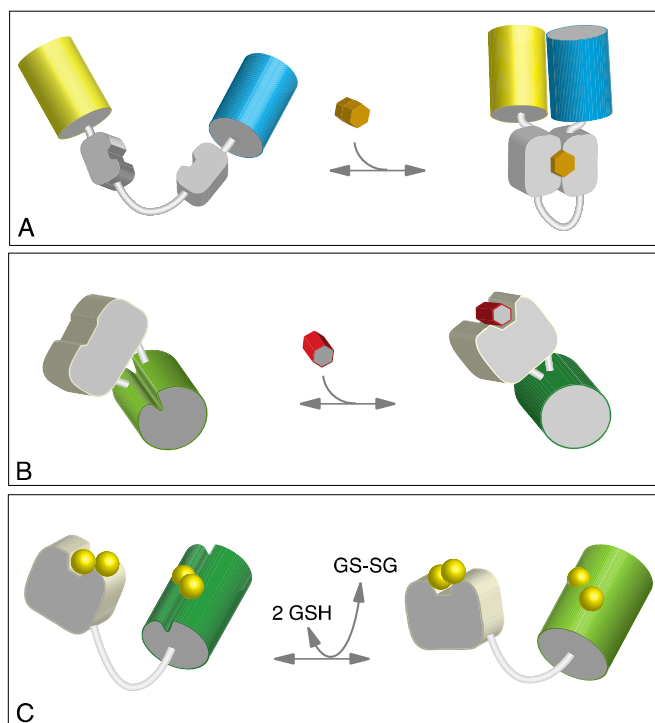
fluorescent protein sensor, multiple classes and modes of sensing have been engineered [6, 8, 9].

#### **4.2.1 Limitations and Deficits in Our Current Tools to Measure Intracellular Redox Molecule Pools**

Our current understanding of intracellular redox pools has been transformed by the development of an increasing class of genetically encoded ratiometric fluorescent probes. The study of thiols and other redox molecules in living systems have particularly hard to investigate. Historical lack of tools to investigate cellular redox molecules have plagued studies of redox biology. In many cases, the best measurement achieved for many cellular redox molecules have been from whole cell lysates [10]. These rudimentary analysis's lack compartmental-specific information, have limited temporal resolution, and are prone to postlysis artifacts such as oxidation and rogue enzyme activities [11]. The development of the roGFP based intracellular sensors and other recent redox sensors have allowed for real time monitoring of redox status, monitoring of compartment specific kinetics, and cellular redox regulation. But our current tool set to measure redox molecules is still limited [12].

Current deficits in the number of molecules that are available to measure with intracellular probes represents an opportunity for the development of new classes of tools for the advancement of redox biology. Currently, a number of tool exists to measure cellular glutathione [13],  $H_2O_2$  [14],  $NAD^+/NADH$  [15], and  $NAD^+/NADPH$  [16], but none exist for important redox couples such as ascorbate/dihydroascorbate [12], and thioredoxins [13, 17]. With these deficits in appropriate tools designed to measure these important redox molecules, and the spectrum of other biologically relevant molecules, new approaches in probe design is needed.

Genetically encoded fluorescent protein sensors for analyte-specific measurements, can be placed into three basic classes (Figure 4.2). The first group, introduced by Tsien and colleagues, [7] are the dual fluorescent protein sensors schematized in Figure 4.2A in which analyte binding modulates the Förster resonance energy transfer (FRET) efficiency between juxtaposed fluorophores. Such sensor designs have been utilized to measure diverse intracellular signals including  $\text{Ca}^{2+}$  [7],  $\text{Zn}^{2+}$  [18],  $\text{Cu}^{2+}$  [19],  $\text{Mg}^{2+}$  [20], ATP [21], glucose [22], glutamine [23], and inositol 1,4,5-trisphosphate [24].

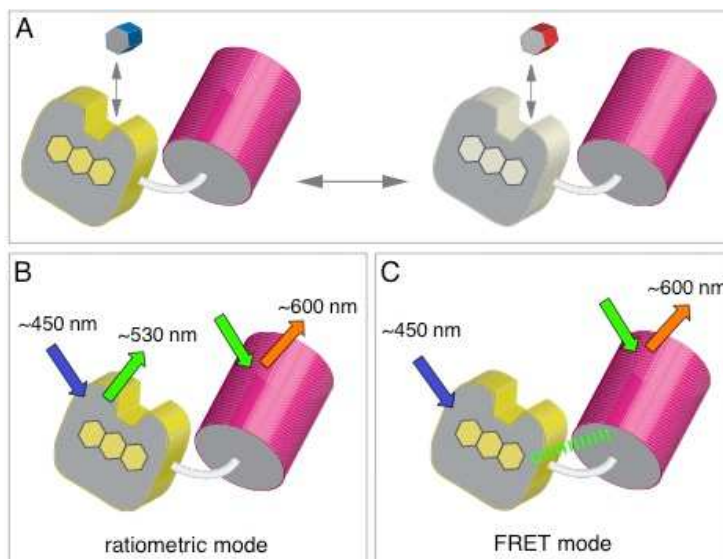


Panel A depicts FRET-based dual fluorescent protein fusion (yellow and cyan cylinders represent variants of green fluorescent protein). Panel B exploits a circularly permuted fluorescent protein fused to a ligand-binding protein (gray). Panel C shows the fusion of a thiol-transferase to a redox-responsive fluorescent protein to generate a glutathione sensor.

### **Figure 4.2: Three types of genetically encoded fluorescent protein sensors**

A second strategy for genetically-encoded sensors features a circularly permuted fluorescent protein with a ligand binding protein inserted between the new N- and C-termini. [25] Conformation changes in the sensor domain modulate the fluorescence of the construct (Figure 4.2B). These circularly-permuted fluorescent constructs have been utilized in a range of sensors including those for Ca<sup>2+</sup> [25], citrate [26], NADH [27], hydrogen peroxide [28], and R- and S-methionine sulfoxide [29].

A third sensor class are genetically encoded single fluorescent proteins incorporating a redox-active disulfide located adjacent to the fluorophore. They were first described by Winther and colleagues [30] and then later fused to the thioltransferase, glutaredoxin 1, to facilitate communication with the intracellular glutathione pool (Figure 4.2C) [31]. Remington *et al.* [32] developed an improved ratiometric probe, roGFP, now often coupled with glutaredoxins, or other thiol/disulfide oxidoreductases, for enhanced specificity towards their cognate substrates (e.g. glutathione, mycothiol, and H<sub>2</sub>O<sub>2</sub>) [33-35].



Panel A: a flavoenzyme (yellow) with strong fluorescence in its oxidized state is fused to a GFP variant (red cylinder). Interaction with a specific substrate of the flavoenzyme ablates the flavin fluorescence and provides for analyte sensing. Two modes of analysis are depicted in panels B and C. In the ratiometric mode the GFP analog is used to normalize for net concentration and spatial presentation of the probe within the sample. Suitable matching of fluorophores permits a significant FRET signal as depicted in panel C.

**Figure 4.3: A new class of genetically encoded probes.**

Figure 4.3 illustrates a new approach to analyte-specific probes based on the fusion of flavoenzymes with GFP or related fluorescent proteins. A number of flavoenzymes are notably fluorescent in their oxidized forms and this fluorescence is usually almost completely ablated on substrate-mediated reduction of the flavin chromophore [36-38]. The selectivity and rapidity that typify enzyme-substrate interactions would be anticipated to facilitate analysis of substrate/product concentration ratios in the chosen flavoenzyme half-reaction.

Fusion to the GFP analog (Figure 4.3A) provides two avenues for analysis. In the first, the GFP can be excited independent of the flavin and thus serve to normalize

the fluorescence of the flavoenzyme component (Figure 4.3B). Such ratiometric normalization has been used in a number of the genetically encoded sensors [39-41]. Alternatively, pairing the flavin donor with a suitable acceptor GFP can exploit FRET between them (Figure 4.3C); this interaction will be eliminated on quenching the fluorescence of oxidized flavin by reduction or complexation.

In this contribution, we present proof of principle for the design, characterization and application of two probes based on fluorescent flavoproteins. We introduce the first ratiometric probe for the redox state for bacterial and lower eukaryotic thioredoxins using *Escherichia coli* thioredoxin reductase. As a second example, we demonstrate sensing NAD<sup>+</sup>/NADH ratios in mammalian cells using a probe based on yeast lipoamide dehydrogenase. Finally, we discuss the performance and limitations of these flavoprotein-GFP probes and suggest avenues for extending their versatility.

### **4.3 Materials and Methods**

#### **4.3.1 Materials.**

5,5'-Dithiobis-(2-nitrobenzoic acid) (DTNB), dithiothreitol (DTT), tris(hydroxypropyl)phosphine (THP), reduced and oxidized nicotinamide adenine dinucleotides (NADH, NAD<sup>+</sup>), and the corresponding phosphorylated derivatives (NADPH, NADP<sup>+</sup>), sodium pyruvate, sodium lactate, phenylmethylsulfonyl fluoride (PMSF), leupeptin, lysozyme, and poly-L-lysine hydrobromide (30-70 KDa) were purchased from Sigma. Isopropyl β-D-1-thiogalactopyranoside (IPTG), ampicillin, and kanamycin were purchased from GoldBio. Size-exclusion PD-10 columns were purchased from GE Healthcare. Genomic DNA sequences were supplied by GeneWiz and DNA primers were from Integrated DNA Technologies.

### **4.3.2 General Procedures.**

Unless otherwise indicated, phosphate buffer containing 50 mM potassium phosphate and 1 mM EDTA adjusted to pH 7.5 was used for all experiments. Proteins were concentrated using Amicon Ultra centrifugal filter units. Visible and ultraviolet spectra were recorded on a Hewlett-Packard 8453 diode-array spectrophotometer. Cuvette fluorescence measurements were conducted on an Aminco Bowman Series 2 Luminescence Spectrometer. Confocal images were captured utilizing a Zeiss LSM 880 laser scanning confocal microscope equipped with a Plan-Neofluar 40x/1.3NA oil-immersion objective. Data were plotted and fitted using GraphPad Prism software. Protein structures were visualized using PyMOL (Schrodinger, LLC).

### **4.3.3 Protein Expression in *E. coli*.**

The expression and purification of *E. coli* thioredoxin 1 (*EcTrx1*) was as previously described.<sup>26</sup> An *E. coli*-optimized DNA sequence for the *E. coli* thioredoxin reductase-mCherry fusion (TrxR-mCherry; Supporting Information) was inserted into a pTrcHisA vector via NheI and HindIII restriction sites. The corresponding G154V mutant (TrxR<sub>GV</sub>-mCherry) was derived from the same vector using the forward and reverse primers shown in Supporting Information. *E. coli* optimized DNA sequences for the G154V mutant of TrxR-mCherry (TrxR<sub>GV</sub>-mCherry), and the LipDH-mCherry were inserted into the pET28a vector via XbaI and NcoI and NcoI and HindIII restriction sites respectively. Transformed BL21(DE3) cells were grown in Luria Bertani (LB) medium containing 50 mg/L of ampicillin (pTrcHisA vectors) or kanamycin (pET28a vectors) and induced at an optical density of 0.6 at 600 nm with 1.0 mM IPTG. After 6 h cells were collected by centrifugation (5000 g, 4 °C, 30 min). Cell pellets from 2 L of culture) were resuspended in 25 mL of

50 mM phosphate buffer, pH 7.5, containing 20% v/v glycerol, 500 mM NaCl, 1 mM phenylmethylsulfonyl fluoride (PMSF), 300  $\mu\text{g}/\text{mL}$  lysozyme, and 1  $\mu\text{M}$  leupeptin. Cells were disrupted by French press using two passes at 10,000 psi. The resulting homogenate was briefly sonicated to shear DNA and centrifuged at 17,000 g. The clarified lysate was rocked for 1 h at 4 °C with 4 mL of nickel affinity resin (Ni-NTA Agarose). The resin was loaded into a 20 mL fritted glass column and washed with 40 mL of 50 mM phosphate buffer, pH 7.5, containing 500 mM NaCl, 20% v/v glycerol followed by 40 and 20 mL of the same solution supplemented with 5 and 20 mM imidazole respectively. The protein constructs were eluted with 20 mL of 50 mM phosphate buffer, pH 7.5, containing 500 mM NaCl and 200 mM imidazole and dialyzed overnight in 50 mM phosphate buffer, pH 7.5, containing 1 mM EDTA and 20% v/v glycerol. Proteins were concentrated by centrifugal filtration to  $\sim 1$  mL and stored at -20 °C.

#### **4.3.4 Protein Handling.**

Concentrations of thioredoxin, mCherry and mRuby2 proteins were calculated using extinction coefficients of 12.9, 72 and 113  $\text{mM}^{-1}\text{cm}^{-1}$  at 280, 587 and 559 nm respectively. Because the oxidized flavin absorbance envelope does not extend beyond 530 nm, the concentrations of mRuby2 and mCherry fusion proteins were determined at 559 and 587 nm respectively. Reduced *Ec*Trx1 was prepared by incubating with a 10-fold molar excess of DTT over total cysteine residues for 1 h at 25 °C. The treated protein (0.7 mL) was then applied to a PD-10 size-exclusion column (GE Healthcare) equilibrated with phosphate buffer. Baseline separation between reduced protein and excess DTT was verified by sampling small volumes of eluent using 5,5'-dithiobis(2-nitrobenzoate) (DTNB). Completely oxidized *Ec*Trx1 was prepared by incubating the

protein, as isolated, with 10 mM potassium ferricyanide in phosphate buffer for 30 min at 25 °C, followed by removal of small molecule reagents on a PD-10 column.

#### **4.3.5 NADPH Reductase Activity of TrxR-mCherry and TrxR<sub>GV</sub>-mCherry.**

Wild type (10 nM) and mutant (1 μM) sensors were compared in a total volume of 200 μL solution containing 50 mM Tris, pH 7.5, 1 mM EDTA, 1 mM DTNB and 25 μM oxidized *EcTrx1* at 25 °C. Reactions were initiated by the addition of 100 μM NADPH. The resulting increase in absorbance was followed at 415 nm and the initial rate from 4 replicate experiments was averaged.

#### **4.3.6 In Vitro TrxR<sub>GV</sub>-mCherry Reduction Assay.**

The probe (1 μM) in 200 μL of 100 mM potassium phosphate solution, pH 7.0, containing 1 mM EDTA together with 10 mM glucose, 50 nM *Aspergillus niger* glucose oxidase and 50 nM bovine liver catalase to lower dissolved oxygen concentrations for prolonged measurements. Samples were then challenged with 10 mM DTT, 10 mM GSH, or 100 μM NADPH at 50 s. The data shown were the average of 3 experiments normalized to the same starting relative fluorescence (exciting and emitting at 456 and 520 nm respectively). The more rapid reduction of the probe with reduced thioredoxin was examined as above, but using 0.1 and 1.0 μM protein concentrations respectively.

#### **4.3.7 Thioredoxin Titration of TrxR<sub>GV</sub>-mCherry.**

Aliquots of the probe (1 μM in the same buffer system used above) were combined with mixtures of reduced and oxidized thioredoxin totaling 200 μM in 200 μL. As before, solutions were gently mixed to avoid undue re-oxygenation of the solution and the fluorescence spectra exciting at 456 nm recorded after 30 s.

#### **4.3.8 In Vivo Trx<sub>R<sub>G</sub>V</sub>-mCherry Reduction Assay.**

Keio parent strain *E. coli* cells[43] containing the probe plasmid were grown overnight in LB broth containing 50 mg/L ampicillin and 1 mM IPTG. One milliliter of an overnight culture was transferred to 10 mL of the same media and grown to an optical density of 1.0 at 600 nm. The cells were collected by centrifugation, resuspended and washed three times in M9 minimal medium before final re-suspension to an optical density of 0.4 in ice-cold M9 medium. As needed, aliquots were warmed to room temperature and mixed with 10 mM DTT, 10 mM GSH, 100  $\mu$ M NADPH or 1  $\mu$ M reduced Trx1 at 50 s to give a final volume of 200  $\mu$ L. Fluorescence measurements (excitation and emission at 456 and 520 nm, respectively) were recorded before and after the addition of reductants. Data were corrected for dilution and represent an average of 3 experiments.

#### **4.3.9 Imaging *E. coli* Cells.**

Plasmid-containing Keio *E. coli* cells were grown overnight in LB broth containing 50 mg/L ampicillin and 1 mM IPTG. A 100 mL flask containing 10 mL of the same medium was inoculated with 1 mL of starter culture. The culture was transferred with a sterile pipette, when the optical density at 600 nm reached 1.0, to an ibidi  $\mu$ -Slide VI 0.4 flow-cell device previously treated with 0.1 mg/ml poly-L-lysine hydrobromide (as described by the manufacturer). After incubation in LB medium at 37 °C for 60 min, the flow cell was transferred to the microscope stage maintained at room temperature. The flow-cell channels were washed with M9 medium at 0.5 mL/min using a syringe pump to remove non-adherent cells prior to imaging using an inverted Zeiss LSM 880 laser scanning confocal microscope equipped with a Plan-Neofluar 40x/1.3NA oil-immersion objective. The 458 and 561 nm laser lines excited

sensor flavin and mCherry fluorophores with corresponding emission band pass limits of 472-552 nm (green channel) and 588-659 nm (red channel) respectively. Images of  $512 \times 200$  pixels were captured every second and processed using Zen 2010D software (Version 7.0.0.223; see later). Where indicated, the composition of the medium flowing through the channels was supplemented with 5 mM DTT or 5 mM diamide during data acquisition.

#### **4.3.10 LipDH-mCherry Reduction and Titration Experiments.**

Reduction studies were performed as described for the thioredoxin reductase probe using 1  $\mu$ M LipDH probe with 10 mM GSH or 100  $\mu$ M NADPH and 0.2  $\mu$ M of the probe with 1  $\mu$ M NADH. Data were adjusted for dilution and the average of 3 experiments normalized to the same starting relative fluorescence. Titrations with NAD<sup>+</sup>/NADH mixtures employed the same procedure used for thioredoxin titrations of the reductase probe (see above). Samples were excited at 456 nm and the resulting fluorescence was recorded at 520 nm. Data shown represent average of 3 experiments.

#### **4.3.11 Mammalian Cell Culture and Imaging.**

Stock HEK293T cells (ATCC CRL-11268) were grown and maintained at 37 °C using 5% CO<sub>2</sub> in Dulbecco's Modified Eagle Medium (DMEM) with high glucose supplemented with 10% fetal bovine serum and 100 units/mL penicillin and streptomycin. Cells (maintained under 20 passages) were grown to 70-90% confluence, trypsinized and about 10,000 cells were used to seed the channels of an ibidi  $\mu$ -Slide VI 0.4 ibiTreat flow cell. After 24 h cells, adherent cells were transiently transfected with a human-optimized DNA sequence for LipDH-mCherry (see

Appendix) that was inserted into a pCMV-Tag2A vector using Lipofectamine 2000 treatment as per product protocol. Media was exchanged for fresh DMEM at 24 h and cells were imaged 48 h after transfection using a flow cell mounting chamber that was maintained at 37 °C in an atmosphere supplemented with 5% CO<sub>2</sub>. During measurements, cells were perfused at 0.5 mL/min with FluoroBrite DMEM (Gibco) supplemented with or without 10 mM pyruvate or lactate.

#### **4.3.12 Image and Data Processing for Bacterial and Mammalian Sensors.**

Each image was recorded in green (472-552 nm) and red (588-659 nm) channels with a ratiometric channel reflecting red divided by green signals. Images were processed using a median filter with a 5x5 kernel size. Green and red channels were false colored with green and red, and comparative images were adjusted equally to exclude over- and under-saturation. The ratiometric channel was false colored with a Rainbow2 lookup table. Using the Zen software, regions of interest containing transfected and untransfected HEK293T cells were manually selected for examination. Data were corrected for a slow photobleaching of the flavin (averaging 24% after 400 measurements). Bleaching was fit to a single exponential and used to correct the signal for the green channel. Insignificant photobleaching of the red channel was encountered over 400 s. In *E. coli*, no photobleaching correction for the TrxR<sub>GV</sub>-mCherry probe was necessary.

#### **4.3.13 Redox Measurements.**

The Nernst equation was used to convert redox potentials to the ratio of a particular redox couple,  $C_{\text{red}}/C_{\text{ox}}$  of standard redox potential,  $E^{\circ}$ :

$$\text{Redox Potential} = E^{\circ} - (RT/nF)\ln[C_{\text{red}}/C_{\text{ox}}]$$

$E^{\circ}$  values used for *E. coli* Trx1 and NAD<sup>+</sup>/NADH were -270 mV [36, 43, 44] and -320 mV [65] respectively.

For *in vivo* redox poise measurements, the fluorescence response values ( $V$ ) for complete oxidation and reduction of the sensor ( $V_{\text{ox}}$  and  $V_{\text{red}}$  respectively) were established as described in the text. The redox poise corresponding to a measured response is then:

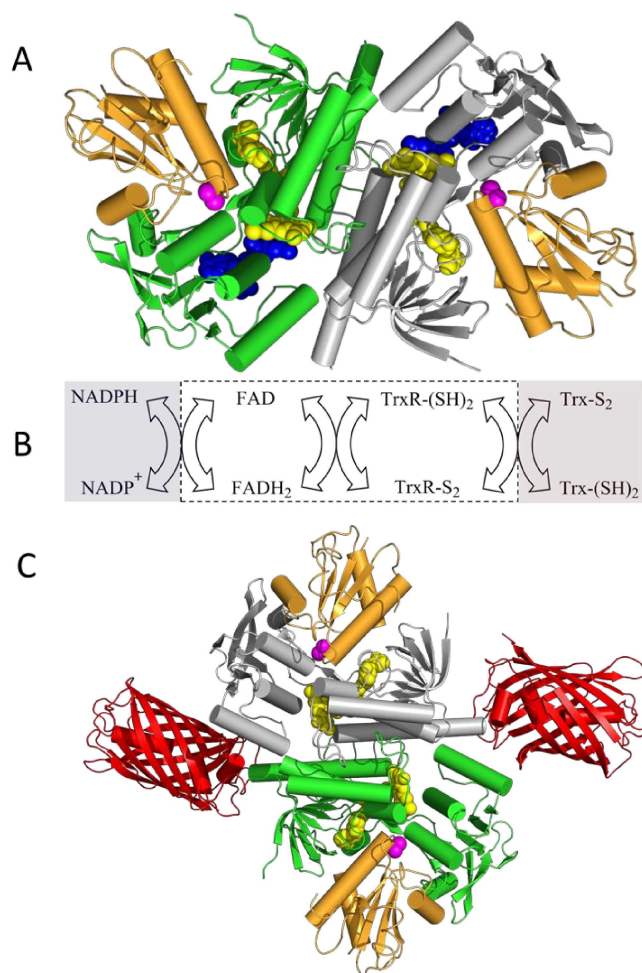
$$\text{Redox Poise} = \text{Sensor Standard Redox Potential} - (RT/nF)\ln[(V - V_{\text{ox}})/(V_{\text{red}} - V)]$$

## 4.4 Results and Discussion

### 4.4.1 Design of a New Probe for Thioredoxin Proteins.

Thioredoxin reductase is a member of the flavoprotein disulfide oxidoreductase superfamily [44-47] and plays important roles in mitigating oxidative stress and redox regulation, together with DNA synthesis and sulfur assimilation [48-52]. Each subunit of the low molecular weight homo-dimeric *E. coli* thioredoxin reductase comprises two domains depicted in Figure 4.4A [53-55]. The first domain contains a bound FAD cofactor which is appreciably fluorescence in its oxidized form. The second domain can undergo a conformation change that brings the flavin cofactor in direct contact with either NADP<sup>+</sup>/NADPH (blue), or the redox active CxxC motif in the reductase (magenta). A cleft between these domains provides for redox communication with thioredoxin (depicted in orange in Figure 4.4A). It should be

noted that there are two thioredoxins in *E. coli* (Trx1 and 2) [51, 52, 56]; both rapidly communicate with the reductase.



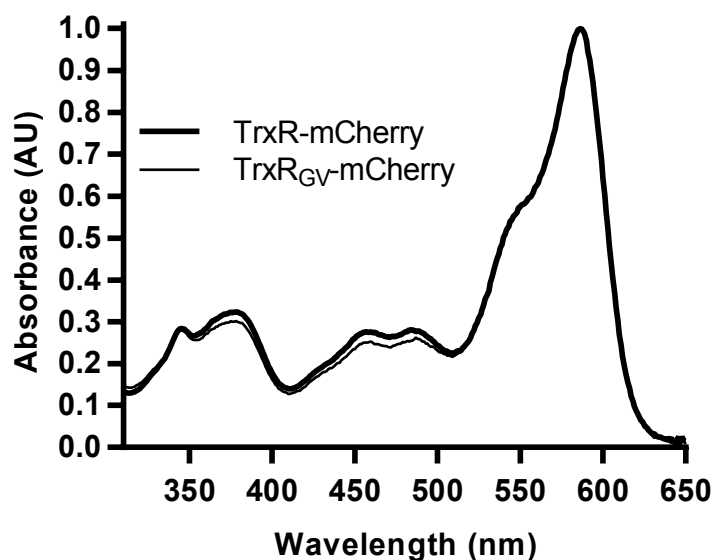
Panel A shows the three dimensional structure of *E. coli* thioredoxin reductase (PDB: 1F6M). The two subunits of this homodimer are depicted in green and grey and the bound thioredoxin (Trx1) is shown in orange. The space-filling representations of the flavin cofactor, the redox active disulfide, and the NADP+ analog, 3-aminopyridine adenine dinucleotide phosphate are in yellow, magenta, and blue respectively. Panel B shows the reductive and oxidative half-reactions without regard to protonation states of the reactants and products. The flavin and redox-active disulfide moieties of the reductase lie within the white box. Panel C is a schematic depiction of the fusion protein attached to the mCherry fluorescent protein (PDB: 2H5Q)

**Figure 4.4: *E. coli* thioredoxin reductase: structure, reactions and probe design.**

Figure 4.4B shows the overall flow of reducing equivalents; in the reductase direction, the pool of NADPH drives the reduction of oxidized intracellular thioredoxin via the mediation of flavin and a redox-active disulfide [45, 47, 57]. We describe later how communication with the NADP<sup>+</sup>/NADPH pool can be disabled to allow this probe to specifically report thioredoxin redox state.

**4.4.2 Expression and Characterization of Thioredoxin Sensors**

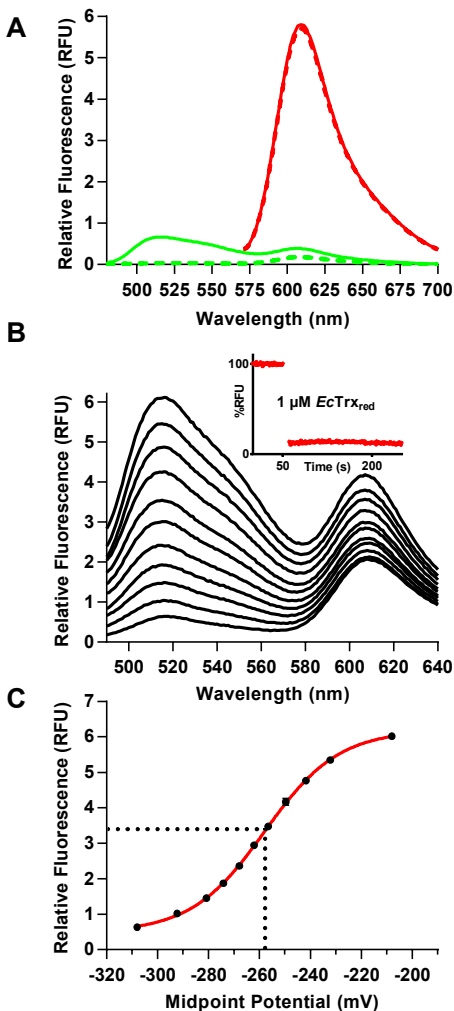
The monomeric fluorescent protein mCherry was initially chosen for the GFP domain component of the thioredoxin sensor (Figure 4.4C). The absorbance and fluorescence characteristics of the resulting *Ec*TrxR-mCherry fusion (TrxR-mCherry) suggest that it would be suitable for the ratiometric imaging depicted in Figure 4.3B. The construct (APPENDIX) was cloned into a pTrcHisA plasmid for expression in *E. coli* BL21-DE3 cells (see Methods). The protein was readily obtained in relatively high yield using the N-terminal HIS-tag. The construct was characterized by absorbance spectrum and found to contain the expected complement of flavin and mCherry (Figure 4.5)



The spectra of TrxR-mCherry and the NADPH binding-compromised mutant, TrxR<sub>GV</sub>-mCherry, were recorded in 50 mM phosphate buffer, pH 7.5, containing 1 mM EDTA. Spectra are normalized using the absorbance at 587 nm.

**Figure 4.5: UV-Vis spectrum of thioredoxin reductase-mCherry sensors.**

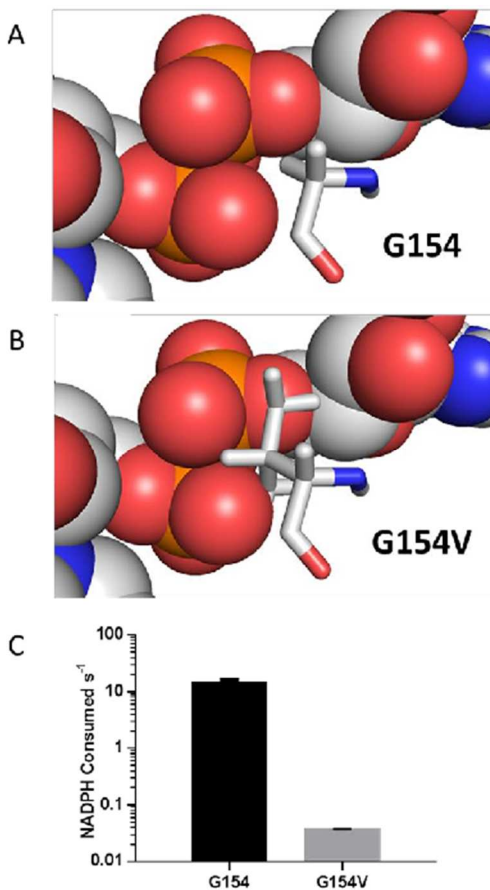
With the probe in hand it was next necessary to disable communication with NADP<sup>+</sup>/NADPH. In a related pyridine nucleotide disulfide oxidoreductase, *E. coli* glutathione reductase [44-47], replacement of a glycine for a valine in the dinucleotide binding site strongly disrupted NADP<sup>+</sup>/NADPH binding [58]. We then prepared the corresponding GLY154VAL mutation in *E. coli* TrxR (Figure 4.7) and found similar ablation of the reactivity towards NADPH ( $391 \pm 16$  fold slower from  $15.0 \pm 0.6$  to  $0.0384 \pm 0.0006$  /s NADPH oxidized/s in the DTNB reductase assay; see Methods); Figure 4.7). This mutation was utilized in all subsequent thioredoxin probes to minimize their response to the intracellular NADPH/NADP<sup>+</sup> pool (see later).



Panel A shows the emission spectra of 1  $\mu\text{M}$  of TrxR<sub>GV</sub>-mCherry before (solid line) and after reduction with 20  $\mu\text{M}$  tris-hydroxypropylphosphine (THP, dashed line; see Methods) exciting into the flavin excitation envelope (456 nm; green curves) or into the mCherry chromophore using 520 nm light (red curves). The inset to panel B shows that the probe responds rapidly to 1  $\mu\text{M}$  reduced thioredoxin. The main panel B and panel C show the response of bound flavin to ratios of reduced and oxidized thioredoxin totaling 200  $\mu\text{M}$ . The fluorescence spectra excited at 456 nm are shown in panel B and the amplitude of the 520 nm signal plotted against the redox potential of the mixture is depicted in panel C.

**Figure 4.6: Characterization of TrxR<sub>GV</sub>-mCherry.**

Emission profiles for the oxidized and reduced TrxR-G154V-mCherry probe (hereafter abbreviated TrxR<sub>GV</sub>-mCherry for convenience) are shown in Figure 4.6A. FAD and mCherry fluorophores were independently excited at 456 nm and 520 nm (green and red spectra respectively). The characteristic oxidized flavin emission centered at ~520 nm is nearly completely quenched on reduction by a water-soluble phosphine (THP) with a small residual bleed through at 610 nm reflecting minor direct excitation of mCherry. The emission spectrum of mCherry for the oxidized and reduced forms of the probe overlay (red spectra Figure 4.6A) and are therefore insensitive to the reduction of the *Ec*TrxR domain. The inset to Figure 4.6B shows that micromolar concentrations of probe and reduced Trx1 equilibrate rapidly. This facile response allows the probe to sense oxidized/reduced Trx ratios (totaling 200  $\mu$ M) as shown in Figure 4.6B and C. Calculating the redox poise of the mixtures using an  $E^{\circ}$  of -270 mV for *E. coli* Trx1 [52, 59, 60] yields a midpoint value of  $-258 \pm 1$  mV (triplicate measurements) for the probe consistent with the published midpoint potentials of the bacterial reductase [61]. The measured redox potential is likely a combination of various *Ec*TrxR redox states resulting from the similarity in redox potentials for flavin and disulfide at the 2- and 4-electron reduced level ( $E^{\circ}$  from -243 to -271 mV respectively).



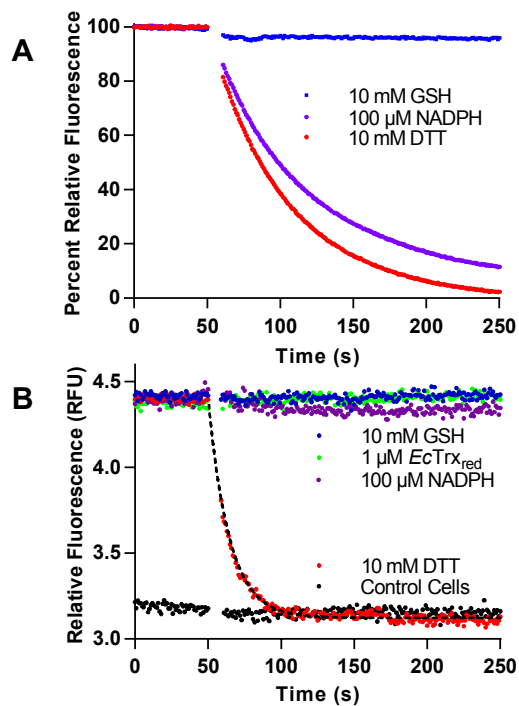
Panel A represents the pyrophosphate moiety of an NADPH analog (red and orange spheres) bound to *E. coli* thioredoxin reductase (PDB 1F6M) with the glycine at position 154 depicted in stick representation. Panel B depicts an in-silico G154V mutation at this position with the expected steric clash between the valine side chain and the pyrophosphate of the pyridine nucleotide. Panel C shows the NADPH reductase activity of native *Ec*TrxR (see Methods) is reduced by  $391 \pm 16$  fold on replacement of G154 by a valine residue.

**Figure 4.7: Suppressing NADPH activity in *E. coli* thioredoxin reductase.**

#### 4.4.3 Thioredoxin Sensor Responds to Intracellular Thioredoxin.

Figure 4.8A shows that TrxR<sub>GV</sub>-mCherry is refractory to reduction by 10 mM GSH and is reduced comparatively slowly by 10 mM DTT. The probe carrying the GLY/VAL mutation is sluggishly reduced by 100  $\mu\text{M}$  NADPH in accord with the data

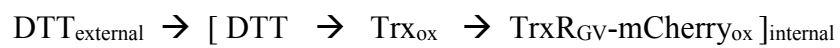
presented earlier (Figure 4.7). *E. coli* thioredoxin reductase is specific for NADPH over NADH [62] and so the probe would be unable to effectively directly communicate with either pyridine nucleotide analog *in vivo*.

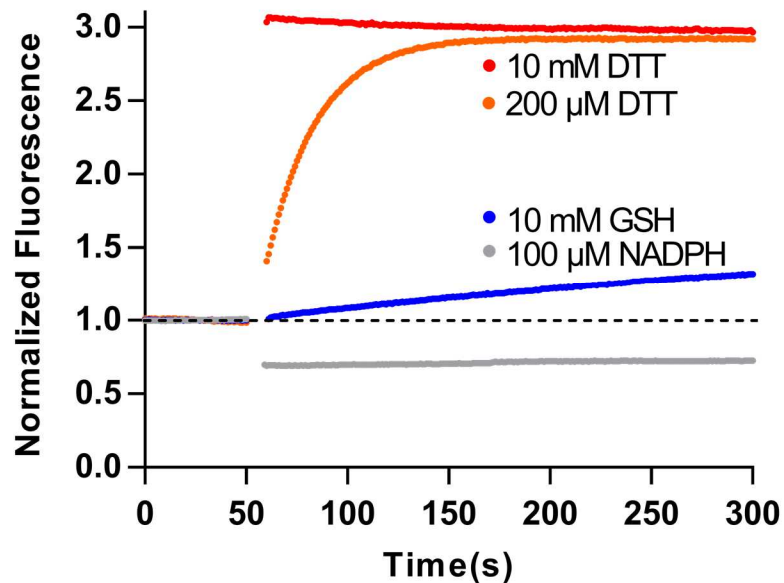


Panel A shows the fluorescence of 1  $\mu\text{M}$  probe mixed at 50 s with 10 mM of GSH or DTT or with 0.1 mM NADPH. Reduction for DTT and NADPH show half-times of  $37 \pm 2$  s and  $48 \pm 2$  s respectively were these analyzed by exponential fit. Panel B represents the fluorescence of *E. coli* cells expressing the thioredoxin probe before and after the addition of the indicated reagents. The lower lines represent a corresponding *E. coli* strain lacking the plasmid for Trx<sub>GV</sub>-mCherry.

**Figure 4.8: Reduction of Trx<sub>GV</sub>-mCherry in vitro and in *E. coli*.**

The sluggish response towards NADPH, and the non-reactivity of TrxR towards GSH provide the impetus to evaluate the probe in *E. coli*. We first examined a suspension of live bacterial cells expressing TrxR<sub>GV</sub>-mCherry in a conventional fluorimeter cuvette (see Methods). Figure 4.8B shows that the indicated concentrations of GSH, NADPH and reduced thioredoxin were ineffective when added to live bacterial cells suspended in M9 minimal media (see Methods). In contrast DTT, being membrane permeant, [63-65] is an effective reductant of the probe in *E. coli*. In this case reduction is about 4-fold faster than that recorded for the probe using the same concentration of DTT (Figure 4.8A). This acceleration of the reduction of intracellular probe likely reflects the mediation of cytosolic thioredoxins following their reduction by internalized DTT:

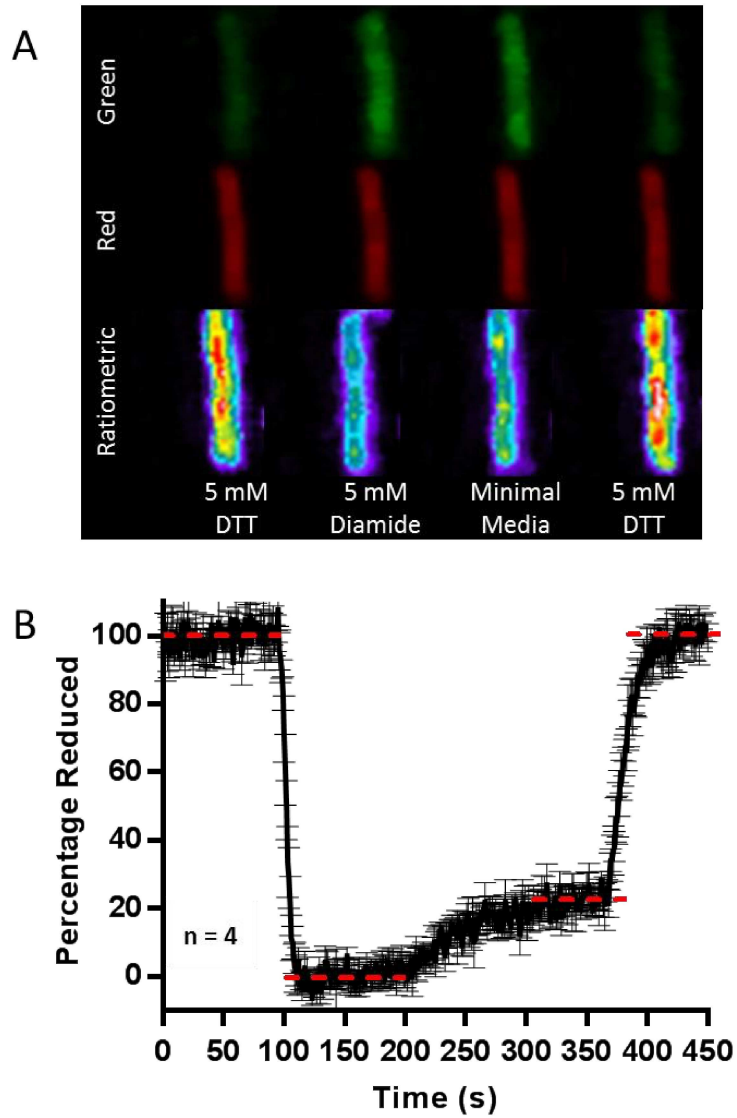




Solutions of 5  $\mu\text{M}$  Trx1 (in 200  $\mu\text{L}$  of 50 mM phosphate buffer, pH 7.5, 25  $^{\circ}\text{C}$ ) were monitored by fluorescence (excitation 290 nm with emission at 350 nm). Potential reductants (100  $\mu\text{M}$  NADPH, 10 mM GSH, 200  $\mu\text{M}$  or 10 mM DTT) were added at 50 s. The lines represent an average of 3 experiments normalized relative to unit initial fluorescence.

**Figure 4.9: Reduction of *Ec*Trx1 followed by tryptophan fluorescence.**

Control experiments confirmed that the direct reduction of Trx1 by DTT is rapid (Figure 4.9). Figure 4.8B also shows that a suspension of the corresponding *E. coli* strain lacking the plasmid for the probe (bottom horizontal data points) is completely unresponsive to treatment with DTT and the other reagents used above. Thus background cellular autofluorescence does not complicate these measurements.

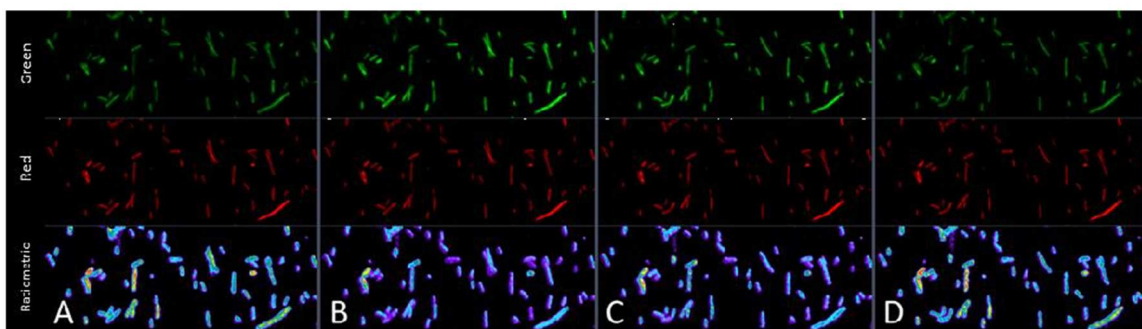


Panel A displays sensor emission of three channels (green, red and ratiometric) of a single *E. coli* cell. Panel B depicts a quantification of the average of four replicate experiments using the ratiometric channel to express the percentage of TrxR<sub>GV</sub>-mCherry reduction.

**Figure 4.10: Interrogating Thioredoxin Redox Poise in Live *E. coli* cells.**

#### 4.4.4 TrxR<sub>GV</sub>-mCherry Sensor Imaged in Live *E. coli* Cells.

Figure 4.10A shows confocal images of an *E. coli* cell expressing TrxR<sub>GV</sub>-mCherry located on the bottom face of a flow chamber. Over 450 s the cell is treated with a series of redox-active permeant reagents dissolved in M9 minimal media. The sensor flavin and mCherry reference were excited using 458 and 561 nm laser lines and the ratiometric channel represents a division of the red by the green channel responses (see Methods). To establish fully reduced and oxidized limiting states, attached bacterial cells were first equilibrated with M9 media containing 5 mM DTT (Figure 4.10) and then exposed to the strong thiol oxidant diamide [66-68] for the next 100 s. Diamide, at 5 mM, effects a rapid recovery of flavin fluorescence (Figure 4.10B; green channel). Diamide was removed by washing with minimal media allowing the intracellular thioredoxin pool to be visualized before the addition of 5 mM DTT to return the cells to their fully reduced state. Throughout the insensitivity of the red channel to cellular redox state (e.g. Figure 4.10A) allowed the red channel to serve as a crucial correction factor for confocal drift and cellular movement as described in Figure 4.3B. A wider field of view captured during the experiment in Figure 4.10 is presented in (Figure 4.11).



Cells were allowed to adhere to the base of poly-L-lysine treated ibidi flow cells. The wells were serially infused with M9 media containing 5 mM DTT, 5 mM diamide, medium alone, and finally 5 mM DTT (Panels A-D, respectively).

**Figure 4.11: Confocal field of view of *E. coli* cells expressing TrxR<sub>GV</sub>-mCherry sensor.**

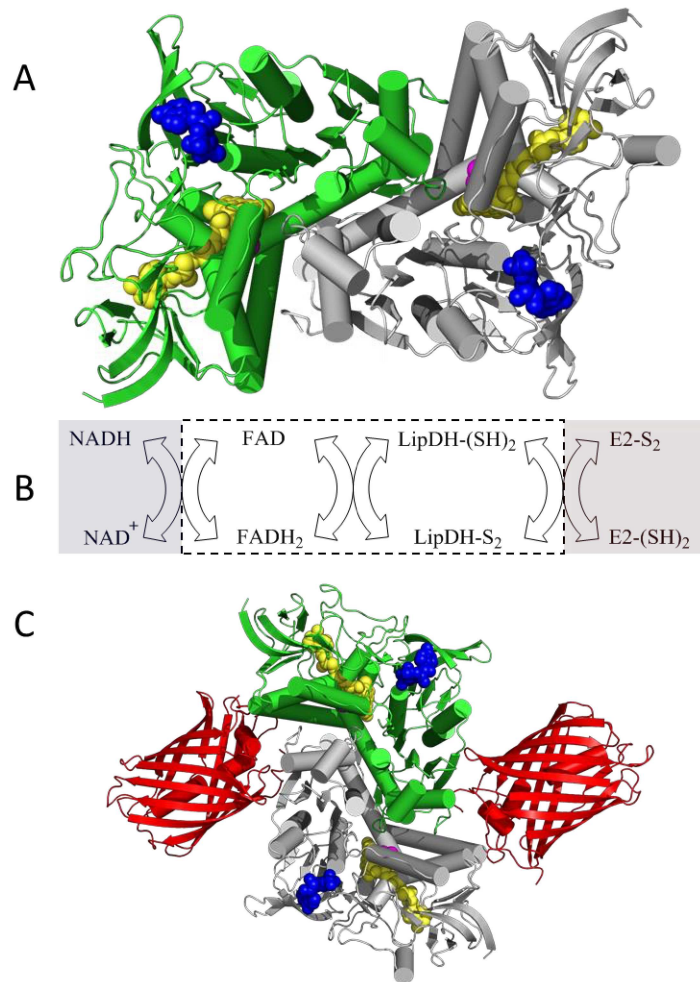
Figure 4.10B shows the quantification of the average of four replicate experiments using the ratiometric channel to express the percentage of TrxR<sub>GV</sub>-mCherry reduction. Utilizing the minimum and maximum limits for the sensor in Figure 4.10B (see Methods), the steady state of the thioredoxin pool in *E. coli* strain used in this work was  $-242 \pm 2$  mV (Figure 4.10B, 4 determinations; see Methods). Under normal, non-stressed, conditions, Trx1 levels are 5- to 15-fold more abundant than Trx2 [49, 69] and therefore Trx1 would be expected to dominate the thioredoxin redox poise. Using a value of  $-270$  mV [52, 59] for the redox potential of Trx1 allows estimation of a 9:1 ratio of oxidized:reduced thioredoxin in *E. coli*. These data are consistent with pioneering work of Holmgren and Fagerstedt [70] who found corresponding ratios of 9:1 to 3:2 oxidized:reduced in quenched extracts of *E. coli*.

While a number of organisms, including bacteria, yeast and plants have thioredoxin/thioredoxin reductase systems resembling that employed above [71, 72],

the TrxR<sub>GV</sub>-mCherry sensor will not communicate effectively with mammalian thioredoxins [71, 72]. The latter electron carriers interact with their cognate mechanistically divergent high molecular weight thioredoxin reductase via a C-terminal cysteine-selenocysteine dipeptide [47, 72].

#### **4.5 Design of a New Probe for NAD<sup>+</sup>/NADH**

To explore whether a flavoenzyme-mCherry fusion could be constructed to sense a key redox pair in mammalian cells we exploited the intrinsic fluorescence of yeast lipoamide dehydrogenase (LipDH) to afford a facile and responsive sensor for NADH/NAD<sup>+</sup>. LipDH is a key enzyme best known for its involvement in role in the pyruvate dehydrogenase,  $\alpha$ -ketoglutarate dehydrogenase, branched chain amino acid dehydrogenase and glycine cleavage multienzyme complexes [73, 74]. We used LipDH from *Saccharomyces cerevisiae* in this work.



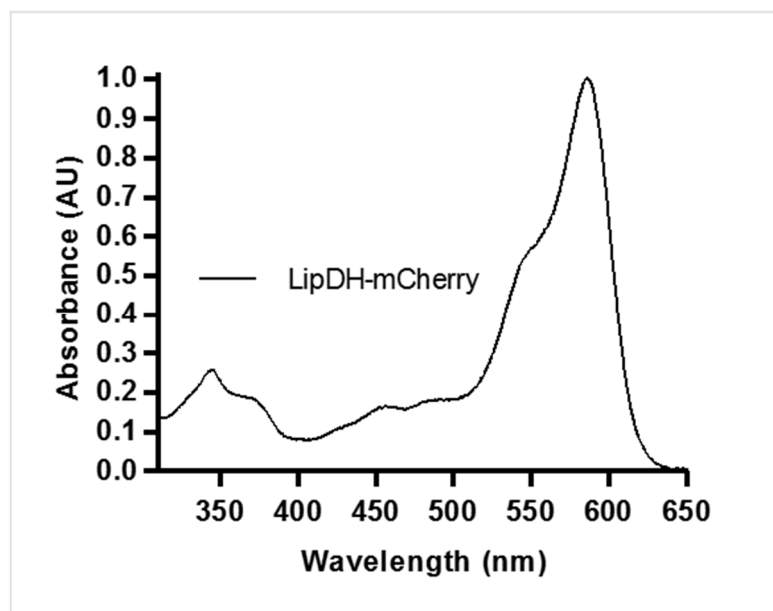
Panel A shows the three dimensional structure of *S. cerevisiae* lipoamide dehydrogenase (PDB: 1V59). The two subunits of this homodimer are depicted in green and grey and bound FAD, redox active disulfide, and  $\text{NAD}^+$  cofactors are shown as space-filling representations colored yellow, magenta, and blue respectively. Panel B shows the reductive and oxidative half reactions without regard to protonation states of the reactants and products. The flavin and redox active disulfide moieties of the dehydrogenase lie within the white box. Panel C is a schematic depiction of the fusion protein attached to the mCherry fluorescent protein (PDB: 2H5Q).

**Figure 4.12: Lipoamide Dehydrogenase: structure, reactions and probe design.**

Figure 4.12A shows a structure of this homodimeric protein; each subunit carries a bound FAD cofactor (yellow) and a binding pocket for NAD<sup>+</sup>/NADH (pyridine nucleotide in blue). The redox-active disulfide that communicates with the flavin prosthetic group within each subunit is shown in magenta and is located at the base of a deep tunnel that serves to isolate the enzyme from non-cognate thiol reductants. Intracellularly the physiological dithiol, dihydrolipoamide, is covalently attached to a lysine residue in a flexible region of dihydrolipoyl acetyl transferase (E2) and serves as the ultimate reductant for NAD<sup>+</sup> via the series of transfers shown from right to left in Panel B. While it might be anticipated that development of a LipDH-based probe for NADH/NAD<sup>+</sup> levels in mammalian cells would require disabling the dihydrolipoamide site, this is only necessary if the sensor is intended for use within the mitochondrial matrix; the lipoyllysine-E2 conjugate is exclusively mitochondrial [75-77]. Here we test the new sensor using cytosolic expression

#### **4.5.1 Expression and Characterization of NAD<sup>+</sup>/NADH Sensor.**

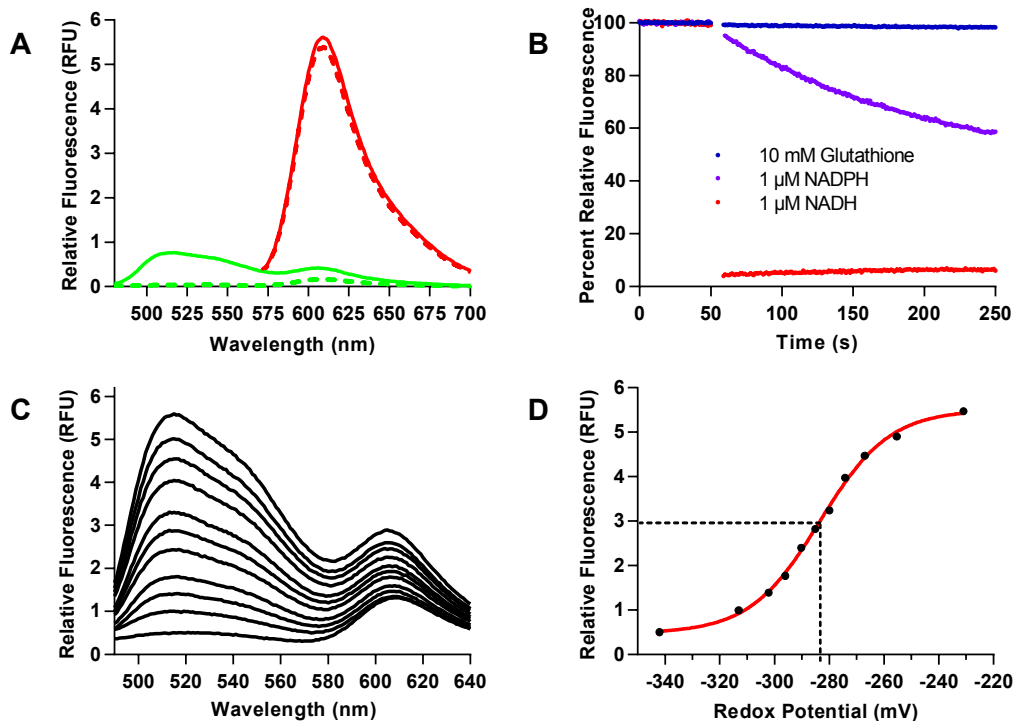
A schematic illustration of the LipDH-mCherry fusion is depicted in Figure 4.12C (with the nucleotide and protein sequences shown in Appendix). The sensor was first characterized after expression in *E. coli* BL21-DE3 cells (see Methods). The purified construct contained the expected complement of flavin and mCherry absorbance contributions (Figure 4.13).



The spectrum was recorded in 50 mM phosphate buffer, pH 7.5, containing 1 mM EDTA, and normalized to 1.0 at 587 nm.

**Figure 4.13: UV-Vis spectrum of the LipDH-mCherry  $\text{NAD}^+/\text{NADH}$  sensor.**

Emission profiles for the oxidized (solid lines) and reduced (dashed lines) LipDH-mCherry probe are shown in Figure 4.14A. FAD and mCherry fluorophores were independently excited at 456 and 520 nm (green and red lines respectively). The oxidized flavin emission at  $\sim 520$  nm is almost completely quenched upon the addition of 20  $\mu\text{M}$  NADH leaving a small residual signal at 610 nm due to weak direct excitation characteristic of mCherry (dashed line). Because of the minimal FRET contribution encountered in Figure 4.14A we again used the probe in a ratiometric mode by independently exciting mCherry at 520 nm as to compensate for any change in the placement or concentration of the fluorophores. As before, the emission spectrum of mCherry is essentially insensitive to reduction of the sensor domain (Figure 4.14A).



Panel A shows the emission spectra of 1  $\mu\text{M}$  of LipDH-mCherry before (solid line) and after reduction with 20  $\mu\text{M}$  NADH (dashed line; see Methods) exciting into the flavin excitation envelope (456 nm; green curves) or into the mCherry chromophore using 520 nm light (red curves). Panel B shows that the probe responds rapidly to 1  $\mu\text{M}$  NADH, while being insensitive to glutathione and NADPH. Panels C and D show the response of bound flavin to ratios of  $\text{NAD}^+$  and NADH totaling 200  $\mu\text{M}$ . The fluorescence spectra excited at 456 nm are shown in panel C and the amplitude of the 520 nm signal plotted against the redox potential of the mixture is depicted in panel D.

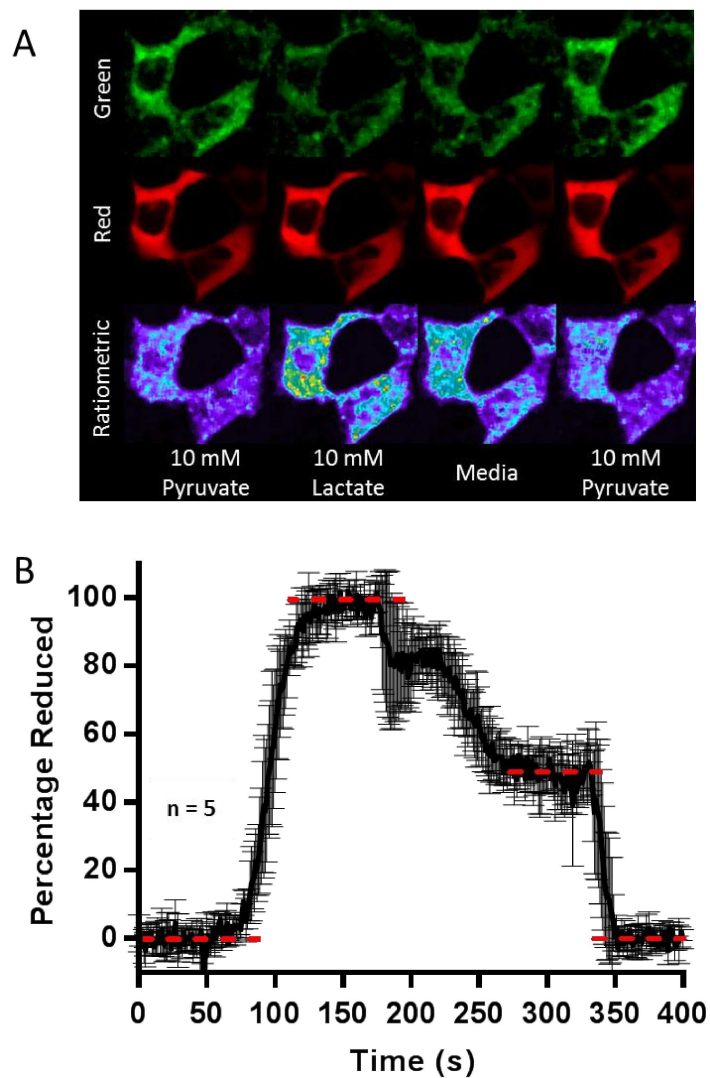
**Figure 4.14: Characterization of LipDH-mCherry.**

Figure 4.14B shows that bleaching of 100 nM probe by 1  $\mu\text{M}$  NADH is complete in the time taken to mix reagents. NADPH is a very poor substrate of LipDH [78-79] and the probe responds slowly to this pyridine nucleotide (Figure 4.14B;  $t_{1/2}$  of >300 s). The probe is unresponsive to 10 mM glutathione as would be expected. Figure

4.14C shows a titration of 1  $\mu\text{M}$  LipDH-mCherry with mixtures of  $\text{NAD}^+$  and NADH totaling 200  $\mu\text{M}$  and panel D plots the fluorescence at 520 nm against the redox potential of the pyridine nucleotide mixtures using a  $E'^{\circ}$  value of -320 mV for NADH [80]. While published redox potentials of the yeast enzyme are not available, our measured midpoint  $-284 \pm 1$  mV (3 determinations) matches the value of -280 mV determined by Matthews and Williams for 2-electron reduction of the pig heart enzyme [81]. This potential corresponds to reduction of the active-site disulfide immediately proximal to the flavin prosthetic group. The resulting thiolate to oxidized flavin charge-transfer complex [44-47] ablates the strong fluorescence of the bound FAD generating the quenching shown in Figure 4.14A and C. Conversion to the 4-electron reduced enzyme with reduction of the flavin occurs at a considerably more negative redox potential of  $\sim -346$  mV [81] and would remain undetected here.

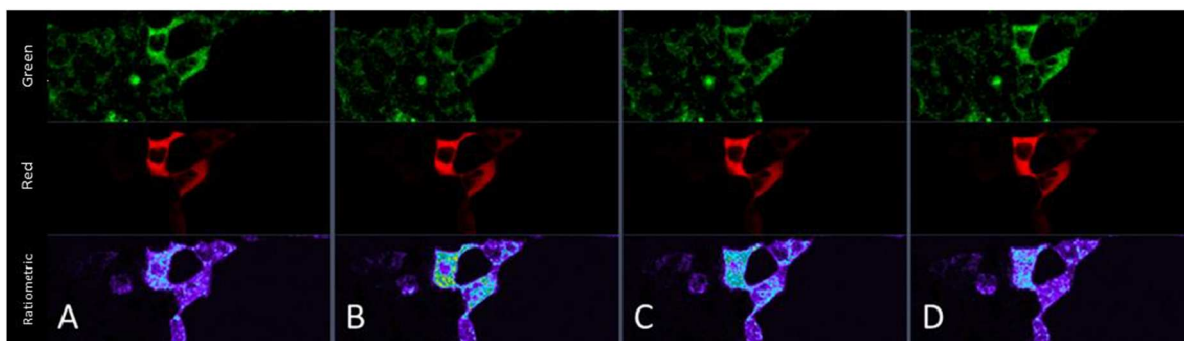
#### **4.5.2 $\text{NAD}^+/\text{NADH}$ Sensor Interacts Reversibly with Intracellular $\text{NAD}^+/\text{NADH}$ .**

After an initial characterization of the LipDH-mCherry, we explored its performance in HEK293T mammalian cells. The sensor sequence was first optimized for expression in human cells and cloned into a pCMV-Tag 2A mammalian expression vector lacking organelle targeting sequences (Appendix) [82]. Cells visualized by confocal (Figures 4.15A and 4.16) show the expected cytosolic expression pattern for the mCherry signal. Using a flow cell (see Methods; 0.5 mL/min DMEM), supplements of 10 mM pyruvate and then 10 mM lactate were used to set the fully oxidized and fully reduced limits of the sensor. Exposure of mammalian cells to these reagents leads to a rapid modulation of intracellular  $\text{NAD}^+/\text{NADH}$  redox pools via the activity of lactate dehydrogenase [83]:



Panel A displays sensor emission of three channels (green, red and ratiometric) of HEK293T cells. Panel B depicts a quantification of the average of five replicate experiments using the ratiometric channel to express the percentage of LipDH-mCherry reduction.

**Figure 4.15: Interrogating NADH/NAD<sup>+</sup> Redox in Live HEK283T Cells.**



HEK293T cells over-expressing LipDH-mCherry are attached to the bottom face of an ibidi flow cells. Solutions flowing over the cells were as described in the Text. Panel A-D contain, respectively, 10 mM pyruvate, 10 mM lactate, media alone, and 10 mM pyruvate.

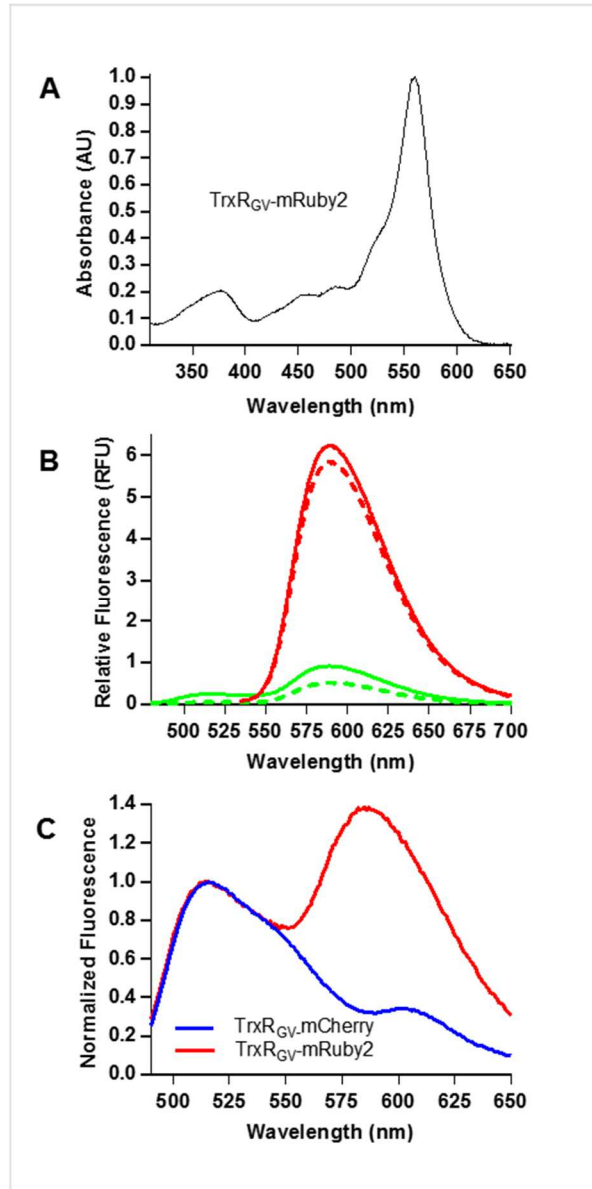
**Figure 4.16: Confocal field of view for one of the NAD<sup>+</sup>/NADH sensor flow cell experiments.**

The data in Figure 4.15A shows a collection of cells in the flow cell and the average of 5 experiments (see Methods) is shown in panel B. In each case the lactate wash was replaced with DMEM medium alone to assess the steady state of the intracellular NAD<sup>+</sup>/NADH pool, prior to a return to the limiting oxidized state upon reintroduction of pyruvate. The green oxidized flavin channel in panel A provides a clear visualization of the NAD<sup>+</sup>/NADH redox state. As before, the red channel is insensitive to media exchange allowing its use as an effective internal correction factor for confocal drift and the movement of live cells. Additional images of these experiments are provided in Figure 4.16. The value of  $47 \pm 6$  % reduction at 300 s in Figure 4.15B corresponds to an NAD<sup>+</sup>/NADH ratio of 18:1 ( $-282 \pm 3$  mV). This ratio falls within the range of values obtained for diverse mammalian cell types and sensors e.g. 10:1 to 830:1 [39, 83-86].

## 4.6 CONCLUSIONS

As described earlier, many elegant prior sensor designs require site-specific splicing of an analyte-response element within a partner GFP domain (e.g. Figure 4.2B) and may entail multiple iterations to obtain a satisfactory response. In addition, the identification of analyte-binding domains that can support sensor development remains a challenge. As an alternate strategy, our proof of principle sensors employ a simple fusion of two components end-to-end. While there is much room for performance enhancements, both the NAD<sup>+</sup>/NADH and thioredoxin probes functioned intracellularly as initially constructed.

A large number of flavin-dependent oxidoreductases can be potentially monitored by a rational selection of the desired reductive or oxidative half-reaction. These facile catalysts would be expected to rapidly respond to specific metabolites at cellularly-relevant concentrations as observed here. An obvious issue for the general application of flavoenzyme-based sensors is the rather limited number of commonly-studied flavoproteins that are highly fluorescent in their oxidized states. While the fluorescence of protein-bound flavins is frequently strongly quenched by neighboring tyrosine and/or tryptophan side chains, several reports show that straightforward mutagenesis can restore fluorescence without ablation of enzymatic activity [87-90]. In addition, the dramatic growth in available genome sequences affords ever increasing opportunities for the identification of new flavoenzyme probe candidates.



Panel A shows the UV-VIS absorbance spectra of the construct normalized to 559 nm. Panel B depicts the emission spectra excited at 456 nm (green) or 520 nm (red) for the oxidized and THP-reduced sensor (solid and dashed lines, respectively). Panel C shows difference spectra between oxidized and THP-reduced probes (TrxR<sub>GV</sub>-mRuby2 and TrxR<sub>GV</sub>-mRuby2) normalized using the flavin emission at 520 nm. The mRuby2 probe shows a much stronger FRET component exciting at 456 nm and emitting at 520nm.

**Figure 4.17: Characterization of the TrxR<sub>GV</sub>-mRuby2 sensor.**

Finally, we note that further developments with these new flavin probes should include the option of utilizing the FRET signal to a suitable GFP acceptor. While the mCherry constructs used here shows minimal FRET interactions, preliminary experiments show that mRuby2 [91] is a considerably superior acceptor (as exemplified in Figure 4.17). In addition to these simple designs, a closer and optimized alignment of the fluorophores might be realized by introducing the GFP at a loop within the native flavoprotein structure. We envisage that these red-shifted FRET-enabled probes will extend the utility of this new class of genetically encoded sensors.

## REFERENCES

1. Shimomura, O., F.H. Johnson, and Y. Saiga, Extraction, purification and properties of aequorin, a bioluminescent protein from the luminous hydromedusan, *Aequorea*. *J Cell Comp Physiol*, 1962. **59**: p. 223-39.
2. Chalfie, M., et al., Green fluorescent protein as a marker for gene expression. *Science*, 1994. **263**(5148): p. 802-5.
3. Inouye, S. and F.I. Tsuji, *Aequorea* green fluorescent protein. Expression of the gene and fluorescence characteristics of the recombinant protein. *Febs Letters*, 1994. **341**(2-3): p. 277-80.
4. Heim, R., D.C. Prasher, and R.Y. Tsien, Wavelength mutations and posttranslational autoxidation of green fluorescent protein. *Proc Natl Acad Sci U S A*, 1994. **91**(26): p. 12501-4.
5. Tsien, R.Y., The green fluorescent protein. *Annual review of biochemistry*, 1998. **67**: p. 509-44.
6. Chudakov, D.M., et al., Fluorescent Proteins and Their Applications in Imaging Living Cells and Tissues. *Physiological Reviews*, 2010. **90**(3): p. 1103-1163.
7. Miyawaki, A., et al., Fluorescent indicators for Ca<sup>2+</sup> based on green fluorescent proteins and calmodulin. *Nature*, 1997. **388**(6645): p. 882-887.
8. Miyawaki, A. and Y. Niino, Molecular spies for bioimaging--fluorescent protein-based probes. *Mol Cell*, 2015. **58**(4): p. 632-43.
9. Lukyanov, K.A. and V.V. Belousov, Genetically encoded fluorescent redox sensors. *Biochim Biophys Acta*, 2014. **1840**(2): p. 745-56.
10. Schwarzlander, M., et al., Dissecting Redox Biology Using Fluorescent Protein Sensors. *Antioxidants & Redox Signaling*, 2016. **24**(13): p. 680-712.
11. Hudson, D.A., S.A. Gannon, and C. Thorpe, Oxidative protein folding: from thiol-disulfide exchange reactions to the redox poise of the endoplasmic reticulum. *Free Radic Biol Med*, 2015. **80**: p. 171-82.

12. Meyer, A.J. and T.P. Dick, Fluorescent protein-based redox probes. *Antioxid Redox Signal*, 2010. **13**(5): p. 621-50.
13. Gutscher, M., et al., Real-time imaging of the intracellular glutathione redox potential. *Nat Methods*, 2008. **5**(6): p. 553-9.
14. Morgan, B., et al., Real-time monitoring of basal H<sub>2</sub>O<sub>2</sub> levels with peroxiredoxin-based probes. *Nature Chemical Biology*, 2016. **12**(6): p. 437-43.
15. Zhao, Y., et al., SoNar, a Highly Responsive NAD<sup>+</sup>/NADH Sensor, Allows High-Throughput Metabolic Screening of Anti-tumor Agents. *Cell Metab*, 2015. **21**(5): p. 777-89.
16. Cameron, W.D., et al., Apollo-NADP(+): a spectrally tunable family of genetically encoded sensors for NADP(+). *Nat Methods*, 2016. **13**(4): p. 352-8.
17. Ostergaard, H., C. Tachibana, and J.R. Winther, Monitoring disulfide bond formation in the eukaryotic cytosol. *The Journal of cell biology*, 2004. **166**(3): p. 337-45.
18. Qiao, W., et al., Zinc binding to a regulatory zinc-sensing domain monitored in vivo by using FRET. *Proc Natl Acad Sci U S A*, 2006. **103**(23): p. 8674-9.
19. Wegner, S.V., et al., Dynamic copper(I) imaging in mammalian cells with a genetically encoded fluorescent copper(I) sensor. *J Am Chem Soc*, 2010. **132**(8): p. 2567-9.
20. Lindenburg, L.H., et al., MagFRET: the first genetically encoded fluorescent Mg<sup>2+</sup> sensor. *PLoS One*, 2013. **8**(12): p. e82009.
21. Imamura, H., et al., Visualization of ATP levels inside single living cells with fluorescence resonance energy transfer-based genetically encoded indicators. *Proc Natl Acad Sci U S A*, 2009. **106**(37): p. 15651-6.
22. Ye, K. and J.S. Schultz, Genetic engineering of an allosterically based glucose indicator protein for continuous glucose monitoring by fluorescence resonance energy transfer. *Anal Chem*, 2003. **75**(14): p. 3451-9.
23. Gruenwald, K., et al., Visualization of glutamine transporter activities in living cells using genetically encoded glutamine sensors. *PLoS One*, 2012. **7**(6): p. e38591.

24. Tanimura, A., et al., Fluorescent biosensor for quantitative real-time measurements of inositol 1,4,5-trisphosphate in single living cells. *J Biol Chem*, 2004. **279**(37): p. 38095-8.
25. Baird, G.S., D.A. Zacharias, and R.Y. Tsien, Circular permutation and receptor insertion within green fluorescent proteins. *Proc Natl Acad Sci U S A*, 1999. **96**(20): p. 11241-6.
26. Honda, Y. and K. Kirimura, Generation of circularly permuted fluorescent-protein-based indicators for in vitro and in vivo detection of citrate. *PLoS One*, 2013. **8**(5): p. e64597.
27. Zhao, Y., et al., Genetically encoded fluorescent sensors for intracellular NADH detection. *Cell Metab*, 2011. **14**(4): p. 555-66.
28. Belousov, V.V., et al., Genetically encoded fluorescent indicator for intracellular hydrogen peroxide. *Nature methods*, 2006. **3**(4): p. 281-6.
29. Tarrago, L., et al., Monitoring methionine sulfoxide with stereospecific mechanism-based fluorescent sensors. *Nat Chem Biol*, 2015. **11**(5): p. 332-8.
30. Ostergaard, H., et al., Shedding light on disulfide bond formation: engineering a redox switch in green fluorescent protein. *Embo J*, 2001. **20**(21): p. 5853-62.
31. Bjornberg, O., H. Ostergaard, and J.R. Winther, Mechanistic insight provided by glutaredoxin within a fusion to redox-sensitive yellow fluorescent protein. *Biochemistry*, 2006. **45**(7): p. 2362-71.
32. Hanson, G.T., et al., Investigating mitochondrial redox potential with redox-sensitive green fluorescent protein indicators. *J Biol Chem*, 2004. **279**(13): p. 13044-53.
33. Bhaskar, A., et al., Reengineering redox sensitive GFP to measure mycothiol redox potential of *Mycobacterium tuberculosis* during infection. *PLoS pathogens*, 2014. **10**(1): p. e1003902.
34. Gutscher, M., et al., Proximity-based protein thiol oxidation by H<sub>2</sub>O<sub>2</sub>-scavenging peroxidases. *J Biol Chem*, 2009. **284**(46): p. 31532-40.
35. Gutscher, M., et al., Real-time imaging of the intracellular glutathione redox potential. *Nature methods*, 2008. **5**(6): p. 553-9.
36. Ghisla, S., et al., Fluorescence and optical characteristics of reduced flavines and flavoproteins. *Biochemistry*, 1974. **13**(3): p. 589-97.

37. Hemmerich, P., G. Nagelschneider, and C. Veeger, Chemistry and molecular biology of flavins and flavoproteins. *FEBS Lett*, 1970. **8**(2): p. 69-83.
38. Visser, A.J., et al., Fluorescence properties of reduced flavins and flavoproteins. *Eur J Biochem*, 1979. **101**(1): p. 13-21.
39. Hung, Y.P., et al., Imaging cytosolic NADH-NAD(+) redox state with a genetically encoded fluorescent biosensor. *Cell Metab*, 2011. **14**(4): p. 545-54.
40. Mukhtarov, M., et al., Calibration and functional analysis of three genetically encoded Cl(-)/pH sensors. *Front Mol Neurosci*, 2013. **6**: p. 9.
41. Kumagai, A., et al., A bilirubin-inducible fluorescent protein from eel muscle. *Cell*, 2013. **153**(7): p. 1602-11.
42. Coddling, J.A., B.A. Israel, and C. Thorpe, Protein Substrate Discrimination in the Quiescin Sulfhydryl Oxidase (QSOX) Family. *Biochemistry*, 2012. **51**(20): p. 4226-35.
43. Datsenko, K.A. and B.L. Wanner, One-step inactivation of chromosomal genes in *Escherichia coli* K-12 using PCR products. *Proc Natl Acad Sci U S A*, 2000. **97**(12): p. 6640-5.
44. Williams, C., Jr., Lipoamide dehydrogenase, glutathione reductase, thioredoxin reductase, and mercuric ion reductase---A family of flavoenzyme transhydrogenases., in *Chemistry and biochemistry of Flavoenzymes*, F. Muller, ed, Editor. 1992, CRC Press: Boca Raton. p. 121-211.
45. Williams, C.H., et al., Thioredoxin reductase two modes of catalysis have evolved. *Eur. J. Biochem.*, 2000. **267**(20): p. 6110-7.
46. Argyrou, A. and J.S. Blanchard, Flavoprotein disulfide reductases: advances in chemistry and function. *Prog Nucleic Acid Res Mol Biol*, 2004. **78**: p. 89-142.
47. Miller, S.M., Flavoprotein disulfide reductases and structurally related flavoprotein thiol/disulfide-linked oxidoreductases, in *Handbook of Flavoproteins*, R. Hille, S.M. Miller, and B.A. Palfey, Editors. 2013, de Gruyter. p. 165-201.
48. Toledano, M.B., et al., The system biology of thiol redox system in *Escherichia coli* and yeast: differential functions in oxidative stress, iron metabolism and DNA synthesis. *Febs Letters*, 2007. **581**(19): p. 3598-607.

49. Miranda-Vizueté, A., et al., Cloning, expression, and characterization of a novel *Escherichia coli* thioredoxin. *J Biol Chem*, 1997. **272**(49): p. 30841-7.
50. Lillig, C.H., et al., New thioredoxins and glutaredoxins as electron donors of 3'-phosphoadenylylsulfate reductase. *J Biol Chem*, 1999. **274**(12): p. 7695-8.
51. Collet, J.F., et al., Thioredoxin 2, an oxidative stress-induced protein, contains a high affinity zinc binding site. *J Biol Chem*, 2003. **278**(46): p. 45325-32.
52. Collet, J.F. and J. Messens, Structure, function, and mechanism of thioredoxin proteins. *Antioxid Redox Signal*, 2010. **13**(8): p. 1205-16.
53. Waksman, G., et al., Crystal structure of *Escherichia coli* thioredoxin reductase refined at 2 Å resolution. Implications for a large conformational change during catalysis. *J. Mol. Biol.*, 1994. **236**(3): p. 800-816.
54. Lennon, B.W., C.H. Williams, Jr., and M.L. Ludwig, Crystal structure of reduced thioredoxin reductase from *Escherichia coli*: structural flexibility in the isoalloxazine ring of the flavin adenine dinucleotide cofactor. *Protein Sci*, 1999. **8**(11): p. 2366-79.
55. Lennon, B.W., C.H. Williams, Jr., and M.L. Ludwig, Twists in catalysis: alternating conformations of *Escherichia coli* thioredoxin reductase. *Science*, 2000. **289**(5482): p. 1190-4.
56. El Hajjaji, H., et al., The zinc center influences the redox and thermodynamic properties of *Escherichia coli* thioredoxin 2. *Journal of molecular biology*, 2009. **386**(1): p. 60-71.
57. Williams, C.H., Jr., Mechanism and structure of thioredoxin reductase from *Escherichia coli*. *Faseb J*, 1995. **9**(13): p. 1267-76.
58. Rescigno, M. and R.N. Perham, Structure of the NADPH-Binding Motif of Glutathione Reductase: Efficiency Determined by Evolution. *Biochemistry*, 1994. **33**(19): p. 5721-5727.
59. Krause, G. and A. Holmgren, Substitution of the conserved tryptophan 31 in *Escherichia coli* thioredoxin by site-directed mutagenesis and structure-function analysis. *J Biol Chem*, 1991. **266**(7): p. 4056-66.
60. Krause, G., et al., Mimicking the active site of protein disulfide-isomerase by substitution of proline 34 in *Escherichia coli* thioredoxin. *J Biol Chem*, 1991. **266**(15): p. 9494-500.

61. O'Donnell, M.E. and C.H. Williams, Jr., Proton stoichiometry in the reduction of the FAD and disulfide of Escherichia coli thioredoxin reductase. Evidence for a base at the active site. *J Biol Chem*, 1983. **258**(22): p. 13795-805.
62. Thelander, L., Thioredoxin reductase. Characterization of a homogenous preparation from Escherichia coli B. *J Biol Chem*, 1967. **242**(5): p. 852-9.
63. Missiakas, D., C. Georgopoulos, and S. Raina, The Escherichia coli dsbC (xprA) gene encodes a periplasmic protein involved in disulfide bond formation. *Embo J*, 1994. **13**(8): p. 2013-20.
64. Cabibbo, A., et al., ERO1-L, a human protein that favors disulfide bond formation in the endoplasmic reticulum. *J Biol Chem*, 2000. **275**(7): p. 4827-33.
65. Wittrup, K.D., Disulfide bond formation and eukaryotic secretory productivity. *Curr. Opin. Biotechnol.*, 1995. **6**(2): p. 203-8.
66. Kosower, N.S. and E.M. Kosower, Diamide: an oxidant probe for thiols. *Methods Enzymol*, 1995. **251**: p. 123-33.
67. Gitler, C., B. Zarmi, and E. Kalef, General method to identify and enrich vicinal thiol proteins present in intact cells in the oxidized, disulfide state. *Analytical biochemistry*, 1997. **252**(1): p. 48-55.
68. Hansen, R.E., D. Roth, and J.R. Winther, Quantifying the global cellular thiol-disulfide status. *Proc Natl Acad Sci U S A*, 2009. **106**(2): p. 422-7.
69. Potamitou, A., A. Holmgren, and A. Vlamis-Gardikas, Protein levels of Escherichia coli thioredoxins and glutaredoxins and their relation to null mutants, growth phase, and function. *J Biol Chem*, 2002. **277**(21): p. 18561-7.
70. Holmgren, A. and M. Fagerstedt, The in vivo distribution of oxidized and reduced thioredoxin in Escherichia coli. *J Biol Chem*, 1982. **257**(12): p. 6926-30.
71. Hirt, R.P., et al., The diversity and evolution of thioredoxin reductase: new perspectives. *Trends Parasitol*, 2002. **18**(7): p. 302-8.
72. Koharyova, M. and M. Kollarova, Thioredoxin system - a novel therapeutic target. *General Physiology and Biophysics*, 2015. **34**(3): p. 221-233.
73. Reed, L.J., A trail of research from lipoic acid to alpha-keto acid dehydrogenase complexes. *J Biol Chem*, 2001. **276**(42): p. 38329-36.

74. Patel, M.S. and T.E. Roche, Molecular biology and biochemistry of pyruvate dehydrogenase complexes. *FASEB J*, 1990. **4**(14): p. 3224-33.
75. Reed, L.J., Multienzyme Complexes. *Accounts of Chemical Research*, 1974. **7**(2): p. 40-46.
76. Olson, M.S., Regulation of the mitochondrial multienzyme complexes in complex metabolic systems. *Ann N Y Acad Sci*, 1989. **573**: p. 218-29.
77. Maas, E. and H. Bisswanger, Localization of the alpha-oxoacid dehydrogenase multienzyme complexes within the mitochondrion. *FEBS Lett*, 1990. **277**(1-2): p. 189-90.
78. Bocanegra, J.A., N.S. Scrutton, and R.N. Perham, Creation of an NADP-dependent pyruvate dehydrogenase multienzyme complex by protein engineering. *Biochemistry*, 1993. **32**(11): p. 2737-40.
79. Blacker, T.S. and M.R. Duchon, Investigating mitochondrial redox state using NADH and NADPH autofluorescence. *Free Radical Biology and Medicine*, 2016. **100**: p. 53-65.
80. Burton, K. and T.H. Wilson, The Free-Energy Changes for the Reduction of Diphosphopyridine Nucleotide and the Dehydrogenation of L-Malate and L-Glycerol 1-Phosphate. *Biochemical Journal*, 1953. **54**(1): p. 86-94.
81. Matthews, R.G. and C.H. Williams, Jr., Measurement of the oxidation-reduction potentials for two-electron and four-electron reduction of lipoamide dehydrogenase from pig heart. *J Biol Chem*, 1976. **251**(13): p. 3956-64.
82. Kim, D.H. and I. Hwang, Direct targeting of proteins from the cytosol to organelles: the ER versus endosymbiotic organelles. *Traffic*, 2013. **14**(6): p. 613-21.
83. Williamson, D.H., P. Lund, and H.A. Krebs, The redox state of free nicotinamide-adenine dinucleotide in the cytoplasm and mitochondria of rat liver. *Biochem J*, 1967. **103**(2): p. 514-27.
84. Zhang, Q., D.W. Piston, and R.H. Goodman, Regulation of corepressor function by nuclear NADH. *Science*, 2002. **295**(5561): p. 1895-7.
85. Sun, F., et al., Biochemical issues in estimation of cytosolic free NAD/NADH ratio. *PLoS One*, 2012. **7**(5): p. e34525.

86. Zhao, Y., et al., In vivo monitoring of cellular energy metabolism using SoNar, a highly responsive sensor for NAD(+)/NADH redox state. *Nat Protoc*, 2016. **11**(8): p. 1345-59.
87. Berry, A., N.S. Scrutton, and R.N. Perham, Switching kinetic mechanism and putative proton donor by directed mutagenesis of glutathione reductase. *Biochemistry*, 1989. **28**(3): p. 1264-9.
88. Maeda-Yorita, K., et al., Properties of lipoamide dehydrogenase altered by site-directed mutagenesis at a key residue (I184Y) in the pyridine nucleotide binding domain. *Biochemistry*, 1991. **30**(51): p. 11788-95.
89. Visser, A.J.W.G., et al., Time-resolved fluorescence of flavin adenine dinucleotide in wild-type and mutant NADH peroxidase. Elucidation of quenching sites and discovery of a new fluorescence depolarization mechanism. *Journal of Physical Chemistry B*, 1998. **102**(50): p. 10431-10439.
90. Mataga, N., et al., Ultrafast fluorescence quenching dynamics of flavin chromophores in protein nanospace. *Journal of Physical Chemistry B*, 1998. **102**(37): p. 7081-7084.
91. Lam, A.J., et al., Improving FRET dynamic range with bright green and red fluorescent proteins. *Nature methods*, 2012. **9**(10): p. 1005-12.

## Appendix A

### CHAPTER 4 DNA AND PROTEIN SEQUENCES

#### DNA Sequences of TrxR-mCherry

GCTAGCATGACTGGTGGACAGCAAATGGGTCGGGATCTGTACGACGATGA  
CGATAAGGATCCAACCCTTATGGGCACGACCAAACACAGTAAACTGCTTA  
TCCTGGGTTTCAGGCCCGGCGGGATACACCGCTGCTGTCTACGCGGCGCGC  
GCCAACCTGCAACCTGTGCTGATTACCGGCATGGAAAAAGGCGGCCAACT  
GACCACCACCGGAAGTGGAAAAGTGGCCTGGCGATCCAAACGATCTGA  
CCGGTCCGTTATTAATGGAGCGCATGCACGAACATGCCACCAAGTTTGAA  
ACTGAGATCATTGATCATATCAACAAGGTGGATCTGCAAAACCGTCCG  
TTCCGTCTGAATGGCGATAACGGCGAATACACTTGCGACGCGCTGATTATT  
GCCACCGGAGCTTCTGCACGCTATCTCGGCCTGCCCTCTGAAGAAGCCTTT  
AAAGGCCGTGGGGTTTCTGCTTGTGCAACCTGCGACGGTTTCTTCTATCGC  
AACCAGAAAGTTGCGGTCATCGGCGGCGGAATACCGCGGTTGAAGAGGC  
GCTGTATCTGTCTAACATCGCTTCGGAAGTGCATCTGATTCACCGCCGTGA  
CGGTTTCCGCGCGGAAAAATCCTCATTAAAGCGCCTGATGGATAAAGTGG  
AGAACGGCAACATCATTCTGCACACCAACCGTACGCTGGAAGAAGTGACC  
GGCGATCAAATGGGTGTCACTGGCGTTCGTCTGCGCGATACGCAAAACAG  
CGATAACATCGAGTCACTCGACGTTGCCGGTCTGTTTGTTGCTATCGGTCA  
CAGCCCGAATACTGCGATTTTTCGAAGGGCAGCTGGAAGTGGAAAACGGCT  
ACATCAAAGTACAGTCGGGTATTCATGGTAATGCCACCCAGACCAGCATT  
CCTGGCGTCTTTGCCGCAGGCGACGTGATGGATCACATTTATCGCCAGGCC  
ATTACTTCGGCCGGTACAGGCTGCATGGCAGCACTTGATGCGGAACGCTA  
CCTCGATGGTTTAGCTGACGCAAAAGTGAGCAAGGGCGAAGAGGATAACA  
TGGCCATCATCAAGGAGTTCATGCGCTTCAAGGTGCACATGGAGGGGCTCC  
GTGAACGGCCACGAGTTCGAGATCGAGGGCGAGGGCGAGGGCCGCCCTA  
CGAGGGCACCCAGACCGCCAAGCTGAAGGTGACCAAGGGTGGCCCCCTGC  
CCTTCGCCTGGGACATCCTGTCCCTCAGTTCATGTACGGCTCCAAGGCCT  
ACGTGAAGCACCCCGCCGACATCCCCGACTACTTGAAGCTGTCCTTCCCCG  
AGGGCTTCAAGTGGGAGCGCGTGATGAACTTCGAGGACGGCGGCGTGGTG  
ACCGTGACCCAGGACTCCTCCCTGCAGGACGGCGAGTTCATCTACAAGGT  
GAAGCTGCGCGGCACCAACTTCCCCTCCGACGGCCCCGTAATGCAGAAGA  
AGACCATGGGCTGGGAGGCCTCCTCCGAGCGGATGTACCCCGAGGACGGC  
GCCCTGAAGGGCGAGATCAAGCAGAGGCTGAAGCTGAAGGACGGCGGCC  
ACTACGACGCTGAGGTCAAGACCACCTACAAGGCCAAGAAGCCCGTGCAG  
CTGCCCCGGCGCCTACAACGTCAACATCAAGTTGGACATCACCTCCACAAC

GAGGACTACACCATCGTGGAACAGTACGAACGCGCCGAGGGCCGCCACTC  
CACCGGCGGCATGGACGAGCTGTACAAGTAAGCTT

### **Primers for G154V Mutation of TrxR**

G154V\_Fwd: GTC ATC GGC GGC GTC AAT ACC GCG GTT  
G154V\_Rev: AAC CGC GGT ATT GAC GCC GCC GAT GAC

### **Protein Sequence of TrxR-mCherry**

MTGGQQMGRDLYDDDDKDPTLMGTTKHSKLLILGSGPAGYTAAVYAARAN  
LQPVLITGMEKGGQLTTTTEVENWPGDPNDLTGPLLMERMHEHATKFETEIIF  
DHINKVDLQNRPFRLNGDNGEYTCDALIATGASARYLGLPSEEAFKGRGVSA  
CATCDGFFYRNQKVAVIGGGNTAVEEALYLSNIASEVHLIHRRDGFRAEKILIK  
RLMDKVENGNIILHTNRTLEEVTGDQMGVTGVRLRDTQNSDNIESLDVAGLF  
VAIGHSPNTAIFEGQLELENGYIKVQSGIHGNATQTSIPGVFAAGDVMMDHIYRQ  
AITSAGTGCMAALDAERYLDGLADAKVSKGEEDNMAIIEFMRFKVHMEGS  
VNGHEFEIEGEGEGRPYEGTQAKLKVTKGGPLPFAWDILSPQFMYGSKAYV  
KHPADIPDYLKLSFPEGFKWERVMNFEDGGVVTVTQDSSLQDGEFIYKVKLR  
GTNFPDGPVMQKKTMGWEASSERMYPEDGALKGEIKQRLKLDGGHYDAE  
VKTTYKAKKPVQLPGAYNVNIKLDITSHNEDYTIVEQYERAEGRHSTGGMDE  
LYK

### **DNA Sequences of LipDH-mCherry (for bacterial expression)**

CCATGGGTCACCATCACCATCATCATGAGAACCTTTACTTTCAAGGCACCA  
TTAACAAAAGTCACGATGTAGTTATCATTGGCGGCGGTCTTGCTGGATATG  
TTGCCGCAATTAAGCGGCCAGTTAGGGTTTAACACCGCTTGTGTGGAAA  
AACGTGGTAAACTGGGGGGTACATGTTTGAATGTTGGGTGCATTCCATCGA  
AAGCCTTACTGAATAATCCCACTTGTTCACCAGATGCACACAGAAGCGC  
AGAAACGTGGTATTGACGTGAACGGCGATATTAAGATTAACGTGGCAAAC  
TTTCAAAAAGCCAAAGATGATGCTGTCAAACA ACTTACGGGTGGTATTGA  
ACTGTTATTCAAAAAGAACAAGGTA ACTTATTATAAAGGAAACGGATCAT  
TTGAGGATGAAACCAAAATTCGTGTGACTCCGGTAGATGGACTGGAAGGT  
ACCGTAAAAGAGGATCATATCTTAGACGTCAAAAATATCATCGTAGCAAC  
AGGTAGCGAAGTGACCCCTTCCCTGGAATTGAAATCGATGAAGAAAAA  
TCGTGAGTAGTACCGGCGCCTTATCCCTGAAAGAAATCCCAAGCGCCTCA  
CCATCATCGGTGGCGGAATTATCGGTCTGGAAATGGGCAGTGTATATAGC  
CGTTTAGGTTCTAAAGTTACGGTAGTCGAATTTCAACCGCAAATTGGCGCA

AGCATGGATGGAGAGGTTGCAAAAGCGACCCAAAAATTTCTGAAGAAACA  
GGGCCTTGACTTTAAACTGAGCACAAAAGTAATTTTCGGCCAAACGCAATG  
ACGATAAAAACGTAGTAGAAATTGTAGTTGAAGACACTAAAACGAACAAA  
CAGGAAAATCTCGAAGCGGAAGTACTTCTGGTTGCGGTCGGTCGCCGCC  
GTACATTGCGGGTTTGGGTGCAGAGAAGATCGGCCTCGAAGTGGACAAAC  
GCGGACGTCTGGTTATCGACGATCAGTTTAATTCTAAATTCCCACATATCA  
AGGTGGTTGGTGACGTTACCTTCGGCCCTATGTTGGCGCACAAAGCAGAA  
GAAGAGGGTATTGCGGCTGTTGAAATGCTGAAAACAGGACACGGTCATGT  
AAATTACAATAATATTCCGAGTGTAATGTATTTCGCACCCCGAAGTGGCGTG  
GGTCGGCAAAACCGAAGAACAATTAAGGAGGCAGGGATTGATTATAAA  
ATTGGGAAATTTCCCTTTGCAGCAAATTCGCGCGCAAAAACCAACCAAGA  
TACCGAAGGTTTCGTGAAAATTTAATCGACAGTAAAACCGAACGCATTCT  
GGGAGCTCATATTATTGGCCCGAACGCGGGTGAGATGATTGCGGAAGCAG  
GTTTGGCTTTAGAATATGGCGCTTCAGCTGAAGATGTGGCTCGTGTCTGTC  
ATGCCCATCCAACATTGAGTGAAGCCTTTAAAGAAGCGAATATGGCAGCG  
TACGATAAAGCCATCCATTGTGTGAGCAAGGGCGAAGAGGATAACATGGC  
CATCATCAAGGAGTTCATGCGCTTCAAGGTGCACATGGAGGGCTCCGTGA  
ACGGCCACGAGTTCGAGATCGAGGGCGAGGGCGAGGGCCGCCCTACGA  
GGGCACCCAGACCGCCAAGCTGAAGGTGACCAAGGGTGGCCCCCTGCCCT  
TCGCCTGGGACATCCTGTCCCCTCAGTTCATGTACGGCTCCAAGGCCTACG  
TGAAGCACCCCGCCGACATCCCCGACTACTTGAAGCTGTCCTTCCCCGAGG  
GCTTCAAGTGGGAGCGCGTGATGAACTTCGAGGACGGCGGCGTGGTGACC  
GTGACCCAGGACTCCTCCCTGCAGGACGGCGAGTTCATCTACAAGGTGAA  
GCTGCGCGGCACCAACTTCCCCTCCGACGGCCCCGTAATGCAGAAGAAGA  
CAATGGGCTGGGAGGCCTCCTCCGAGCGGATGTACCCCGAGGACGGCGCC  
CTGAAGGGCGAGATCAAGCAGAGGCTGAAGCTGAAGGACGGCGGCCACT  
ACGACGCTGAGGTCAAGACCACCTACAAGGCCAAGAAGCCCGTGCAGCTG  
CCCGGCGCCTACAACGTCAACATCAAGTTGGACATCACCTCCCACAACGA  
GGACTACCCATCGTGGAACAGTACGAACGCGCCGAGGGCCGCCACTCCA  
CCGGCGGCATGGACGAGCTGTACAAGTAAGCTT

**Protein Sequences of LipDH-mCherry (for bacterial expression)**

MGHHHHHHENLYFQGTINKSHDVVIIGGGPAGYVAAIKAAQLGFNTACVEKR  
GKLGGTCLNVGCIPSKALLNNSHLFHQMHTAQKRGIDVNGDIKINVANFQK  
AKDDAVKQLTGGIPELLFKKNKVTTYKNGSFEDETKIRVTPVDGLEGTVKED  
HILDVKNIIVATGSEVTPFPGIEIDEEKIVSSTGALSLEIPKRLTIIGGGIIGLEMG  
SVYSRLGSKVTVVEFQPQIGASMDGEVAKATQKFLKKQGLDFKLSTKVISAK  
RNDDKNVVEIVVEDTKTNKQENLEAEVLLVAVGRRPYIAGLGAEKIGLEVDK  
RGRLVIDDQFNSKFPKIKVVGDVTFGPMLAHKAEIEGIAAVEMLKTDGHGHVN  
YNNIPSVMYSHPEVAWVGKTEEQLKEAGIDYKIGKFPFAANSRAKTNQDTEG  
FVKILIDSKTERILGAHIIGPNAGEMIAEAGLALAYGASAEDVARVCHAHPTLS

EAFKEANMAAYDKAIHCVSKGEEDNMAIIKEFMRFKVHMEGSVNGHEFEIEG  
EGEGRPYEGTQTAKLKVTKGGPLPFAWDILSPQFMYGSKAYVKHPADIPDYL  
KLSFPEGFKWERVMNFEDEGGVVTVTQDSSLQDGEFIYKVKLRGTNFPDGPV  
MQKKTMGWEASSERMYPEDGALKGEIKQRLKLDGGHYDAEVKTTYKAKK  
PVQLPGAYNVNIKLDITSHNEDYTIVEQYERAEGRHSTGGMDELYK

### DNA Sequence of TrxR<sub>Gv</sub>-mRuby2

TCTAGAAATAATTTTGTTTAACTTTAAGAAGGAGATATAATGACTGGTGGGA  
CAGCAAATGGGTCGGGATCTGTACGACGATGACGATAAGGATCCAACCCT  
TATGGGCACGACCAAACACAGTAAACTGCTTATCCTGGGTTTCAGGCCCGG  
CGGGATACACCGCTGCTGTCTACGCGGCGCGCCAACCTGCAACCTGTG  
CTGATTACCGGCATGGAAAAAGGCGGCCAACTGACCACCACCACGGAAGT  
GGAAAACCTGGCCTGGCGATCCAAACGATCTGACCGGTCCGTTATTAATGG  
AGCGCATGCACGAACATGCCACCAAGTTTGAAACTGAGATCATTTTTGATC  
ATATCAACAAGGTGGATCTGCAAACCGTCCGTTCCGTTCTGAATGGCGAT  
AACGGCGAATACTTTGCGACGCGCTGATTATTGCCACCGGAGCTTCTGCA  
CGCTATCTCGGCCTGCCCTCTGAAGAAGCCTTTAAAGGCCGTGGGGTTTCT  
GCTTGTGCAACCTGCGACGGTTTCTTCTATCGCAACCAGAAAGTTGCGGTC  
ATCGGCGGCGTGAATACCGCGGTTGAAGAGGCGCTGTATCTGTCTAACAT  
CGCTTCGGAAGTGCATCTGATTCACCGCCGTGACGGTTTCCGCGCGGAAAA  
AATCCTCATTAAGCGCCTGATGGATAAAGTGGAGAACGGCAACATCATTC  
TGCACACCAACCGTACGCTGGAAGAAGTGACCGGCGATCAAATGGGTGTC  
ACTGGCGTTCGTCTGCGGATACGCAAAACAGCGATAACATCGAGTCACT  
CGACGTTGCCGGTCTGTTTGTGCTATCGGTCACAGCCCGAATACTGCGAT  
TTTCGAAGGGCAGCTGGAACCTGGAAAACGGCTACATCAAAGTACAGTCGG  
GTATTCATGGTAATGCCACCCAGACCAGCATTCTGCGCTTTTGCCGCAG  
GCGACGTGATGGATCACATTTATCGCCAGGCCATTACTTCGGCCGGTACAG  
GCTGCATGGCAGCACTTGATGCGGAACGCTACCTCGATGGTTTAGCTGACG  
CAAAAGTCAGCAAAGGCGAGGAACTGATTAAGAGAATATGCGCATGAA  
AGTAGTGATGGAAGGCAGTGTTAATGGGCATCAGTTTAAGTGAAGTGGT  
AGGGAGAGGGTAACCCGTATATGGGTACGCAGACCATGCGTATCAAAGTT  
ATTGAGGGTGGTCCGCTTCCTTTCGCGTTTGATATCCTTGCTACCTCCTTTA  
TGTATGGCTCTCGCACGTTTATTAATATCCGAAAGGAATTCCTGATTTTTT  
TAAACAATCATTTCCGGAAGGCTTTACATGGGAACGTGTTACGCGTTATGA  
AGACGGCGGCGTCTGTTACTGTCATGCAAGATACCTCACTGGAAGATGGCT  
GCCTGGTCTATCACGTCCAGGTTCTGTTGAGTTAATTTTCCGTCAAATGGTC  
CTGTGATGCAGAAAAAGACAAAGGGTTGGGAACCGAACACGGAAATGAT  
GTATCCGGCGGATGGGGGTCTGCGCGGCTACACACATATGGCTCTTAAAG  
TTGATGGTGGCGGGCATCTGTCTTGCAGCTTCGTGACGACCTATCGCAGCA  
AAAAACGGTGGGGAACATCAAATGCCTGGCATTTCATGCTGTCGACCAC  
CGCTGGAACGTCTGGAAGAATCCGACAATGAAATGTTTGTGGTGCAGCG

TGAACACGCGGTGGCGAAATTCGCTGGCCTGGGTGGCGGTATGGACGAGC  
TCTATAAAGGGAGCGGCCATCACCATCACCATCACTAACCATGG

### **Protein Sequence of TrxR<sub>Gv</sub>-mRuby2**

MTGGQQMGRDLYDDDDKDPTLMGTTKHSKLLILGSGPAGYTAAVYAARAN  
LQPVLITGMEKGGQLTTTTEVENWPGDPNDLTGPLLMERMHEHATKFETEIIF  
DHINKVDLQNRPFRLNGDNGEYTCDALIATGASARYLGLPSEEAFKGRGVSA  
CATCDGFFYRNQKVAVIGGVNTAVEEALYLSNIASEVHLIHRRDGFRAEKILIK  
RLMDKVENGNILHTNRTLEEVTGDQMGVTGVRLRDTQNSDNIESLDVAGLF  
VAIGHSPNTAIFEGQLELENGYIKVQSGIHGNATQTSIPGVFAAGDVMMDHIYRQ  
AITSAGTGCMAALDAERYLDGLADAKVSKGEELIKENMRMKVVMEGSVNG  
HQFKCTGEGEGNPYMGQTMRIVIEGGPLPFAFDILATSFMYGSRFTFIKYPK  
GIPDFFKQSFPEGFTWERVTRYEDGGVVTVMQDTSLEDGCLVYHVQVRGVNF  
PSNGPVMQKKTGWEPNTEMMYPADGGLRGYTHMALKVDGGGHLSCSFVT  
TYRSKKTVGNIKMPGIHAVDHRLERLEESDNEMFVVQREHAVAKFAGLGGG  
MDELYKGSQHSHHHHH

### **DNA Sequence of LipDH-mCherry (for mammalian expression)**

GGATCCCACAATTAACAAGTCCCATGACGTGGTCATCATCGGAGGGCGGAC  
CTGCCGGCTACGTCCGCGCTATCAAGGCCGCCAGCTGGGCTTTAATACCG  
CTTGCGTGGAGAAGAGAGGCAAGCTGGGCGGCACATGCCTGAATGTGGGA  
TGTATCCCTTCCAAGGCCCTGCTGAACAATTCCCACCTGTTCCACCAAATG  
CACACCGAGGCCCAAAAAGGGGCATCGATGTGAACGGCGACATCAAGA  
TCAACGTCGCCAATTTTCAGAAGGCCAAAGACGACGCCGTGAAACAGCTC  
ACAGGCGGCATTGAGCTGCTCTTTAAGAAGAATAAAGTGACCTACTACAA  
GGGCAACGGCTCCTTCGAGGATGAGACCAAGATTAGAGTGACCCCTGTGG  
ACGGCCTCGAAGGCACCGTCAAAGAGGACCATATTCTGGACGTGAAAAAC  
ATCATTGTGGCCACCGGCTCCGAGGTCACCCCTTCCCCGGCATTGAGATC  
GATGAAGAGAAGATTGTGTCCAGCACCGGCGCCCTGTCCCTGAAGGAGAT  
CCCCAAAAGACTCACCATCATCGGAGGGCGGCATCATCGGCTTAGAAATGG  
GCAGCGTCTATAGCAGGCTGGGCTCCAAGGTGACCGTCGTCGAGTTCCAG  
CCTCAAATCGGAGCCAGCATGGACGGCGAAGTGGCCAAAGCCACCCAGAA  
GTTCTGAAGAAGCAAGGCCTCGACTTCAAAGTGTCCACCAAGGTGATCA  
GCGCTAAAAGGAACGACGACAAAAACGTGGTGGAGATCGTGGTCGAGGA  
CACAAAGACCAACAAGCAGGAGAATCTGGAAGCCGAAGTGCTCCTGGTCG  
CCGTGGGCAGAAGGCCTTACATTGCCGACTGGGCGCCGAAAAGATCGGA  
CTGGAAGTGGACAAGAGGGGCAGGCTCGTGATCGATGACCAGTTCAACTC  
CAAGTTCCCCACATCAAGGTCGTGGGAGACGTGACCTTTGGCCCCATGCT  
GGCCACAAGGCCGAAGAAGAGGGAATTGCCGCCGTCGAAATGCTGAAG

ACAGGCCACGGCCATGTGAACTACAACAATATCCCCAGCGTGATGTACTC  
CCATCCTGAGGTCGCTTGGGTCGGCAAAACAGAGGAGCAGCTCAAAGAGG  
CCGGCATTGACTACAAGATCGGCAAGTTCCTTCGCCGCCAACAGCAGA  
GCCAAGACAAATCAGGACACCGAGGGCTTCGTGAAGATTCTGATCGACAG  
CAAGACAGAGAGAATCCTGGGCGCTCACATCATCGGCCCTAATGCCGGCG  
AGATGATTGCCGAGGCTGGACTGGCCCTCGAATACGGCGCCAGCGCTGAG  
GATGTGGCTAGGGTCTGTACGCCCATCCCACCTCTCCGAGGCCTTCAAG  
GAGGCTAACATGGCCGCCTACGACAAGGCTATCCACTGTGTGTCAAAGG  
GGAAGAAGACAACATGGCTATCATAAAAGAATTTATGCGGTTCAAAGTTC  
ACATGGAAGGGTCCGTTAATGGTCATGAGTTCGAGATTGAGGGGCGAAGGA  
GAGGGCAGACCGTACGAAGGAACACAGACGGCAAAACTGAAGGTCACCA  
AGGGCGGTCCGCTGCCTTTCGCGTGGGATATACTGTACCCCCAGTTTATGT  
ACGGAAGCAAAGCGTATGTCAAGCACCCGGCGGACATCCCAGATTATCTC  
AAACTGTCCTTCCCCGAAGGTTTCAAATGGGAAAGGGTAATGAACTTCGA  
GGATGGTGGAGTCGTCACAGTTACACAAGATTCTTCTTTCAGGACGGCGA  
GTTTATCTACAAGGTCAAAGTGGGGGCACCAACTTCCCTTCTGACGGACC  
CGTAATGCAAAAAAAGACGATGGGGTGGGAGGCTTCATCAGAGCGCATGT  
ACCCAGAGGATGGGGCTCTGAAGGGCGAGATCAAGCAGCGGCTGAAGCT  
GAAAGACGGAGGACACTACGACGCGGAAGTGAAAATACTTACAAAGCA  
AAAAAGCCGGTACAAGTCCCAGGGGCATATAATGTAAACATCAAAGTGA  
CATTACGAGCCACAATGAGGACTACACGATAGTCGAACAGTACGAACGGG  
CGGAAGGAAGACACTCTACAGGTGGGATGGACGAAGTCTATAAGTGACTC  
GAG

### **Protein Sequences of LipDH-mCherry (for mammalian expression)**

MDYKDDDDKARADPTINKSHDVVIIGGGPAGYVAAIKAAQLGFNTACVEKR  
GKLGGTCLNVGCIPSKALLNNSHLFHQMHTAQKRGIDVNGDIKINVANFQK  
AKDDAVKQLTGGIELLFKKNKVTTYKNGSFEDETKIRVTPVDGLEGTVKED  
HILDVKNIIVATGSEVTPFPGIEIDEEKIVSSTGALSLEIPKRLTIIGGGIIGLEMG  
SVYSRLGSKVTVVEFQPQIGASMDGEVAKATQKFLKKQGLDFKLSTKVISAK  
RNDDKNVVEIVVEDTKTNKQENLEAEVLLVAVGRRPYIAGLGAEKIGLEVDK  
RGRLVIDDQFNSKFPHIKVVGDVTFGPMLAHKAEEEGIAAVEMLKTGHGHVN  
YNNIPSVMYSHPEVAWVGKTEEQLKEAGIDYKIGKFPFAANSRAKTNQDTEG  
FVKILIDSKTERILGAHIIGPNAGEMIAEAGLALAYGASAEDVARVCHAHPTLS  
EAFKEANMAAYDKAIHCVSKGEEDNMAIIEFMRFKVHMEGSVNGHEFEIEG  
EGEGRPYEGTQTAKLKVTGGPLPFAWDILSPQFMYGSKAYVKHPADIPDYL  
KLSFPEGFKWERVMNFEDGGVVTVTQDSSLQDGEFIYKVKLRGTNFPSPDGPV  
MQKKTMGWEASSERMYPEDGALKGEIKQRLKLDGGHYDAEVKTTYKAKK  
PVQLPGAYNVNIKLDITSHNEDYTIVEQYERAEGRHSTGGMDELYK